

Electronic Thesis and Dissertation Repository

---

8-24-2012 12:00 AM

## Ionothermal Synthesis of High Silica Zeolites in Deep Eutectic Solvents (DES)

Zheng Sonia Lin  
*The University of Western Ontario*

Supervisor  
Dr. Yining Huang  
*The University of Western Ontario*

Graduate Program in Chemistry  
A thesis submitted in partial fulfillment of the requirements for the degree in Master of Science  
© Zheng Sonia Lin 2012

Follow this and additional works at: <https://ir.lib.uwo.ca/etd>

 Part of the [Inorganic Chemistry Commons](#), and the [Materials Chemistry Commons](#)

---

### Recommended Citation

Lin, Zheng Sonia, "Ionothermal Synthesis of High Silica Zeolites in Deep Eutectic Solvents (DES)" (2012).  
*Electronic Thesis and Dissertation Repository*. 722.  
<https://ir.lib.uwo.ca/etd/722>

This Dissertation/Thesis is brought to you for free and open access by Scholarship@Western. It has been accepted for inclusion in Electronic Thesis and Dissertation Repository by an authorized administrator of Scholarship@Western. For more information, please contact [wlsadmin@uwo.ca](mailto:wlsadmin@uwo.ca).

**Ionothermal Syntheses of High Silica Zeolites in Deep Eutectic Solvents (DES)**

(Spine title: Ionothermal Syntheses of High Silica Zeolites)

(Thesis format: Integrated Article)

by

Zheng Sonia Lin

Graduate Program in Chemistry

A thesis submitted in partial fulfillment  
of the requirements for the degree of  
Master of Science

The School of Graduate and Postdoctoral Studies  
The University of Western Ontario  
London, Ontario, Canada

© Zheng Sonia Lin 2012

THE UNIVERSITY OF WESTERN ONTARIO  
School of Graduate and Postdoctoral Studies

**CERTIFICATE OF EXAMINATION**

Supervisor

Examiners

\_\_\_\_\_  
Dr. Yining Huang

\_\_\_\_\_  
Dr. Mark S. Workentin

Supervisory Committee

\_\_\_\_\_  
Dr. Yang Song

\_\_\_\_\_  
Dr. Ajay K. Ray

The thesis by

**Zheng Sonia Lin**

entitled:

**Ionothermal Syntheses of High Silica Zeolites in Deep Eutectic Solvents  
(DES)**

is accepted in partial fulfillment of the  
requirements for the degree of  
Master of Science

\_\_\_\_\_  
Date

\_\_\_\_\_  
Chair of the Thesis Examination Board

## Abstract

Phase-pure high silica zeolites have been synthesized using different deep eutectic solvents for the first time. ZSM-5 was made in tetrapropylammonium bromide/pentaerythritol. The reaction is affected by the amounts of seeding, water content, and organic structure-directing agent (SDA). Sodalite and ZSM-39 were prepared in tetramethylammonium chloride (TMACl)/1, 6-hexanediol by using the mineralizing agents NaOH and  $\text{NH}_4\text{F}$ , respectively. In urea/choline chloride, ZSM-5, Beta, ZSM-39, and ZSM-11 were made by using different organic SDAs in the presence of fluoride. The reaction temperature and the choice of organic SDA affect the type of structures being produced.

The crystallization of ZSM-39 in TMACl/1, 6-hexanediol was studied by powder X-ray diffraction, NMR spectroscopy, and SEM. Amorphous silica first arrange themselves around the  $\text{TMA}^+$  and then reorganize to form the larger cages. The larger cages are joined together as the smaller cages are formed, trapping the  $\text{F}^-$  in the framework.

## Keywords

ionic liquids, ionothermal, deep eutectic solvents, high silica zeolites, structure-directing agent, ZSM-5, Beta, ZSM-39, ZSM-11, crystallization, seeding

*To my dear parents*

## Acknowledgments

First and foremost, I wish to express my deepest appreciation to my supervisor, Dr. Yining Huang for his supervision and interest in this project. I am most grateful to the guidance, insightful thoughts, suggestions, and encouragement he has given me throughout this work. This thesis would not have been possible without his help and his incredible efficiency in proof-reading my draft copies.

I wish to express my gratitude to my examiners, Dr. Mark S. Workentin, Dr. Yang Song, and Dr. Ajay K. Ray for reading my thesis and providing valuable advices, and also to Dr. Richard Puddephatt for being the chair of the examination board of my thesis. Furthermore, I wish to thank Dr. Styaliani Conostas for being on my thesis supervisory committee.

I want to extend my gratitude to Dr. Nicholas Payne and Dr. Lyudmila Goncharova for their interesting courses. I would like to thank Dr. Matthew Willans, the NMR manager, for his dedication and technical help. Also, I want to express my thanks to Ms. Grace Yau (Earth Science) for the powder X-ray diffraction experiments. I wish to thank Tim Goldhawk at the Western Nanofabrication Facility for helping me to take SEM images and EDX data for my samples.

It has been an honour to work with Dr. Andre Sutrisno, Margaret Hanson-Clarke, Lu Zhang, Jun Xu, Tetyana Levchenko, Adam MacIntosh, Yue Hu, Donghan Chen, and Peng He in the Huang's Group. I appreciate their friendly help and especially want to thank Donghan who helped me to obtain the SEM pictures for the zeolite samples. I want to say thank you to all my friends for their support and encouragement.

Finally, I would like to thank my dear and beloved parents, who have always been so supportive and so believed in my abilities throughout my studies.

## Table of Contents

<b>CERTIFICATE OF EXAMINATION</b> .....	ii
<b>Abstract</b> .....	iii
<b>Dedication</b> .....	iv
<b>Acknowledgments</b> .....	v
<b>Table of Contents</b> .....	vi
<b>List of Tables</b> .....	x
<b>List of Figures</b> .....	xi
<b>List of Appendices</b> .....	xv
<b>List of Abbreviations</b> .....	xvi
<b>Chapter 1 : Introduction</b> .....	1
1.1 Zeolite molecular sieves .....	1
1.1.1 General background .....	1
1.1.2 Applications .....	1
1.2 Structures of zeolites.....	2
1.2.1 Structure naming of zeolites .....	2
1.2.2 ZSM-5 (MFI) .....	3
1.2.3 ZSM-11 (MEL).....	3
1.2.4 Sodalite (SOD).....	4
1.2.5 ZSM-39 (MTN) .....	5
1.2.6 Zeolite Beta (BEA) .....	6
1.3 Synthesis of zeolites .....	7
1.3.1 Hydrothermal synthesis .....	7
1.3.2 Formation mechanism.....	7
1.3.3 Organic structure-directing agents (SDAs).....	8

1.3.4	Mineralizing agent .....	9
1.3.5	Seeding.....	9
1.3.6	Non-aqueous synthesis.....	10
1.3.7	Ionothermal syntheses of porous materials.....	10
1.4	Research objectives and motivations.....	11
1.5	References.....	13
<b>Chapter 2 : Experimental.....</b>		<b>16</b>
2.1	Sample preparations.....	16
2.1.1	Zeolite synthesis in DES .....	16
2.1.2	Calcination .....	16
2.2	Characterization.....	17
2.2.1	Powder X-ray diffraction (PXRD).....	17
2.2.2	Solid state nuclear magnetic resonance spectroscopy .....	19
2.2.2.1	Overview .....	19
2.2.2.2	Magic-angle spinning (MAS).....	20
2.2.2.3	High power proton decoupling (HPDEC) .....	21
2.2.2.4	Cross polarization (CP) .....	21
2.2.3	Scanning electron microscopy (SEM) and energy dispersive X-ray spectroscopy (EDX).....	23
2.3	Synthesis of <i>N, N</i> -dipropylhexamethyleneiminium iodide (DPHMII).....	23
2.4	Synthesis of <i>N, N</i> -diethyl-3, 5- <i>cis</i> -dimethylpiperidinium iodide (DECDMPI).....	24
2.5	References.....	25
<b>Chapter 3 : Tetraalkylammonium Salt/Alcohol Mixtures as Deep Eutectic Solvents (DES) for Syntheses of High-Silica Zeolites.....</b>		<b>26</b>
3.1	Introduction.....	26
3.2	Experimental.....	29
3.2.1	Syntheses of high-silica zeolites .....	29



3.2.2	Characterization .....	31
3.3	Results and Discussion .....	32
3.3.1	MFI synthesized using TPABr as the organic SDA .....	32
3.3.1.1	NH <sub>4</sub> F as the mineralizing agent.....	32
3.3.1.2	NaOH as the mineralizing agent.....	41
3.3.2	Attempts to synthesize other zeolites using different DES.....	43
3.3.2.1	TEACl/pentaerythritol .....	43
3.3.2.2	Sodalite (SOD) and ZSM-39 (MTN) .....	46
3.4	Conclusions.....	48
3.5	References: .....	49
<b>Chapter 4 : Ionothermal Synthesis of High-Silica Zeolites in Urea/Choline Chloride Deep Eutectic Solvent (DES) .....</b>		<b>52</b>
4.1	Introduction.....	52
4.2	Experimental.....	54
4.2.1	Syntheses of high-silica zeolites .....	54
4.2.2	Characterization .....	56
4.3	Results and Discussion .....	58
4.3.1	Tetrapropylammonium bromide (TPABr).....	62
4.3.2	Tetraethylammonium hydroxide (TEAOH) .....	64
4.3.3	Tetramethylammonium chloride (TMACl) .....	68
4.3.4	<i>N, N</i> -dipropylhexamethylene imminium iodide (DPHMII) and <i>N, N</i> -diethyl-3, 5-dimethylpiperidinium iodide (DECDMPI) .....	69
4.4	Conclusions.....	74
4.5	References: .....	75
<b>Chapter 5 : Preliminary Studies on the Formation of ZSM-39 (MTN) Zeolite in Tetramethylammonium Chloride (TMACl)/1, 6-Hexandiol Deep Eutectic Mixture.....</b>		<b>79</b>
5.1	Introduction.....	79

5.2 Experimental Section.....	81
5.2.1 Sample preparation .....	81
5.2.2 Sample characterization .....	82
5.3 Results and Discussion .....	92
5.4 Conclusions.....	97
5.5 References.....	98
<b>Chapter 6 : Conclusions and Future Works.....</b>	<b>101</b>
6.1 Conclusions.....	101
6.2 Future Works .....	102
<b>Appendices.....</b>	<b>103</b>
<b>Curriculum Vitae .....</b>	<b>105</b>

## List of Tables

Table 2.1 Main nuclear spin interactions which can occur in solid.....	20
Table 3.1 Effects of seeding, amount of H <sub>2</sub> O, and TPABr:PE on ZSM-5 synthesis using the fluoride route; T = 170 °C. The PXRD patterns for the samples listed in this table are shown in Appendix A.....	33
Table 3.2 ZSM-5 samples synthesized using different Al sources in the presence of NaOH; T = 170 °C. The PXRD patterns of the samples listed in this table are shown in Appendix B. .....	42
Table 3.3 Silicalite-1 sample synthesized using TEACl as the template; T = 170 °C.....	44
Table 3.4 Mole ratios of SOD and MTN samples synthesized using TMACl as the template; T = 140 °C. M. I. = mineralizing agent.....	46

## List of Figures

Figure 1.1 (a) Pentasil unit. (b) Framework of zeolite ZSM-5. A layer of component pentasil chains is indicated by shading. (c) Channel structure of ZSM-5. ....	3
Figure 1.2 (a) Framework of zeolite ZSM-11. A layer of pentasil chains is shown by shading. <sup>1</sup> (b) Channel structure of ZSM-11. ....	4
Figure 1.3 Structure of (a) SOD framework and (b) $\beta$ -cage. ....	4
Figure 1.4 (a) Structure showing the tiling in ZSM-39 (MTN). (b) The two types of cages in ZSM-39. ....	5
Figure 1.5 Framework of zeolite Beta (a) Polymorph A, (b) Polymorph B, and (c) Polymorph C. The vertices represent the silicon atoms of the framework. The oxygen atoms are not shown for the purpose of clarity. The connections between each layer is in red. ....	6
Figure 1.6 Mechanism for formation of ZSM-5 (adapted with permission). ....	8
Figure 2.1 A schematic diagram showing the diffraction process of X-rays and derivation of Bragg's Law. ....	18
Figure 2.2 A diagram showing the arrangement of X-ray source, sample, and the detector.	18
Figure 2.3 An illustration of magic-angle spinning (MAS) with the sample rotor. ....	21
Figure 2.4 Pulse sequence of a cross-polarization experiment. ....	22
Figure 3.1 The structure of (a) pentaerythritol and (b) 1, 6-hexanediol. ....	28
Figure 3.2 PXRD patterns of (a) Silicalite-1 using TPABr and $\text{NH}_4\text{F}$ (A2), (b) aluminosilicate ZSM-5 synthesized in NaOH medium (D2), (c) Silicalite-1 using TEACl and $\text{NH}_4\text{F}$ (E1), (d) Sodalite (F1), and (e) ZSM-39 (F2). ....	34
Figure 3.3 SEM images of an as-synthesized ZSM-5 using $\text{F}^-$ as the mineralizing agent. ....	35

Figure 3.4 $^{29}\text{Si}$ MAS NMR spectra of (a) Silicalite-1 using TPABr and $\text{NH}_4\text{F}$ , (b) Al-containing ZSM-5 synthesized in NaOH medium, (c) Silicalite-1 synthesized using TEACl and $\text{NH}_4\text{F}$ , (d) Sodalite, and (e) ZSM-39.....	36
Figure 3.5 $^{13}\text{C}$ CP MAS NMR spectra of (a) pentaerythritol, (b) Silicalite-1 using TPABr and $\text{NH}_4\text{F}$ , (c) ZSM-5 synthesized in NaOH medium, (d) Silicalite-1 using TEACl and $\text{NH}_4\text{F}$ , and (e) ZSM-39.....	38
Figure 3.6 $^{19}\text{F}$ MAS NMR spectra of Silicalite-1 synthesized in $\text{NH}_4\text{F}$ media using (a) TPABr, (b) TEACl as templates, and (c) ZSM-39. Spinning side bands are indicated by “*”.	40
Figure 3.7 SEM images of ZSM-5 samples synthesized using (a-b) $\text{Al}(\text{O-}i\text{Pr})_3$ , (c-d) $\text{NaAlO}_2$ , and (e-f) $\text{Al}_2(\text{SO}_4)_3$ as Al sources.....	42
Figure 3.8 $^{27}\text{Al}$ MAS NMR spectra of ZSM-5 (a-c) synthesized in NaOH media using (a) $\text{Al}(\text{O-}i\text{Pr})_3$ , (b) $\text{NaAlO}_2$ , (c) $\text{Al}_2(\text{SO}_4)_3$ as Al sources, (d) sodalite, and (e) ZSM-39.....	43
Figure 3.9 SEM images of as-synthesized ZSM-5 using TEACl as the organic SDA.....	44
Figure 3.10 (a) Framework of MFI viewed down axis-b; all T-sites are numbered. (b) $^{29}\text{Si}$ MAS spectrum of as-made MFI using TEACl as the template. The numbers above the peaks correspond to the different T-sites. A small section of the framework showing neighboring Si-9 atoms. ....	45
Figure 3.11 SEM images of as-made (a-b) sodalite, and (c-d) ZSM-39.....	48
Figure 4.1 organic SDAs used for syntheses of ZSM-11: (a) <i>N, N</i> -dipropylhexamethyleneiminium iodide (DPHMII), and (b) <i>N, N</i> -diethyl-3,5-dimethylpiperidinium iodide (DECDMPI).....	54
Figure 4.2 PXRD patterns of as-synthesized (A.S.) (a) MFI, (b) BEA, (c) MTN from $\text{TMA}^+$ , (d) MTN from DPHMII, and (e) MEL from DPHMII, (f) MEL from DECDMPI. ....	58
Figure 4.3 $^{29}\text{Si}$ MAS spectra of as-synthesized (a) MFI, (b) BEA, (c) MTN from $\text{TMACl}$ , (d) MTN from DPHMII, (e) MEL from DPHMII, and (f) MEL from DECDMPI.....	59

Figure 4.4 $^{13}\text{C}$ CP MAS spectra of as-synthesized (a) MFI, (b) BEA, (c) MTN from TMACl, (d) MTN from DPHMII, (e) MEL prepared using DPHMII as the organic SDA, and (f) MEL prepared using DECDMPI as the organic SDA. The numbers in (e) and (f) are peak assignments corresponding to the different carbon sites on the DPHMII and DECDMPI templates shown in Figure 4.14. ....	60
Figure 4.5 $^{19}\text{F}$ MAS spectra of as-synthesized (a) MFI, (b) BEA, (c) MTN from TMACl, (d) MTN from DPHMII, (e) MEL prepared using DPHMII as the organic SDA, and (f) MEL prepared using DECDMPI as the organic SDA. The spinning side bands are indicated by “*” and “o” .....	61
Figure 4.6 SEM images showing (a) an overview and (b) a single crystal of the as-made Silicalite-1. ....	64
Figure 4.7 $^{27}\text{Al}$ MAS spectra of as-made BEA (a) and calcined BEA (b).....	65
Figure 4.8 $[4^35^4]$ cage in BEA. ....	66
Figure 4.9 SEM images showing (a) an overview and (b) expanded view of as-synthesized BEA.....	66
Figure 4.10 PXRD pattern of calcined BEA.....	67
Figure 4.11 $^{29}\text{Si}$ MAS spectrum of calcined BEA. ....	67
Figure 4.12 SEM images showing (a) an overview and (b) expanded view of as-synthesized TMA-MTN. ....	69
Figure 4.13 SEM images showing (a) an overview and (b) expanded view of as-synthesized MTN from a reaction mixture containing DPHMII at 170 °C. ....	70
Figure 4.14 DPHMII (a) and DECDMPI (b). The carbon atoms are labeled to represent the peak assignments for $^{13}\text{C}$ MAS spectra in Figure 4.4 (e) and (f).....	71
Figure 4.15 SEM images showing (a) an overview and (b) expanded view of as-synthesized DPHMI-MEL.....	72

Figure 4.16 SEM images showing (a) an overview and (b) expanded view of as-synthesized DECDMP-MEL.....	73
Figure 4.17 PXRD pattern of the solid obtained after 24 days of reaction using DECDMPI as the organic SDA.....	74
Figure 5.1 Two types of cages that build up ZSM-39: (a) [5 <sup>12</sup> ] and (b) [5 <sup>12</sup> 6 <sup>4</sup> ].....	80
Figure 5.2 PXRD patterns of samples obtained from reactions stopped at different time intervals.....	84
Figure 5.3 <sup>29</sup> Si MAS NMR spectra of samples obtained from reactions stopped at different time intervals.....	85
Figure 5.4 <sup>1</sup> H → <sup>29</sup> Si CP MAS NMR spectra of samples obtained from reactions stopped at early stages of crystallization (24-50 hr). Contact time = 0.5 ms.....	86
Figure 5.5 <sup>1</sup> H → <sup>29</sup> Si CP MAS NMR spectra of a 50 hr sample (ct = 10 ms) and a 72 hr sample (for comparison). The framework structure of ZSM-39 with T-sites assigned are shown. <sup>27</sup> .....	87
Figure 5.6 : <sup>13</sup> C CP MAS NMR spectra of samples obtained from reactions stopped at different time intervals. TMAm <sup>+</sup> : trimethylammonium ion .....	88
Figure 5.7 <sup>19</sup> F MAS NMR spectra of samples obtained from reactions stopped at different time intervals. Spinning speed = 12 kHz. The spinning side bands are shown by “*” and “o”. TMAF = tetramethylammonium fluoride.....	89
Figure 5.8 SEM images of samples obtained from reactions stopped at 48 hr (a-b), 50 hr (c-d), 66 hr (e-f), and 72 hr (g-h).....	90
Figure 5.9 SEM images of samples obtained from reactions stopped at (a) 4, and (b) 14 days. ....	91

## **List of Appendices**

Appendix A: PXRD patterns of Silicalite-1 samples listed in Table 3.1.....	103
Appendix B: PXRD patterns of aluminosilicate ZSM-5 samples prepared using different sources of aluminum. These are the PXRD patterns for the samples listed in Table 3.2....	104



## List of Abbreviations

AlPO <sub>4</sub>	Aluminophosphates
[Bmim]Br	1-butyl-3-methyl-imidazolium bromide
BEA	Beta
CP	Cross polarization
CSA	Chemical shift anisotropy
ct	Contact time
δ	Chemical shift
DECDMPI	<i>N, N</i> -diethyl-3, 5- <i>cis</i> -dimethylpiperidinium iodide
DES	Deep eutectic solvent
DPHMII	<i>N, N</i> -dipropylhexamethyleneiminium iodide
[emim]Br	1-ethyl-3-methyl-imidazolium bromide
EDX	Energy dispersive X-ray spectroscopy
HPDEC	High power proton decoupling
IL	Ionic liquid
IZA	International Zeolite Association
IZA-SC	International Zeolite Association-Structure Commission
MAS	Magic-angle spinning
MEL	Mobil Eleven
MFI	Mobil Five
MOF	Metal-organic framework
MTN	Mobil Thirty-Nine
NMR	Nuclear magnetic resonance
PE	Pentaerythritol
ppm	Parts per million (chemical shift)
PXRD	Powder X-ray diffraction
r.f.	Radio-frequency
SEM	Scanning electron microscopy
Si/Al	Silicon to aluminum ratio
SOD	Sodalite
SDA	Structure-directing agent
SSNMR	Solid-state nuclear magnetic resonance
TMACl	Tetramethylammonium chloride
TEACl	Tetraethylammonium chloride
TMS	Tetramethylsilane
TON	Theta-1

TPABr	Tetrapropylammonium bromide
TPAOH	Tetrapropylammonium hydroxide
T-site	Tetrahedral site
TTMSS	Tetrakis(trimethylsilyl)silane
wt.	Weight

## Chapter 1 : Introduction

### 1.1 Zeolite molecular sieves

#### 1.1.1 General background

The term “zeolite” comes from Greek, meaning “boiling stone.” Zeolites were first discovered in 1756 by the Swedish mineralogist, Axel Fredrik Cronstedt, who observed that upon boiling the mineral stilbite, a large amount of steam was produced from the water that has been previously absorbed by the material. Zeolites are a group of crystalline, highly-porous silicate and aluminosilicate materials with open three-dimensional frameworks of tetrahedral silica or alumina anions strongly bonded at all corners via oxygen atoms. Depending on the chemical composition and the crystal structure of the particular zeolite involved, the structures of zeolite contain (-Si-O-Al-) or (-Si-O-Si-) linkages that form pores of uniform diameter and enclose regular internal cavities and channels of discrete sizes and shapes. The pore size of zeolites can range from 3 to 10 Å. Cations and water molecules are contained within the enclosed cavities of zeolites and are loosely bound to the lattice, contributing to zeolites’ ability to perform ion exchange. The water molecules can be reversely driven off in most zeolites, allowing for gas adsorption and water adsorption/desorption based on the size and shape of the absorbed molecule.<sup>1</sup>

#### 1.1.2 Applications

Zeolites are involved in many industrial and chemical applications due to their varieties in structure, chemical composition, thermal and hydrothermal stabilities. For instance, due to the negatively charged nature of the framework, synthetic zeolites are often used as ion exchangers. They act as water softeners in detergents because the  $\text{Ca}^{2+}$  and  $\text{Mg}^{2+}$  are captured into the framework.<sup>2</sup>

For many years, zeolites have very important in the petrochemical industry. They are used in fluidic catalytic cracking where the high molecular weight hydrocarbons are broken down into smaller alkane molecules and olefins.<sup>1</sup> Because the channels and pores

of zeolites vary in shapes and sizes depending on the framework type, they are also used as shape-selective catalysts. For example, zeolite ZSM-5 is responsible for the conversion of meta-xylene to para-xylene. The confined space inside the zeolites allows the isomerization to take place faster. This zeolite has both straight and sinusoidal channels. Within these channels, para-xylene has a much high diffusion coefficient than meta-xylene and therefore diffuses out from the straight channels faster than the other.<sup>3</sup>

The applications of zeolites have been expanded into many different ways. By introducing transition metals into the framework, zeolites can become powerful catalysts for many different types of reactions. For example, titanium silicalite-1 (TS-1), where titanium is introduced into ZSM-5, is an excellent catalyst for a variety of chemical reactions, such as olefin epoxidation and the oxidation of alcohol to aldehydes.<sup>4</sup> The area of zeolite films and membranes has also been investigated for applications in separation processes and semiconductors.<sup>5-7</sup> More recently, zeolites have also been explored for potential applications in tissue engineering since the surface of the zeolites can be functionalized with bioactive agents.<sup>8</sup>

## 1.2 Structures of zeolites

### 1.2.1 Structure naming of zeolites

The description of zeolite frameworks are assigned by the International Zeolite Association-Structure Commission (IZA-SC). The different zeolite framework structures are named using three-letter codes which compose of only Roman letters. These codes are usually derived from the Type Materials and represent the framework topology of the zeolites and do not reflect crystal symmetries or composition of the materials. For instance, the full name of zeolite ZSM-5 is Zeolite Socony Mobil-Five, while the abbreviated name is Mobil Five. The three-letter code for this framework is MFI.

As of December 2011, 201 framework type codes have been assigned by the IZA-SC. For the purpose of this thesis, five framework types will be discussed in the following sections.

### 1.2.2 ZSM-5 (MFI)

ZSM-5 was first developed by Mobil Oil: The framework of ZSM-5 contains pentasil units that are made up of eight five-membered rings of linked tetrahedra (Figure 1.1a).<sup>9</sup> The ZSM-5 units join through edges to form chains which extend along the  $z$ -axis (Figure 1.1b).<sup>1,9</sup> The adjacent sheets in MFI are related by an inversion centre.<sup>9</sup> The overall network of MFI contains two types of intersecting channels. One is sinusoidal, running parallel to  $[001]$ , and the other is straight and parallel to  $[010]$  (Figure 1.1c).<sup>1,9</sup> ZSM-5, at high temperatures, is orthorhombic (space group  $Pnma$ ) but experiences phase transition at lower temperatures (300-350 K) and becomes monoclinic (space group  $P2_1/n$ ).<sup>10-11</sup> The silicate form of ZSM-5, Silicalite-1, is charge neutral, and therefore it cannot act as a catalyst. However, the aluminosilicate form of MFI is negatively charged; there must be a positive charge in order to keep the material charge neutral. When there is a presence of proton ( $H^+$ ), the zeolite becomes acidic and can be utilized for acid-catalyzed reactions.<sup>1</sup> The all-silica form of ZSM-5 is called silicalite-1.

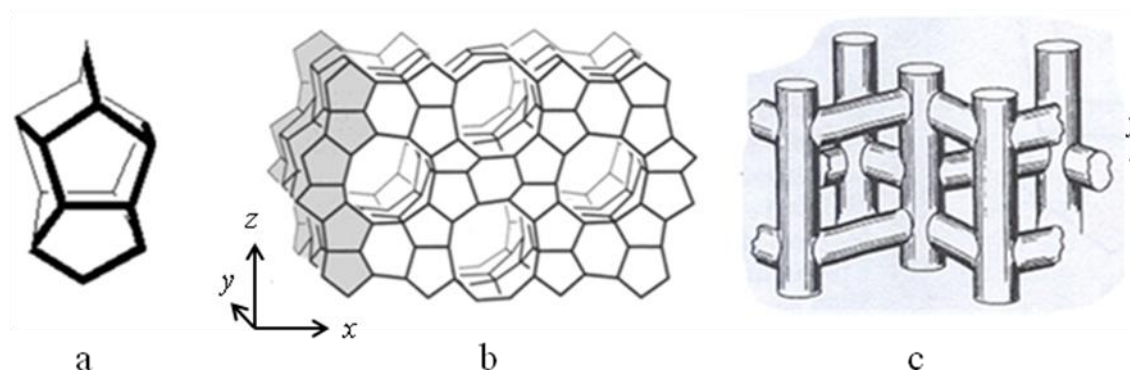


Figure 1.1 (a) Pentasil unit.<sup>1</sup> (b) Framework of zeolite ZSM-5.<sup>1</sup> A layer of component pentasil chains is indicated by shading.<sup>1</sup> (c) Channel structure of ZSM-5.<sup>9</sup>

### 1.2.3 ZSM-11 (MEL)

A zeolite framework closely related to ZSM-5 is ZSM-11 (Mobil Eleven, MEL), which is tetragonal (space group  $I-4m2$ ). ZSM-11, like ZSM-5, is also made up of pentasil chains (Figure 1.2a).<sup>1</sup> Nevertheless, in MEL, the sheets are joined together by a mirror plane instead rather than by a centre of inversion.<sup>1</sup> This makes the two intersecting 10-membered ring channels straight rather than sinusoidal (Figure 1.2b).<sup>1,12</sup>

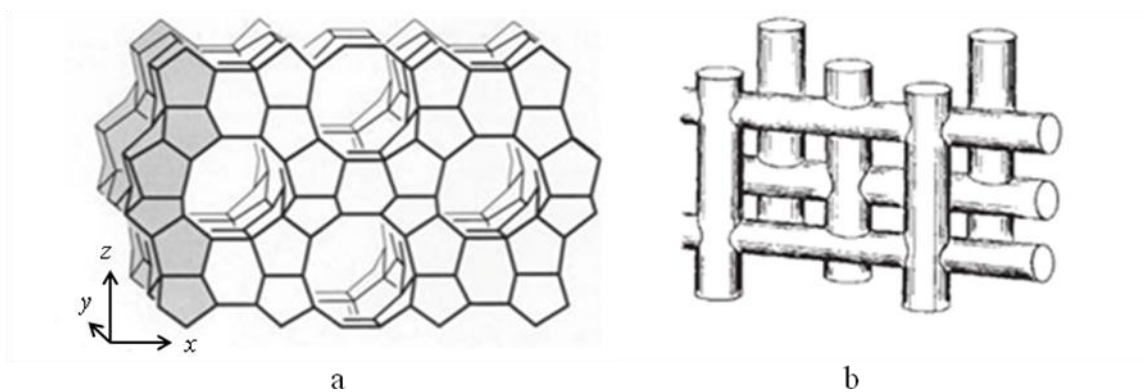


Figure 1.2 (a) Framework of zeolite ZSM-11. A layer of pentasil chains is shown by shading.<sup>1</sup> (b) Channel structure of ZSM-11.<sup>12</sup>

#### 1.2.4 Sodalite (SOD)

Sodalite (SOD), the simplest zeolite, has a cubic topology with space group  $Im\bar{3}m$ . The structure of sodalite is composed of  $\beta$ -cages which are polyhedrons containing truncated octahedra (Figure 1.3a). Each  $\beta$ -cage contains eight six membered ringed windows and six four membered ringed windows ( $[4^66^8]$ ) (Figure 1.3b).<sup>13</sup> The  $\beta$ -cage has an internal diameter of  $\sim 6\text{\AA}$ , allowing for the capturing of small molecules such as  $\text{CO}_2$ .

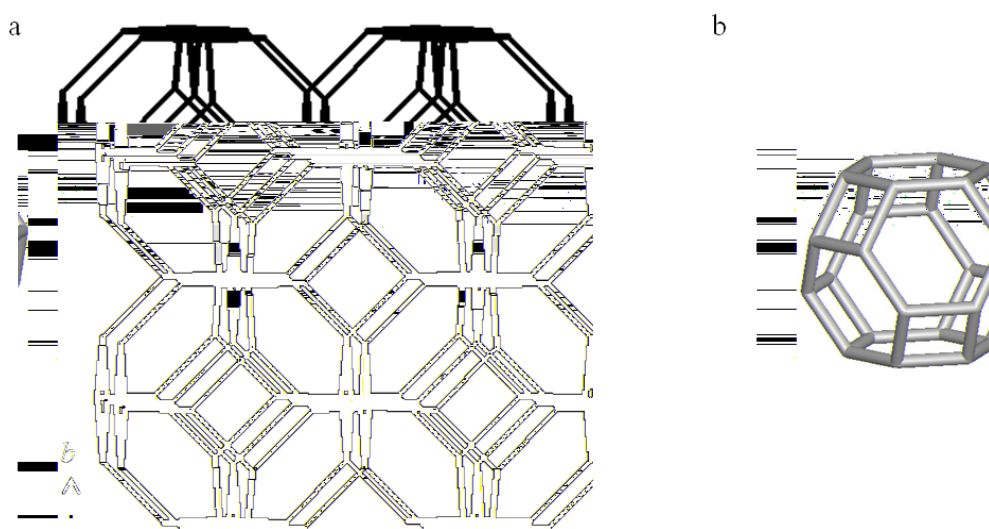


Figure 1.3 Structure of (a) SOD framework and (b)  $\beta$ -cage.

### 1.2.5 ZSM-39 (MTN)

Zeolite ZSM-39 (Mobil Thirty-Nine, MTN) is the silicate analogue of the 17Å cubic gas hydrate dodecasil-3C.<sup>14-15</sup> The space group of ZSM-39 is Fd-3m. The tiling of the MTN framework is shown in Figure 1.4a. There are two types of cages in MTN (Figure 1.4b): The smaller one is made up of 12 five-membered rings ( $[5^{12}]$ ), and the larger one is made up by 12 five-membered rings and four six-membered rings ( $[5^{12}6^4]$ ). The smaller cavity is around 5.7 Å, while the size of the larger cavity is around 7.5 Å. Due to the small size of the cages, MTN has a very limited sorption capacity.<sup>16-19</sup> However, since ZSM-39 is a clathrate, any molecules that enter the framework will become trapped. Studying this host-guest interaction will provide a better understanding of the molecular interactions between the framework and the entrapped species.

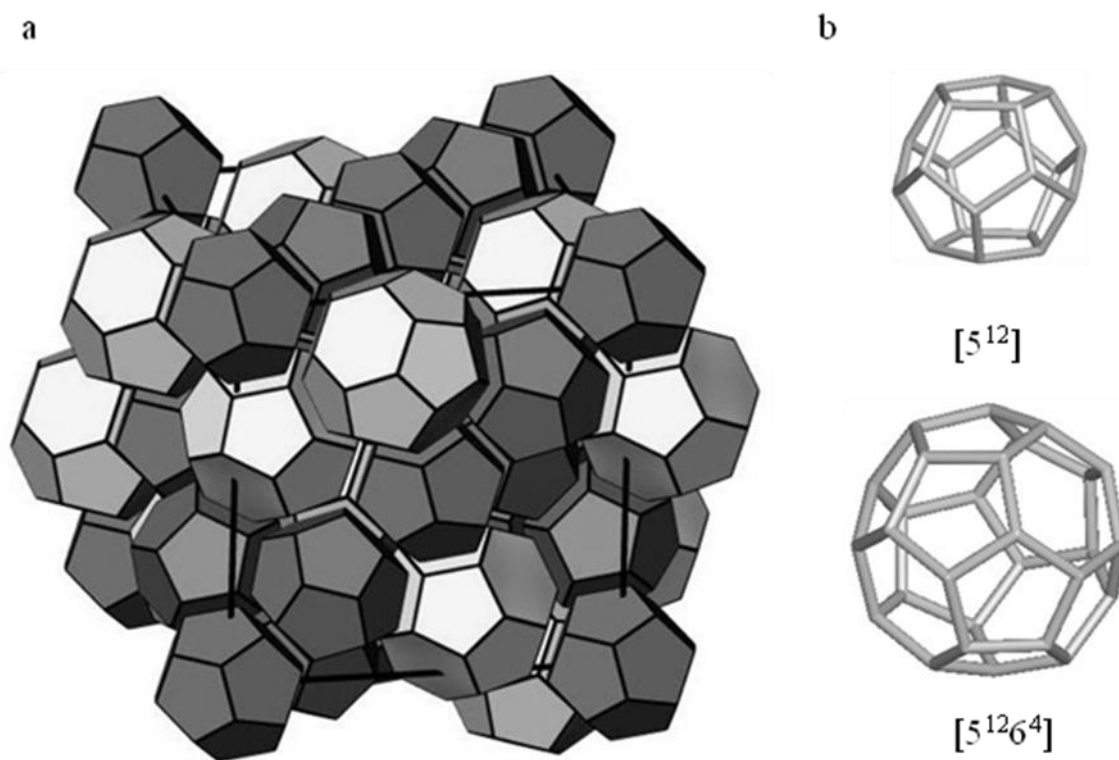


Figure 1.4 (a) Structure showing the tiling in ZSM-39 (MTN). (b) The two types of cages in ZSM-39.

### 1.2.6 Zeolite Beta (BEA)

The framework of zeolite beta (BEA) is shown in Figure 1.5. Zeolite beta is a highly disordered structure consisting of three polymorphs: Polymorph A, Polymorph B, and Polymorph C.<sup>20-22</sup> The stacking patterns of a building unit layer for the three different polymorphs are shown in Figure 1.5. However, the neighboring layers are stacked on top of each other in a random fashion. Therefore, the final structure formed is usually highly faulted. The eventual three dimensional frameworks will contain 12-membered ringed channels in the *a*- and *b*-directions that are independent of the stacking sequence along the *c*-direction.<sup>20</sup>

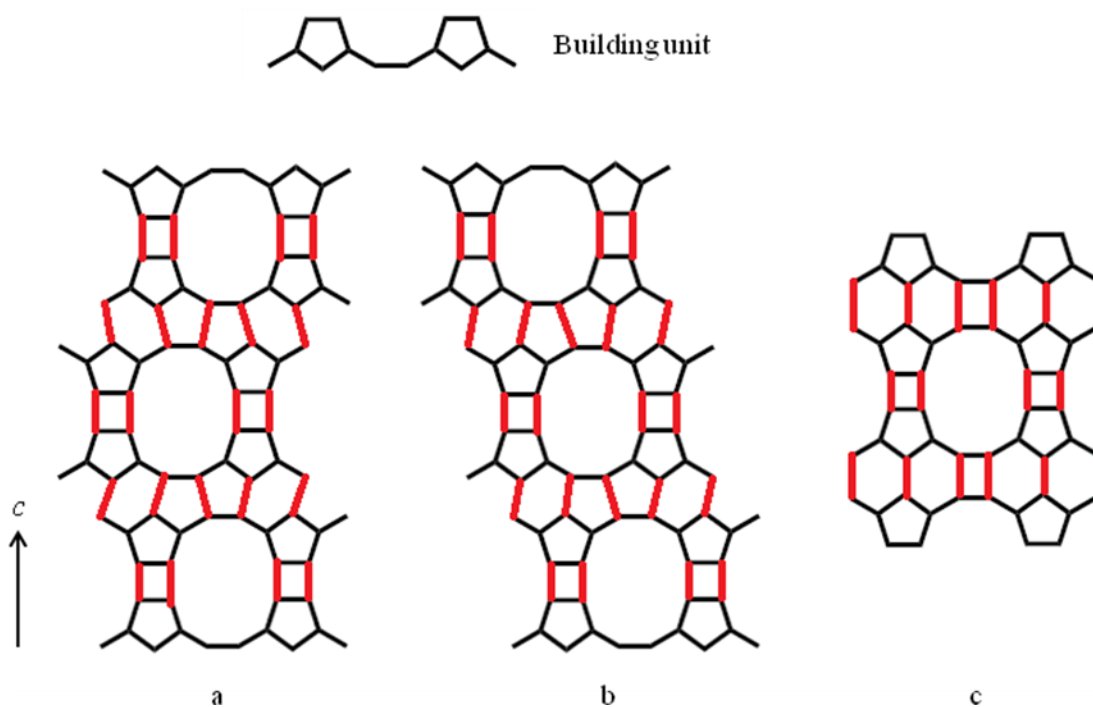


Figure 1.5 Framework of zeolite Beta (a) Polymorph A, (b) Polymorph B, and (c) Polymorph C. The vertices represent the silicon atoms of the framework. The oxygen atoms are not shown for the purpose of clarity. The connections between each layer is in red.



## 1.3 Synthesis of zeolites

### 1.3.1 Hydrothermal synthesis

Hydrothermal synthesis is a technique for preparing crystalline materials in aqueous solutions at high temperatures and pressure. It is the typical route for the syntheses of many microporous materials, including zeolites. For zeolites, they are usually prepared by mixing a base, silica, water, and an organic structure-directing agent (often tetraalkylammonium ions) inside a Teflon-lined stainless autoclave which is subjected to a reaction temperature of 150-200 °C.<sup>23</sup> The advantage of hydrothermal synthesis is the production of crystals with higher quality. Furthermore, under the presence of high amounts of water, the reaction mixture is more homogenized. Nevertheless, the high water content also generates high autogenous pressure which requires the use of the stainless steel autoclaves.

### 1.3.2 Formation mechanism

The crystallization process of zeolites is quite complicated, because it is affected by many factors such as temperature, the homogeneity of the reaction mixture, source of silica, etc. Figure 1.6 shows the general scheme for the formation of ZSM-5.<sup>24</sup> The silica in the starting material are quite hydrophobic. The presence of organic cations, often known as the organic structure-directing agent (SDA), allows the silica species to form a hydration sphere around it. Depending on the structure of the organic species involved, the interaction between the silica and the organic molecules can vary. The penetration of water into this hydration is minimized when there is an energetically favourable interaction between the organic SDA and the silica molecules.<sup>25</sup> Once the hydration spheres form, the aggregation of these small species form what is called the primary units.<sup>24</sup> The primary units may then join together later on to become bigger aggregates. Usually, the crystallization process starts with the aggregation of amorphous materials into a gel phase, allowing the formation of nuclei within the gel.<sup>26-27</sup> When crystal growth starts, the smaller units can also diffuse to the surface of the growing crystals, which eventually yields the zeolite product with a three-dimensional network.<sup>24</sup>

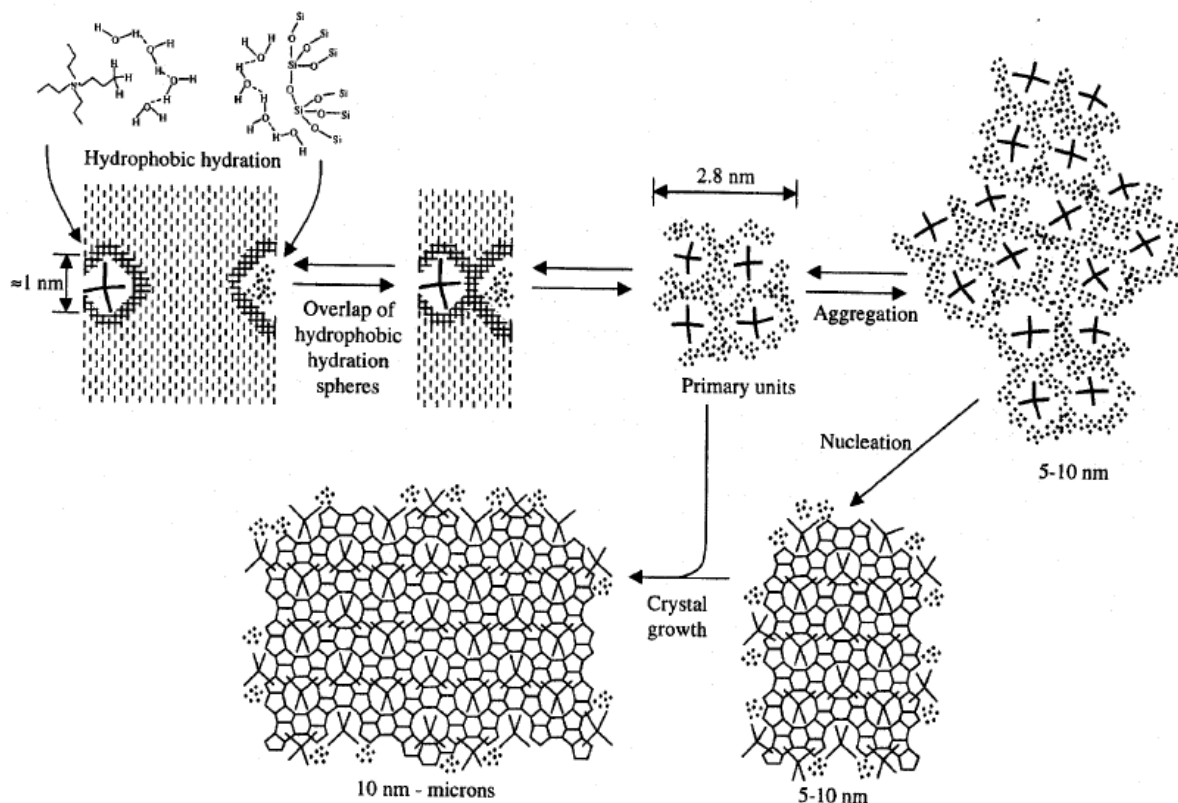


Figure 1.6 Mechanism for formation of ZSM-5 (adapted with permission).<sup>24</sup>

### 1.3.3 Organic structure-directing agents (SDAs)

Many organic species, especially the quaternary ammonium cations, amines, and alcohols have been explored and employed in the synthesis of microporous materials since the 1960s.<sup>28</sup> It has been found that these organic molecules are often occluded inside the cages of the final framework being formed. In the realm of zeolite synthesis, the addition of organic molecules allows the production of high-silica zeolites ( $\text{SiO}_2/\text{Al}_2\text{O}_3 > 20$ ). The higher silica content in the zeolites results in less defect sites and higher thermal stability. Furthermore, from the zeolite formation mechanism point of view, the introduction of these organic species into reactions will lead to a variety of framework types being produced. This is because the differences in the chemical structure of the organic molecules will induce different interactions between the organic SDA and the silica present in the reaction mixture. Therefore, the organic species have a structure-directing effect on the type of zeolite being formed and are known as the

structure-directing agent (SDA).<sup>24</sup> However, depending on the synthesis conditions, it is not uncommon that different structures share the same SDA, or the same structure can be formed by different SDAs.<sup>29</sup> This case will be seen in the later chapters of the thesis.

#### 1.3.4 Mineralizing agent

An important component of the reaction mixtures for zeolite syntheses is the mineralizing agent, which helps to dissolve the silica and alumina species in the reaction mixture and is responsible for the formation of Si-O-Si or Si-O-Al bridges. Zeolite syntheses were often performed at high pH in the presence of hydroxide ions. In the 1970s, Flanigen discovered that silicalite-1 can be prepared using  $F^-$  species as the mineralizing agent at near neutral pH. It has been found that the use of  $F^-$  yields zeolite crystals with larger sizes and fewer defects.<sup>30</sup>

The fluoride route has then been explored by many researchers, not only for pure silica zeolites, but also for zeolites having substituted heteroatoms and the zeolite-like material, aluminophosphates.<sup>29</sup> Furthermore, in certain cases, a framework cannot be formed without the presence of  $F^-$ . The all silica zeolites produced via the  $F^-$  route are strictly hydrophobic and do not have the abilities to act as ion exchangers. Nevertheless, these siliceous species are of interests to many people, not only for the discoveries of new synthetic framework types, but also the fact that  $F^-$  ions are often occluded inside the all silica zeolites. There are three forms where  $F^-$  can exist inside the cages of a zeolite. The first case would be  $F^-$  is ion-paired with the organic SDA. In the second case,  $F^-$  can be trapped inside a small cage or in between walls or channels to act as a counter ion for the organic SDA. In the third case, the  $F^-$  is covalently bonded to a silicon atom which now becomes pentacoordinated.<sup>31</sup> For these reasons, it has been argued that  $F^-$  ions have structure-directing effects on zeolite formation.

#### 1.3.5 Seeding

As mentioned previously, the crystallization of zeolites occur through the aggregation of amorphous gel. For nucleation to take place, small nuclei must be formed in order to have surfaces for the crystals to grow on. Crystal growth can happen on the surface of the seed crystals. Also, there are microcrystallites which were initially adhered

to the seed surface and later became washed off by the solvents in the reaction mixture. These microcrystalline particles also provide surface area for the building units to aggregate. Therefore, the rate of crystallization is often sped up by adding seeds to the reaction, because the time it takes for any nuclei to be formed is much shorter.<sup>32-34</sup>

### 1.3.6 Non-aqueous synthesis

The area of non-aqueous synthesis has been explored by different researchers over the past few decades. The first example would be the synthesis of sodalite in the presence of ethylene glycol by Bibby and Dale.<sup>35</sup> It has been shown that ZSM-5, ZSM-35, ZSM-39, octadecasil (AST), P1, Beta, and ZSM-48 can be made in ammonia using the F<sup>-</sup> route.<sup>36</sup> Another example is the production of large ferrierite (FER) crystals in pyridine.<sup>37</sup> Recently, a new strategy for preparing microporous materials has been developed by Morris *et al.*—ionothermal synthesis.<sup>38</sup>

### 1.3.7 Ionothermal syntheses of porous materials

Ionic liquids (ILs) are a class of solvents with a melting point of below 100 °C. However, since the temperatures required for the syntheses of most zeolites or zeolite-like materials are in the range of 150-200 °C, an IL used for this purpose is a salt with a melting point below this range. Compared to hydrothermal synthesis, the use of IL produces lower autogenous pressure. Furthermore, the organic component of an IL can act both as a solvent and also an SDA. The formation of microporous materials involves the interactions between the growing framework, solvent, and SDA. It has been argued that by using IL as the solvent, the competition between solvent/growing crystals and solvent/SDA can be minimized.<sup>38</sup> The use of ionic liquids has produced many new classes of porous materials, such as the aluminophosphates, coordination polymers and metal organic frameworks.<sup>38-41</sup>

A type of IL is called the deep eutectic solvent (DES). A deep eutectic solvent is a system with two components resulting in a melting point lower than the pure substance form of both. Dong reported the first DES method of synthesizing aluminophosphates materials in a quaternary ammonium salt/pentaerythritol mixture.<sup>40</sup> As discussed in 1.3.3, the presence of organic SDA is extremely important for the successful synthesis of

the desired framework. Therefore, ideally speaking, desired products can be obtained by mixing a second compound with the organic SDA responsible for the formation of zeolite of interest.

Despite many new frameworks have been synthesized in the presence of ILs, little work has been done on the preparation of highly siliceous materials under ionothermal conditions. This is mainly due to the poor solubility of silica in ILs, causing the investigations in this area to be rather challenging. Until now, there have been only a few reports on the syntheses of siliceous frameworks in IL. It has been found that sodalite can be synthesized in 1-ethyl-3-methyl-imidazolium bromide ([emim]Br).<sup>42-43</sup> Yan's group synthesized ZSM-5 by microwave-heating a mixture formed from 1-butyl-3-methylimidazolium [Bmim] bromide and a dry-gel precursor containing the ZSM-5 structure-directing agent (SDA), TPAOH.<sup>44</sup> Another example of MFI synthesis was reported by Morris's group. The group found that silicalite-1 can be made in the presence of fluoride by using [Bmim] bromide/hydroxide mixture with the addition of a small amount of H<sub>2</sub>O. The siliceous zeolites produced in this type of reagent composition can be composed of phase-pure silicalite-1 (MFI) or a mixture of Theta-1 (TON) and MFI.<sup>45</sup> For all the syntheses mentioned above, a small amount of water must be added to the reaction mixture for the zeolites to be formed. These examples show that despite the difficulties of dissolving the reactants in ILs, by carefully optimizing the reaction conditions, siliceous materials can still be made. Comparing Yan's and Morris's results, we can see that, like in hydrothermal syntheses, the presence of the organic SDA species is extremely important for the production of phase-pure frameworks.

## 1.4 Research objectives and motivations

While there is much research done on the exploration of new materials, investigations in different synthetic methodologies for high-silica zeolites remain attractive. High-silica zeolites are excellent heterogeneous catalysts since they exhibit less defects and high thermal stabilities. The current challenges in the preparation of silica-based microporous materials are as follows:

- (1) The solubility of starting materials in the ILs

(2) The synthesis of phase-pure structures

(3) The reproducibility of results

To circumvent these problems, seeding, choices of mineralizing agent and the organic SDA were employed to yield highly crystalline siliceous samples. Also, more knowledge about the silica chemistry under ionothermal conditions is required for the development in the area of silicate and aluminosilicate preparation in IL and for the discoveries of new framework structures.

This thesis focuses on two types of IL systems. In total, five zeolites with different framework types have been synthesized under ionothermal conditions: MFI, SOD, MTN, MEL and BEA. The effects of different components on the production of zeolite using tetraalkylammonium salt/alcohol DES are discussed in Chapter 3 of the work. Chapter 4 demonstrates the preparation of several phase-pure zeolites by using different organic SDAs in urea/choline chloride mixture. Finally, the formation mechanism of MTN in the presence of tetramethylammonium chloride/1, 6-hexanediol mixture was studied in the attempt to gain a better understanding of the chemistry involved in ionothermal synthesis of high-silica zeolites.

## 1.5 References

1. Bekkum, H. v.; Jacobs, P. A.; Flanigen, E. M.; Jansen, J. C., *Introduction to Zeolite Science and Practice*. 2001.
2. Flanigen, E. M., *Pure Appl. Chem.* **1980**, 52 (9), 2191-2211.
3. Rees, L. V. C., *Nature* **1989**, 340 (6232), 356-356.
4. Clerici, M. G. In *Titanium silicalite-1*, Wiley-VCH Verlag GmbH & Co. KGaA: 2009; pp 705-754.
5. Garces, J. M. In *Observations on zeolite applications*, Materials Research Society: 1999; pp 551-566.
6. Kulprathipanja, S., *Zeolites in Industrial Separation and Catalysis*. Weinheim : Wiley-VCH: 2010.
7. Yan, Y.; Li, S.; Li, Z., *Zeoraito* **2003**, 20, 111-120.
8. El-Gindi, J.; Benson, K.; De Cola, L.; Galla, H.-J.; Seda Kehr, N., *Angew. Chem. Int. Ed.* **2012**, 51 (15), 3716-3720.
9. Kokotailo, G. T.; Lawton, S. L.; Olson, D. H.; Olson, D. H.; Meier, W. M., *Nature* **1978**, 272 (5652), 437-438.
10. Grau-Crespo, R.; Acuay, E.; Ruiz-Salvador, A. R., *Chem. Commun.* **2002**, (21), 2544-2545.
11. Hay, D. G.; Jaeger, H.; West, G. W., *J. Phys. Chem.* **1985**, 89 (7), 1070-1072.
12. Kokotailo, G. T.; Chu, P.; Lawton, S. L.; Meier, W. M., *Nature* **1978**, 275 (5676), 119-120.
13. Meier, W. M.; Olson, D. H.; Baerlocher, C., *Zeolites* **1996**, 17 (1-2), 1-229.
14. Claussen, W. F., *J. Chem. Phys.* **1951**, 19 (2), 259-260.
15. Claussen, W. F., *J. Chem. Phys.* **1951**, 19 (11), 1425-1426.
16. Long, Y.; He, H.; Zheng, P.; Wu, G.; Wang, B., *J. Inclusion Phenom. Macrocyclic Chem.* **1987**, 5 (3), 355-362.
17. Marler, B.; Dehnbostel, N.; Eulert, H. H.; Gies, H.; Liebau, F., *J. Inclusion Phenom. Macrocyclic Chem.* **1986**, 4 (4), 339-349.
18. Schlenker, J. L.; Dwyer, F. G.; Jenkins, E. E.; Rohrbaugh, W. J.; Kokotailo, G. T.; Meier, W. M., *Nature* **1981**, 294 (5839), 340-342.

19. Zheng, P.; Wang, B.; Wu, G., *Chem. J. Chinese Univ.* **1988**, 9, 1.
20. Newsam, J. M.; Treacy, M. M. J.; Koetsier, W. T.; Gruyter, C. B. D., *Proceedings of the Royal Society of London. Series A, Mathematical and Physical Sciences* **1988**, 420 (1859), 375-405.
21. Corma, A.; Navarro, M. T.; Rey, F.; Rius, J.; Valencia, S., *Angew. Chem. Int. Ed.* **2001**, 40 (12), 2277-2280.
22. Corma, A.; Moliner, M.; Cantón, Á.; Díaz-Cabañas, M. J.; Jordá J. L.; Zhang, D.; Sun, J.; Jansson, K.; Hövmandler, S.; Zou, X., *Chem. Mater.* **2008**, 20 (9), 3218-3223.
23. Arganer, R. J.; Landolt, G. R. US3702886, 1972.
24. de Moor, P. P. E. A.; Beelen, T. P. M.; Komanschek, B. U.; Beck, L. W.; Wagner, P.; Davis, M. E.; van Santen, R. A., *Chem. Eur. J.* **1999**, 5 (7), 2083-2088.
25. Petrovic, I.; Navrotsky, A.; Davis, M. E.; Zones, S. I., *Chem. Mater.* **1993**, 5 (12), 1805-1813.
26. Subotic, B., *ACS Symp. Ser.* **1989**, 398, 110-123.
27. Schoeman, B. J., *Zeolites* **1997**, 18 (2-3), 97-105.
28. Barrer, R. M.; Denny, P. J., *J. Chem. Soc.* **1961**, (Mar), 971.
29. Caullet, P.; Paillaud, J. L.; Simon-Masseron, A.; Soulard, M.; Patarin, J., *C.R. Chim.* **2005**, 8 (3-4), 245-266.
30. Flanigen, E. M.; Bennett, J. M.; Grose, R. W.; Cohen, J. P.; Patton, R. L.; Kirchner, R. M.; Smith, J. V., *Nature* **1978**, 271 (5645), 512-516.
31. Koller, H.; Wolker, A.; Eckert, H.; Panz, C.; Behrens, P., *Angew. Chem. Int. Ed.* **1997**, 36 (24), 2823-2825.
32. Gora, L.; Strelitzky, K.; Thompson, R. W.; Phillips, G. D. J., *Zeolites* **1997**, 19 (2-3), 98-106.
33. Gora, L.; Strelitzky, K.; Thompson, R. W.; Phillips, G. D. J., *Zeolites* **1997**, 18 (2-3), 119-131.
34. Rees, L. V. C.; Thompson, R. W., *Zeolites* **1997**, 19 (5-6), 317-317.
35. Bibby, D. M.; Dale, M. P., *Nature* **1985**, 317 (6033), 157-158.
36. Millar, D. M.; Garces, J. M. In *Synthesis of crystalline porous solids in ammonia*, Materials Research Society: 1999; pp 1535-1542.



37. Kuperman, A.; Nadimi, S.; Oliver, S.; Ozin, G. A.; Garces, J. M.; Olken, M. M., *Nature* **1993**, *365* (6443), 239-242.
38. Cooper, E. R.; Andrews, C. D.; Wheatley, P. S.; Webb, P. B.; Wormald, P.; Morris, R. E., *Nature* **2004**, *430* (7003), 1012-1016.
39. Kitagawa, S.; Kitaura, R.; Noro, S., *Angew. Chem. Int. Ed.* **2004**, *43* (18), 2334-2375.
40. Dong, J. X.; Liu, L.; Li, X. P.; Xu, H.; Li, J. P.; Lin, Z., *Dalton T.* **2009**, (47), 10418-10421.
41. Ferey, G., *Chem. Soc. Rev.* **2008**, *37* (1), 191-214.
42. Ma, Y. C.; Wang, S. J.; Song, Y. L.; Xu, Y. P.; Tian, Z. J.; Yu, J. Y.; Lin, L. W., *Chinese. J. Inorg. Chem.* **2010**, *26* (11), 1923-1926.
43. Ma, Y. C.; Xu, Y. P.; Wang, S. J.; Wang, B. C.; Tian, Z. J.; Yu, J. Y.; Lin, L. W., *Chem. J. Chinese. U.* **2006**, *27* (4), 739-741.
44. Cai, R.; Liu, Y.; Gu, S.; Yan, Y. S., *J. Am. Chem. Soc.* **2010**, *132* (37), 12776-12777.
45. Morris, R. E.; Wheatley, P. S.; Allan, P. K.; Teat, S. J.; Ashbrook, S. E., *Chem. Sci.* **2010**, *1* (4), 483-487.

## Chapter 2 : Experimental

### 2.1 Sample preparations

#### 2.1.1 Zeolite synthesis in DES

The typical procedure is as follows: A mixture containing the mineralizing agent, the organic SDA, alcohol or urea/choline chloride, were mixed quantitatively and ground using a mortar and a pestle. Calcined seeds was added to the mixture and ground if the formation of the zeolite of interest required the presence of seed crystals. The ground solid mixture was then transferred to a 40 mL Teflon container. To this mixture, a source of colloidal silica was added. In the case of the preparation of zeolite beta, since the organic SDA is in the form of solution, fumed silica was used instead of colloidal silica. The components were hand-mixed using a spatula until a sticky white paste is formed inside the Teflon cup. The Teflon container was then placed inside a stainless steel autoclave and the reaction mixture would be heated at around 140-170 °C for 19-28 days depending on the type of reaction. For studies in which the reaction intermediates were obtained, the reactions were taken out at different time intervals.

Once the reactions are completed, the product was obtained by filtration after being three successive washes using deionized water. The filtered solid was washed with methanol several times and with deionized water again. The product was dried in the oven at 100 °C for 24 hours.

#### 2.1.2 Calcination

Calcination is a thermal treatment which removes the organic SDA and water components inside the pores of a zeolite. Selected samples were calcined in a furnace at 350/500 °C.

## 2.2 Characterization

### 2.2.1 Powder X-ray diffraction (PXRD)

Most of the zeolite samples we prepared are under 100  $\mu\text{m}$  in size; therefore, powder X-ray diffraction (PXRD) is employed as a method for sample analysis instead of single-crystal X-ray diffraction.

Table 2.1 shows the diffraction process of X-ray on a crystal. X-ray diffraction is a scattering phenomenon, since the incoming X-ray beam is scattered by the atoms in the crystals. Some of these scatterings lead to constructive interference, producing a X-ray diffraction pattern. In Figure 2.1,  $\theta$  represents the angle between the incident beam and the lattice plane, and  $d$  is the  $d$ -spacing. The Bragg's equation:

$$n\lambda = 2d \sin\theta \quad (\text{Equation 1})$$

describes the relationship between the wavelength, angle of the incident beam, and the interplanar distance.  $n$  is the order of reflection in integral values of  $\geq 1$ .<sup>1</sup> The diffractograms patterns obtained show peak intensities as a function of  $2\theta$ . The detector is placed at an angle of  $2\theta$  to collect the diffracted beams reflected at angle  $\theta$  from the crystals.

The powder X-ray diffractograms of our samples were collected on a conventional Rigaku powder diffractometer with  $\text{Co-K}\alpha$  radiation ( $\lambda = 1.7902 \text{ \AA}$ ). The range of  $2\theta$  values is from  $5^\circ$  to  $65^\circ$ .

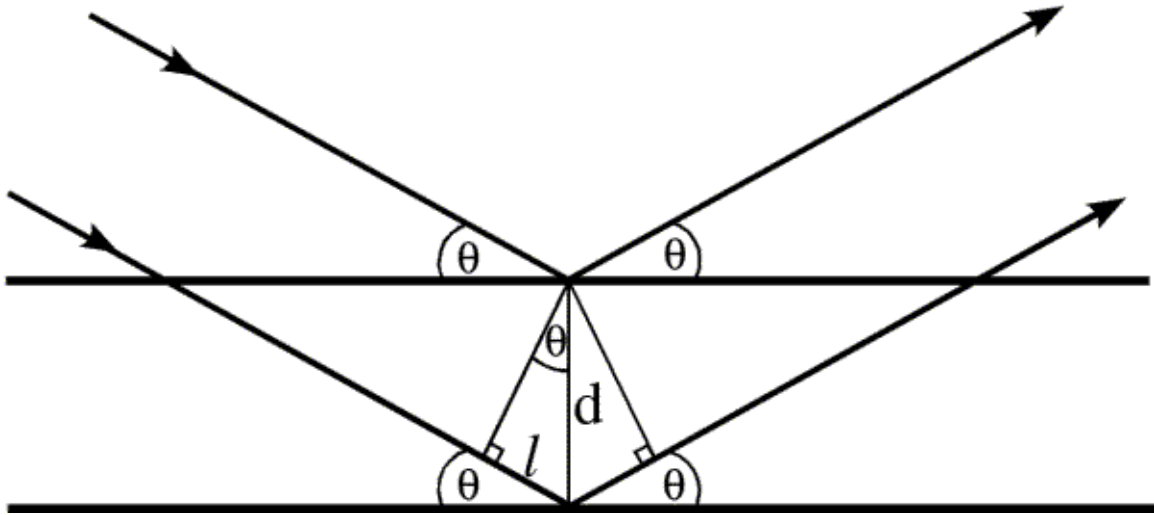


Figure 2.1 A schematic diagram showing the diffraction process of X-rays and derivation of Bragg's Law.

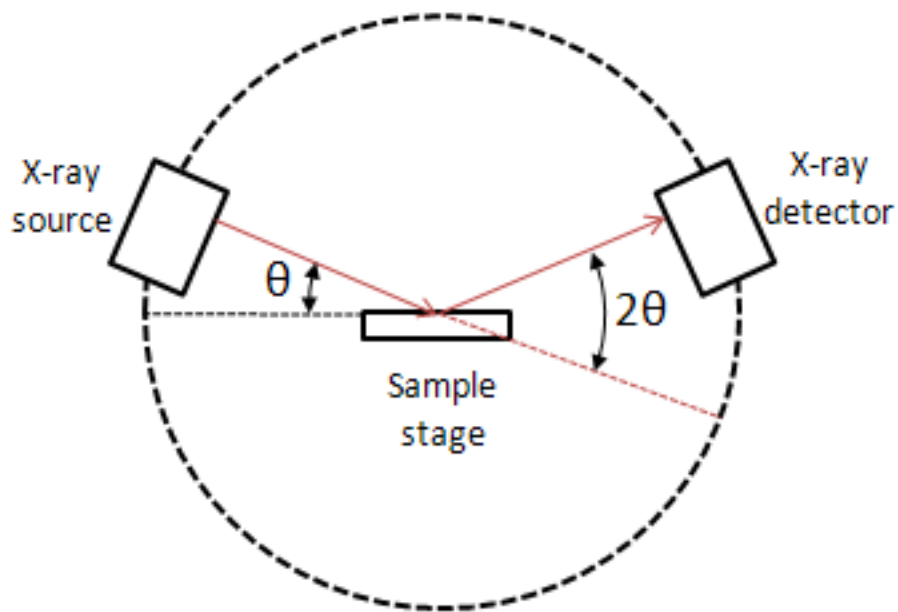


Figure 2.2 A diagram showing the arrangement of X-ray source, sample, and the detector.

## 2.2.2 Solid state nuclear magnetic resonance spectroscopy

### 2.2.2.1 Overview

Nuclear magnetic resonance (NMR) spectroscopy is a powerful analytical tool that probes the nuclear spin interactions of the nuclei directly, thus allowing the detailed information of the local chemical environments of the atoms of interest. This technique can be used for both solution and solid analyses for inorganic and organic species. However, solid state NMR (SSNMR) is much more challenging than solution NMR. In solution NMR, the molecules have free and random motions in all possible directions. These rapid motions average out the orientation dependent interactions to give the sharp isotropic peak in the solution NMR spectra. Thus, the signals observed in solution NMR are very narrow and resolved. On the other hand, in a solid sample, molecules have very restricted motions. The anisotropic or orientation dependent interactions are then observed on the NMR spectrum. Therefore, SSNMR spectra often consist of wide and unresolved peaks. Some of the main nuclear spin interactions are summarized in Table 2.1. In order to obtain structural information in solids, high-resolution NMR spectroscopic techniques must be employed. One of the mostly widely used line-narrowing technique in SSNMR is magic-angle spinning (MAS), which shall be discussed in the next.<sup>2</sup>

Table 2.1 Main nuclear spin interactions which can occur in solid.

Type of Nuclear Interaction	Magnitude (kHz)	Nature of Interaction
Zeeman interaction	$10^3$ - $10^6$	Interaction of nuclear spin with the external magnetic field
Chemical shielding	$0$ - $10^2$	The shielding effect on the nucleus of the fields produced by the surrounding electrons
J-coupling	$0$ - $10^1$	Interactions of the nuclear spins through chemical bonds
Dipolar coupling	$0$ - $10^2$	Interaction through space between two nuclear spins
Quadrupolar interaction	$0$ - $10^6$	Occurs in spin $> \frac{1}{2}$ nuclei. It is due to the interactions of the nuclear electric quadrupole moment with the non-zero electric field gradient (due to non-spherical charge distribution) around the nucleus

### 2.2.2.2 Magic-angle spinning (MAS)

Among these interactions outlined in Table 2.1, chemical shielding, dipolar coupling, and quadrupolar interactions are time dependent when the sample is being spun inside the rotor. E.R. Andrew and I.J. Lowe found that, by rotating the sample mechanically at an angle of  $54.74^\circ$  to the external magnetic field (Figure 2.3) at a rate faster than the dipolar coupling line width, the dipolar coupling will be suppressed.<sup>3</sup> By removing the dipolar coupling effect, narrow resonances consisting of the isotropic signals can be obtained, resulting in high resolution NMR spectra. Sometimes, MAS cannot completely remove the effects of chemical shielding. When the spinning rate is

less than the chemical shift anisotropy (CSA), a series spinning sidebands appears. The separations between the sidebands are equal to the spinning speed of the rotor. Therefore, by spinning the sample at two different speeds, the isotropic signals, which do not change with the spinning rate, can be identified.

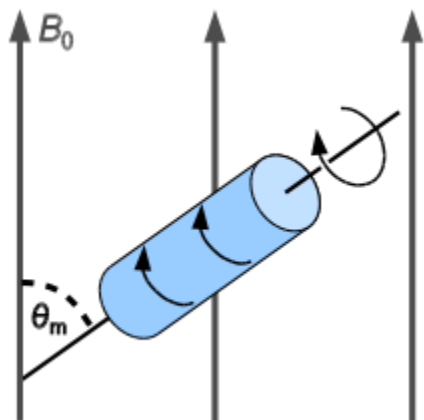


Figure 2.3 An illustration of magic-angle spinning (MAS) with the sample rotor.

### 2.2.2.3 High power proton decoupling (HPDEC)

For many dilute spin-1/2 nuclei, such as  $^{13}\text{C}$  and  $^{29}\text{Si}$ , the homonuclear coupling is usually less significant due to their low natural abundances. However, the presence of  $^1\text{H}$  can lead to severe line broadening due to the heteronuclear coupling between the dilute spin-1/2 nuclei and  $^1\text{H}$ . This heteronuclear interaction can be eliminated by applying a strong and continuous radio frequency (r.f.) field (at a frequency higher than the heteronuclear coupling interaction between the dilute and abundant spin nuclei) at the Larmor frequency of the spin abundant nuclei. This causes rapid transition of the abundant nuclei between two spin states, so the net effect on the dilute spin nuclei is zero.<sup>2</sup>

### 2.2.2.4 Cross polarization (CP)

Cross polarization (CP) is a technique that is used to improve the signal-to-noise ratio of the dilute spin nuclei by transferring the polarization from an abundant spin nucleus, such as  $^1\text{H}$ , to the dilute spin, such as  $^{13}\text{C}$ . The pulse sequence of a CP

experiment is illustrated in Figure 2.4. For CP to work, the following Hartmann-Hahn condition must be met:

$$\gamma_S B_{1S} = \gamma_I B_{1I} \quad (\text{Equation 2})$$

where  $S$  denotes the dilute spin, while  $I$  denotes the abundant spin.  $\gamma$  is the gyromagnetic ratio, which is a property of the nucleus of interest. Nuclei with low sensitivities have a low  $\gamma$ .  $B_1$  is the strength of the r.f. field. In a CP experiment, a  $90^\circ$  pulse is applied to the abundant spin. The period during which cross polarization occurs is called the contact time. The contact time needs to be set so that the r.f. field of the dilute spin is equal to the r.f. field of the abundant spin. Based on this condition, the signal-to-noise ratio of the dilute spin will be enhanced by  $\gamma_I/\gamma_S$ . Furthermore, since the abundant spins are usually strongly dipolar coupled, they tend to have a large fluctuating magnetic field, meaning that the relaxation time for the spin abundant nuclei is much shorter. Thus, in this case, one does not need to wait for the long relaxation time of the dilute spin nuclei.<sup>4-5</sup>

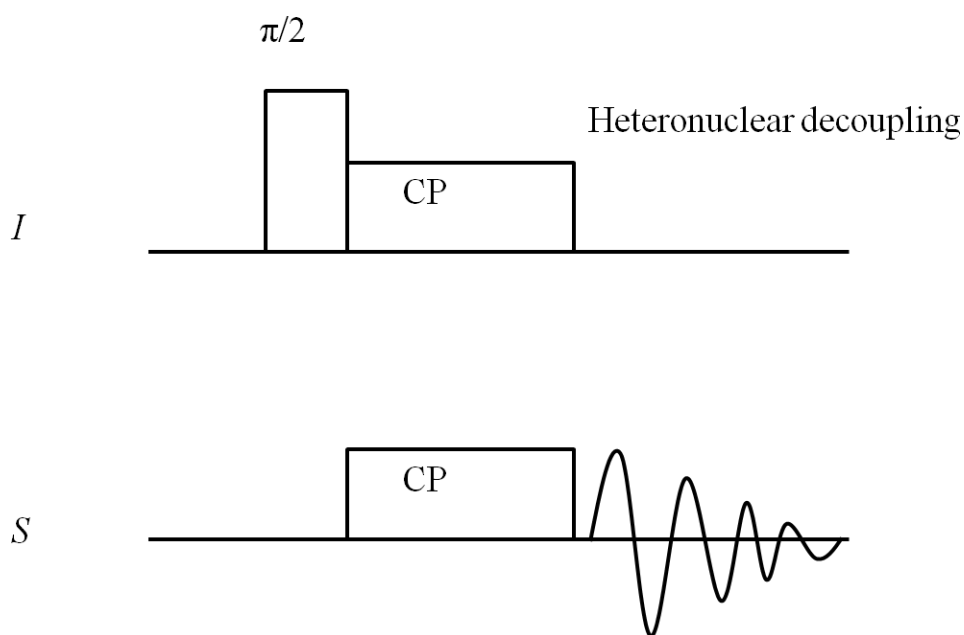


Figure 2.4 Pulse sequence of a cross-polarization experiment.



### 2.2.3 Scanning electron microscopy (SEM) and energy dispersive X-ray spectroscopy (EDX)

Scanning electron microscopy (SEM) is a characterization technique which allows the observation of three-dimensional images of a material's surface. In SEM, the area of examination of the sample is irradiated by a beam of electron which raster across the surface. As the beam of electron interacts with the surface of the material, different signals, such as backscattered electrons, X-rays, photons, and secondary electrons (electrons generated by primary irradiation), are produced. Among these, the secondary electrons produced are detected. Due to the narrowness of the electron beam, high resolution images can be produced.<sup>6</sup>

Energy dispersive X-ray spectroscopy (EDX) is a surface characterization technique which allows elemental analysis of the sample of interest. As a beam of high-energy electron is aimed at the sample surface, electrons on the inner shells of the atoms on the sample may be excited. The excited inner shell electron (secondary electron) is ejected, creating a hole, which then became filled in by an electron from a high energy shell. This results in the irradiation of an energy which has the difference between the higher energy shell and the ground state, known as X-ray. Since each element has its own atomic structure, this type of radiation is different for different elements. Therefore, by analyzing the X-ray irradiation of the sample surface, elemental identification and a semi-quantification of the elements detected can be obtained.<sup>6</sup>

For SEM images to be obtained, the surface of the specimen must be conductive. Therefore, the zeolite samples were coated with a 3 nm thick amorphous osmium using the Osmium Plasma Coater.

## 2.3 Synthesis of *N*, *N*-dipropylhexamethyleneiminium iodide (DPHMII)

*N*, *N*-dipropylhexamethyleneiminium iodide (DPHMII) is the organic SDA for zeolite ZSM-11.<sup>7</sup> 25 g of hexamethyleneimine (99%, Sigma Aldrich) was added to a stirring mixture containing 200 mL methanol (CALEDON) and 36 g of potassium bicarbonate (99.7%, Sigma Aldrich). The round bottom flask containing the reaction

mixture was put in an oil bath at a temperature of around 50 °C. 1-iodopropane (99%, Sigma Aldrich) was added dropwise to the reaction mixture. The reaction mixture was allowed to react for 72 hours, the time at which it turned dark brown. Methanol was then removed by rotary evaporation. Chloroform (CALEDON) was added to the solid; the resulting mixture was stirred for three hours. The brown liquid containing the crude was separated from the solid by suction filtration. The brown crude product was obtained by removing the solvent under vacuum. Recrystallization was performed using ethanol/2-propanol (CALEDON). The mixture was put in the freezer overnight before the crystals were recovered by suction filtration. If the resulting product is slightly yellow, it must be washed in ethyl acetate until it is completely white.

## 2.4 Synthesis of *N, N*-diethyl-3, 5-*cis*-dimethylpiperidinium iodide (DECDMPI)

*N, N*-diethyl-3, 5-*cis*-dimethylpiperidinium iodide (DECDMPI) is also an organic SDA for MEL type framework.<sup>8</sup> The preparation of DECDMPI is similar to that of DPHMII outlined in Section 2.3, except the iodoethane (99 %, Sigma Aldrich) is used instead of 1-iodopropane.

## 2.5 References

1. Bragg, W. L., *Proc. R. Soc.* **1913**, 89A, 248.
2. Ernst, M., *J. Magn. Reson.* **2003**, 162 (1), 1-34.
3. Hennel, J. W.; Klinowski, J., *Top. Curr. Chem.* **2005**, 246, 1-14.
4. Hartmann, S. R.; Hahn, E. L., *Phys. Rev.* **1962**, 128 (5), 2042.
5. Wilson, M. A.; Pugmire, R. J.; Zilm, K. W.; Goh, K. M.; Heng, S.; Grant, D. M., *Nature* **1981**, 294 (5842), 648-650.
6. Goldstein, J.; Newbury, D.; Joy, D.; Lyman, C.; Echlin, P.; Lifshin, E.; Sawyer, L.; Michael, J., *Scanning Electron Microscopy and X-Ray Microanalysis*. 3 ed.; Springer: 2003; p 1-2.
7. Fecant, A.; Bats, N. Preparation of MEL-type zeolites and their use. FR2914635A1, 2008.
8. Nakagawa, Y. Preparation of zeolite ZSM-11 using a 3,5-dimethylpiperidinium templating agent. US5645812A, 1997.

## **Chapter 3 : Tetraalkylammonium Salt/Alcohol Mixtures as Deep Eutectic Solvents (DES) for Syntheses of High-Silica Zeolites**

### **3.1 Introduction**

Zeolites are a group of silicates and aluminosilicate microporous materials that are often used in ion-exchange, catalysis, and adsorption processes. These applications were made possible due to the presence of regular internal cavities and channels of discrete sizes and shapes which are unique to each type of zeolite.<sup>1</sup> Typically, zeolite crystals are synthesized hydrothermally at 150-200 °C in a sealed steel autoclave by mixing a base, silica, water (the solvent), and an organic structure-directing agent (SDA).<sup>2</sup> Recently, a new method, ionothermal synthesis, has been developed for the preparation of aluminophosphates (AlPO<sub>4</sub>s), metal-organic frameworks (MOFs) and coordination polymers.<sup>3-19</sup>

An ionic liquid (IL) is usually defined as a salt that is fluidic at ambient temperature (<100 °C).<sup>20</sup> However, as mentioned in the previous paragraph, the reactions to make zeolites are usually conducted at temperatures higher than 100 °C. Therefore, an ionic liquid can then be defined as any salt with a melting point below the range of 150-200 °C for the purpose of our studies.<sup>3</sup> The first reported work in this area was for the preparation of aluminophosphates materials and involved the use of 1-ethyl-3-methylimidazolium bromide ([emim]Br) and urea/choline chloride deep eutectic solvents (DESs).<sup>3</sup> There are several advantages of using IL in syntheses. In this case, the IL serves as both the organic SDA and the solvent, which means the competition between solvent and the SDA for the growing crystalline materials is minimized. Also, by using ILs as the solvent, the vapour pressure is reduced significantly.<sup>21</sup> A DES, which is a mixture composed of two different salts that results in a melting point depression. In the context of synthesizing microporous framework materials, a DES can be prepared by making an alcohol/quaternary ammonium salt mixture.<sup>22</sup> To be ideal for the preparation of zeolite and zeolitic materials, the melting of such a mixture needs to be below 130 °C.

The organic SDA plays an important role in the structure formation of the zeolite framework.<sup>22</sup> Dong's group was able to prepare different types of  $\text{AlPO}_4$ s by varying the organic SDA present in the reaction mixture containing pentaerythritol.<sup>22</sup> This work has shown that  $\text{AlPO}_4$  structures can be formed under the presence of alcohol.<sup>22</sup>

While much attention has been put into the discoveries of making new framework structures using ILs, there are also interests in improving synthetic strategies used in zeolite preparation. In the past few decades, there were examples of preparing silicates and aluminosilicates in a non-aqueous environment. Bibby and Dale first reported that sodalite can be synthesized in ethylene glycol.<sup>23</sup> Reports have shown that zeolite ZSM-5 (MFI) can be prepared in the presence of ethanol,<sup>24</sup> glycerol,<sup>25</sup> and in a mixture of ethylenediamine and triethylamine.<sup>26</sup> The ZSM-39 (MTN) zeolite, which is isostructural with the  $17\text{\AA}$  cubic gas hydrate, has also been synthesized in non-aqueous conditions in morpholine and pyrrolidine/mepiquat mixture under the presence of HF.<sup>27-29</sup> These early examples have shown that zeolites can be made in a reaction mixture containing alcohol or amine species.

Although much effort has been made in zeolite preparation through non-aqueous route, the number of studies remains quite limited. As for ionothermal synthesis, there have been few reports on the study of high-silica zeolites, despite the fact that a lot of work has been done on the syntheses of zeolite-like materials. This is probably due to the poor solubility of silica in the reaction mixture in the presence of low water content, which is essential for the hydrolysis silica and the polycondensation of silicate species.<sup>30</sup> Furthermore, many syntheses of zeolites are carried at high pH in the presence of hydroxide ions.<sup>1</sup> The sources for the hydroxide ions are usually NaOH or KOH. The solubility of these species is lowered significantly in the absence or low presence of water.

According to our best knowledge, there are only three reported syntheses of zeolites using ILs. Sodalite was synthesized in 1-ethyl-3-methylimidazolium bromide ([emim]Br) under the presence of  $\text{OH}^-$  at high pH.<sup>31-32</sup> Yan's group synthesized ZSM-5 by microwave-heating a mixture formed from 1-butyl-3-methylimidazolium [Bmim]

bromide and a dry-gel precursor containing the ZSM-5 organic structure-directing agent (SDA), TPAOH.<sup>33</sup> Morris's group reported the synthesis of several siliceous zeolites in a fluoride medium by using the [Bmim] bromide/hydroxide IL. The products could be either phase-pure Silicalite-1 (MFI) or a mixture of Theta-1 (TON) and MFI.<sup>34</sup> This suggests that the presence of TPA<sup>+</sup> is important in the formation of phase-pure ZSM-5. Furthermore, for all of the cases listed above, a small amount of water must be present to ensure the successful production of zeolite materials. This indicates that water is crucial for the formation of silicate and aluminosilicate materials in IL. Furthermore, these examples also indicate that in order to have consistency in the final products, the presence of an organic SDA that is specific for the desired final framework is extremely important.

The main difficulties in generating silicate and aluminosilicate frameworks in ILs are poor solubility of starting materials and the lack of reproducible results. To overcome these problems, we have used colloidal silica and various organic SDAs which help to give the desired products. Under our experimental conditions, no extra water was added to the initial reaction mixture. All the water content in the reaction mixture came exclusively from the reactants. In this work, we demonstrated the successful syntheses of three zeolite types: ZSM-5, sodalite (SOD), and ZSM-39. The Silicalite-1 syntheses were performed in both fluoride and hydroxide media using colloidal silica as the silica source and a deep eutectic mixture composed of a template, tetrapropylammonium bromide (TPABr) or tetraethylammonium chloride (TEACl), and pentaerythritol (PE). The aluminosilicate ZSM-5 was prepared in the NaOH environment. SOD and MTN type zeolite were produced in tetramethylammonium chloride (TMACl)/1, 6-hexanediol mixture in the presence of NaOH and NH<sub>4</sub>F, respectively.

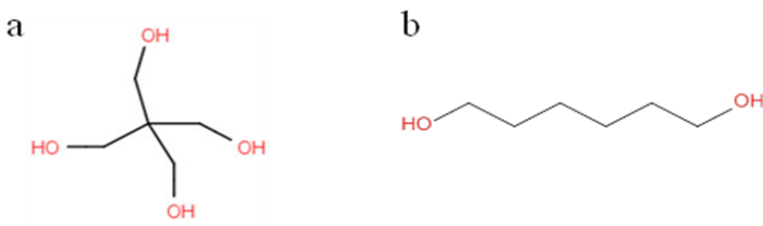


Figure 3.1 The structure of (a) pentaerythritol and (b) 1, 6-hexanediol.

## 3.2 Experimental

### 3.2.1 Syntheses of high-silica zeolites

#### **Synthesis of Silicalite-1 (MFI) using TPABr**

The typical procedure is as follows: Ammonium fluoride ( $\geq 98\%$ , Alfa Aesar), pentaerythritol (98+%, Alfa Aesar), tetrapropylammonium bromide (98%, Sigma-Aldrich), and dry as-synthesized ZSM-5 (from hydrothermal synthesis using TPABr) were mixed quantitatively and ground using a mortar and a pestle. The ground solid mixture was then transferred to a 40mL Teflon container. To this mixture, a source of colloidal silica (Ludox HS-40, Ludox CL-X, or Ludox TM-50, Sigma-Aldrich) was added. The silica contents in Ludox HS-40, Ludox CL-X, and Ludox TM-50 are 40 weight (wt.) %, 45 wt. %, and 50 wt. % suspension in  $H_2O$ , respectively. The components were hand-mixed using a spatula until a sticky white paste is formed inside the Teflon cup. The Teflon container was then placed inside a stainless steel autoclave and the reaction mixture would be heated at around 150-170 °C for 19-24 days. For instance, in one of the syntheses, 2.5 g TPABr, 3.0 g PE, 1.0 g  $NH_4F$ , and 0.05 g as-made ZSM-5 seeds were mixed and ground. 2.5 g Ludox HS-40 was then added to the ground mixture. For every 2.5 g of Ludox HS-40, there is 1.5 g of  $H_2O$ . The typical molar composition of the initial batch is:  $1SiO_2$ : 1.6  $NH_4F$ : 1.3-1.7 pentaerythritol: 0.25-0.56 TPABr: 3-5  $H_2O$ .

#### **Synthesis of aluminosilicate ZSM-5 (MFI) using TPABr**

The preparation of aluminosilicates ZSM-5 is similar to the procedures described in the previous section except the  $NH_4F$  was replaced by NaOH (99%, Caledon), and a source of aluminum was added. The sources of aluminum can be Alumina (~8%  $H_2O$ , Strem Chemicals), aluminum isopropoxide (98+%, Sigma-Aldrich), or aluminum sulphate hydrate (98%, Sigma-Aldrich). Tetrapropylammonium bromide, pentaerythritol, sodium hydroxide, an aluminum source, and 5% ZSM-5 seeds were mixed and ground using a mortar and a pestle. The ground mixture was transferred to a Teflon container and Ludox HS-40 was added. The ingredients were hand-mixed using a

spatula until a semi-transparent, mobile liquid gel was formed. The Teflon container was put inside a stainless steel autoclave. The gel would be reacted for 21-28 days at 170 °C. The typical molar composition of the initial batch is: 1 SiO<sub>2</sub>: 0.1 NaOH: 1.3-1.7 pentaerythritol: 0.56 TPABr: 0.02 Al: 5 H<sub>2</sub>O. For instance, in a synthesis that uses Al(O-*i*Pr)<sub>3</sub> as the Al source, 5.0 g Ludox HS-40 was added to a ground mixture of 5.0 g TPABr, 6.0 g PE, 0.2 g NaOH, 0.14 g Al(O-*i*Pr)<sub>3</sub>, and 0.1 g as-synthesized ZSM-5 seeds. The reagents were hand-mixed; reaction time for this batch was 25 days at 170 °C.

### **Synthesis of Silicalite-1 using TEACl**

The synthesis of ZSM-5 using tetraethylammonium chloride monohydrate (≥98.0%, Sigma Aldrich) as the template is similar to the procedures outlined in 2.2, except the template was changed to TEACl from TPABr. The mole ratios of the reagents are: 1SiO<sub>2</sub>: 1.6 NH<sub>4</sub>F: 1.3 pentaerythritol: 0.8 TEACl: 5.8 H<sub>2</sub>O.

### **Synthesis of sodalite**

The source of silica used was Ludox HS-40 (Sigma-Aldrich). The eutectic mixture was composed of tetramethylammonium chloride (TMACl, 97%, Sigma-Aldrich) and 1, 6-hexanediol (97%, Sigma-Aldrich). The reaction was performed at a temperature of 140 °C. The mineralizing agent was sodium hydroxide (99%, Caledon). Ludox HS-40 was added to the eutectic mixture, mineralizing agent, and alumina. No extra water was added. The reagents were then hand-mixed using a spatula. The mole ratios of the starting materials were 1.0 SiO<sub>2</sub>: 2.1 TMACl: 2.4 1, 6-hexanediol: 2.2 NaOH: 0.7 NaAlO<sub>2</sub>: 5.3 H<sub>2</sub>O.

### **Synthesis of ZSM-39 (MTN)**

The reagents used in the synthesis of ZSM-39 were similar to those mentioned in "**Synthesis of sodalite**", except the mineralizing agent was changed from NaOH to NH<sub>4</sub>F. In this case, ZSM-39 was synthesized instead of SOD. The mole ratios of the starting materials were 1.0 SiO<sub>2</sub>: 2.1 TMACl: 2.4 1, 6-hexanediol: 2.2 NH<sub>4</sub>F: 0.7 NaAlO<sub>2</sub>: 5.3 H<sub>2</sub>O.



## Product Isolation

The product was obtained by filtration after being three successive washes using deionized water. The filtered solid was washed with methanol several times and with deionized water again. The product was dried in the oven at 100 °C for 24 hours.

### 3.2.2 Characterization

The powder x-ray diffractograms of the products were collected on a conventional Rigaku powder diffractometer with Co-K $\alpha$  radiation ( $\lambda = 1.79 \text{ \AA}$ ). The data for the X-ray diffraction (XRD) patterns were collected from 5° to 65° of 2 $\theta$  values.

Selected samples were analyzed by SEM and EDX; these experiments were done at Western Nanofabrication Facility. A thin layer of amorphous osmium (3 nm) was coated onto the sample using the Osmium Plasma Coater. SEM and EDX experiments were performed using LEO (Zeiss) 1540XB FIB/SEM. EDX data were obtained from different spots of the sample. The Si/Al ratios for selected samples were calculated by take an average of the values of the different locations.

The solid-state NMR spectra were recorded on an Infinity Plus 400 spectrometer which has a wide-bore magnet. The  $^{79}\text{Br}$  signal from KBr was used to set the magic angle of 54.7°.  $^{13}\text{C}$  cross polarization (CP),  $^{29}\text{Si}$ ,  $^{27}\text{Al}$ , and  $^{19}\text{F}$  magic-angle spinning (MAS) NMR spectra were obtained for some of the samples. The Larmor frequencies for  $^1\text{H}$ ,  $^{29}\text{Si}$ ,  $^{27}\text{Al}$ ,  $^{19}\text{F}$  and  $^{13}\text{C}$  are 399.5, 79.4, 104.1, 375.9, and 100.5 MHz, respectively. A 7.5 mm HXY probe was used to acquire one pulse  $^{29}\text{Si}$  MAS spectra. The chemical shifts for the  $^{29}\text{Si}$  spectra were referenced to the standard tetramethylsilane (TMS,  $\delta = 0$  ppm) by using tetrakis(trimethylsilyl)silane (TTMSS) as the secondary standard. TTMSS has two peaks, one at -9.8 ppm and the other at -125.2 ppm. The resonance at -9.8 ppm was used as the reference peak. The spinning rate was 4.0 kHz. The pulse angle was 45° with a pulse delay of 60 s. The  $^{27}\text{Al}$  MAS spectra were obtained by using a 5.0 mm HFX probe with a spinning rate of 8 kHz. A pulse angle of 30° with a pulse delay of 1 s was used. The reference standard used for setting the  $^{27}\text{Al}$  NMR chemical shift was  $\text{Al}(\text{NO}_3)_3$  ( $\delta = 0$  ppm).  $^{19}\text{F}$  MAS NMR were carried out using the 4.0 mm HXY probe

with a pulse angle of  $30^\circ$  and a pulse delay of 10 s. The  $^{19}\text{F}$  shifts were referenced to  $\text{CFCl}_3$  ( $\delta = 0$  ppm) by employing  $\alpha, \alpha, \alpha$ -trifluorotoluene ( $-63.7$  ppm) as the external reference. The isotropic signal was determined by spinning the sample at two different speeds. Finally, the  $^{13}\text{C}$  CP MAS experiments were performed using the 4.0 mm HXY probe. TTMSS was used to set up the Hartmann-Hahn matching condition. The spinning speed for these samples was 10 kHz. The  $^1\text{H}$   $90^\circ$  pulse length was  $4.5\ \mu\text{s}$ . The contact time used was 2 ms, and the pulse delay was 10 s. Adamantane was used as a secondary standard to reference the  $^{13}\text{C}$  chemical shifts to TMS ( $\delta = 0$  ppm). Adamantane has two  $^{13}\text{C}$  signals at 28.8 and 38.2 ppm. The latter of the two was used as the reference peak for our samples.

### 3.3 Results and Discussion

#### 3.3.1 MFI synthesized using TPABr as the organic SDA

##### 3.3.1.1 $\text{NH}_4\text{F}$ as the mineralizing agent

Silicalite-1 was synthesized in  $\text{F}^-$  medium with  $\text{NH}_4\text{F}$  being the mineralizing agent and using 5% seeding. An experiment done in the absence of seeds produced amorphous material, indicating that the presence of seeds was necessary for the formation of the zeolites under our reaction conditions (Table 3.1, Sample A1). The growth of highly siliceous zeolites requires the hydrolysis of silica, which has a very low solubility in alcohol. This slows down the reaction rate significantly compared to the processes that occur in hydrothermal conditions containing high water content. By adding seeds to the reaction mixture increases the surface area available for the solute to adhere and become part of the solid component.

For experiments that investigate the effect of seeding, Ludox HS-40 was used as the silica source (Table 3.1, Samples A1-A4). A PXRD pattern of an as-synthesized Silicalite-1 sample prepared by using calcined MFI seeds is shown in Figure 3.2a. The mole ratios of the reagents in the initial batch were 1  $\text{SiO}_2$ : 0.7 TPABr: 1.3 PE: 1.6  $\text{NH}_4\text{F}$ : 5  $\text{H}_2\text{O}$ . The water was from the colloidal silica, and no extra water was added. When no seeds were added to the reaction mixture, there were no signs of crystallization even after 19 days at  $170^\circ\text{C}$ . When 5% (by weight) of as-synthesized ZSM-5 seeds were added,

phase-pure MFI was produced under the same condition. However, as the amounts of seeds present in the initial batch decreased, the reaction time became longer. Also, the product yields dropped significantly from 70% (5% seeding) to 20% (1% seeding). The increase of crystallization rate when seeds were present was probably due to the increase in the available surface area. Decreasing the amounts of seeds resulted in smaller surface area and less nuclei available for crystal growth, thus lowering the rate at which the solute became integrated into the solid phase from solution. This decrease in crystallization rate results in lower product yield in a given period of reaction.<sup>35</sup>

Table 3.1 Effects of seeding, amount of H<sub>2</sub>O, and TPABr:PE on ZSM-5 synthesis using the fluoride route; T = 170 °C. The PXRD patterns for the samples listed in this table are shown in Appendix A.

Sample	Type of Ludox	Amount of seeds added (wt % with respect to silica)	TPABr:PE (moles)	H <sub>2</sub> O:SiO <sub>2</sub> (moles)	Reaction time (days)	Yield (%)	Framework Type
A1	HS-40	0	0.42	5.0:1	19	0	/
A2	HS-40	5	0.42	5.0:1	19	70	MFI
A3	HS-40	3	0.42	5.0:1	21	40	MFI
A4	HS-40	1	0.42	5.0:1	21	19	MFI
B1	CL-X 45%	5	0.42	4.1:1	17	51	MFI
B2	TM-50	5	0.42	3.3:1	21	25	MFI
C1	HS-40	5	0.22	5.0:1	22	35	MFI
C2	HS-40	5	0.17	5.0:1	27	50	MFI
C3	HS-40	5	0.13	5.0:1	27	24	MFI

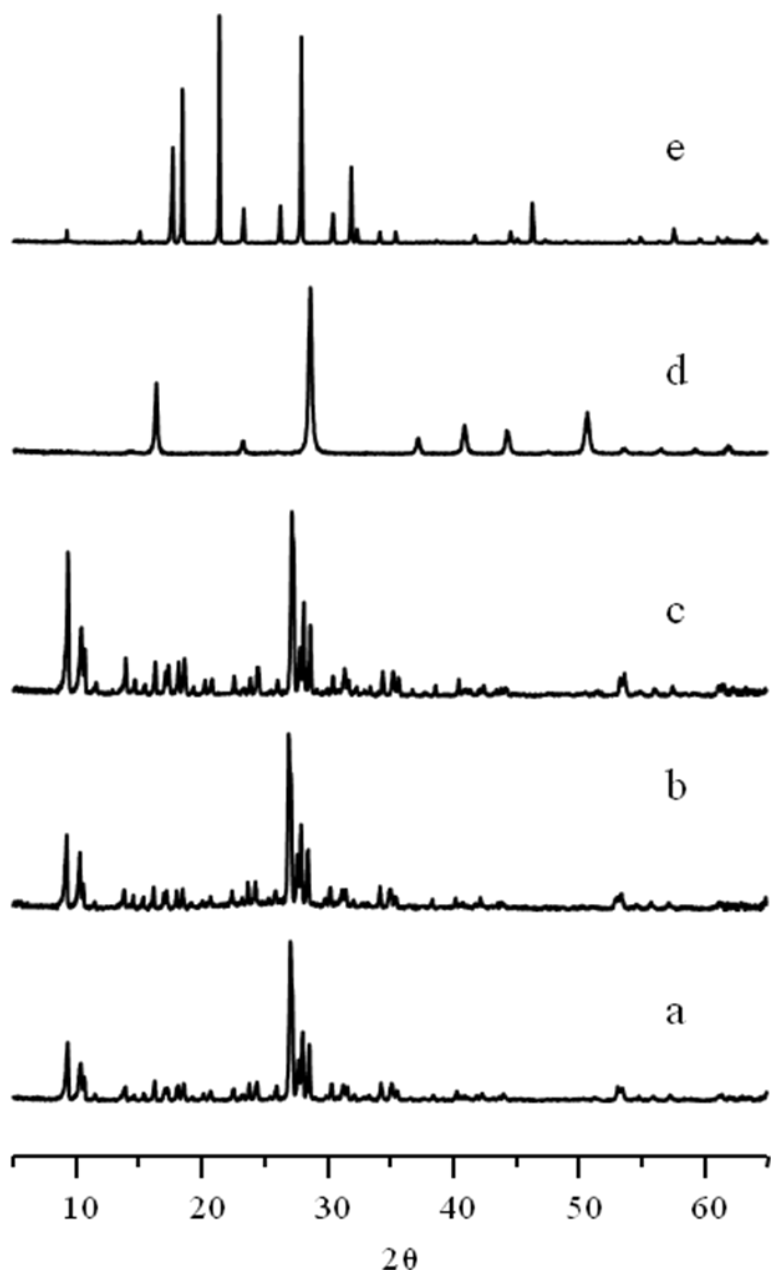


Figure 3.2 PXR D patterns of (a) Silicalite-1 using TPABr and  $\text{NH}_4\text{F}$  (A2), (b) aluminosilicate ZSM-5 synthesized in NaOH medium (D2), (c) Silicalite-1 using TEACl and  $\text{NH}_4\text{F}$  (E1), (d) Sodalite (F1), and (e) ZSM-39 (F2).

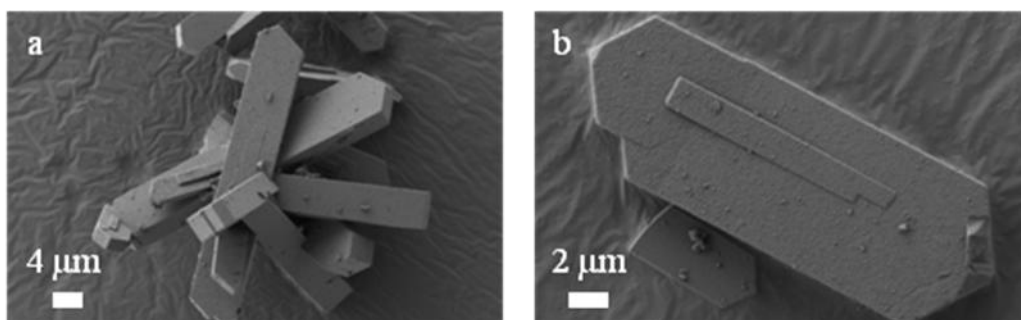


Figure 3.3 SEM images of an as-synthesized ZSM-5 using  $F^-$  as the mineralizing agent.

Figure 3.3a shows the SEM image of a sample synthesized using Ludox HS-40 and 5% calcined seeds. The crystals are long, flat needles and are heavily intergrown into each other to form a star shape. Figure 3.3b is the picture for a selected crystal, showing that it is twinned. The  $^{29}\text{Si}$  MAS NMR spectrum (Figure 3.4a) of an as-synthesized sample shows broad features that are characteristic of MFI.<sup>36</sup> The intensities of the peaks in the  $Q^4$  region (Si atoms bonded to four other Si atoms via oxygen linkages) are much higher than those in  $Q^3$  (Si atoms bonded to one  $-\text{OH}$  and three other Si atoms via oxygen linkages), the reaction was indeed complete, and the quality of the sample is very high. The as-synthesized ZSM-5 is orthorhombic and contains 12 crystallographically inequivalent tetrahedral sites (T-sites). The signals peaks shown on the  $^{29}\text{Si}$  MAS are quite broad due to the severe overlapping of these signals.<sup>37</sup>

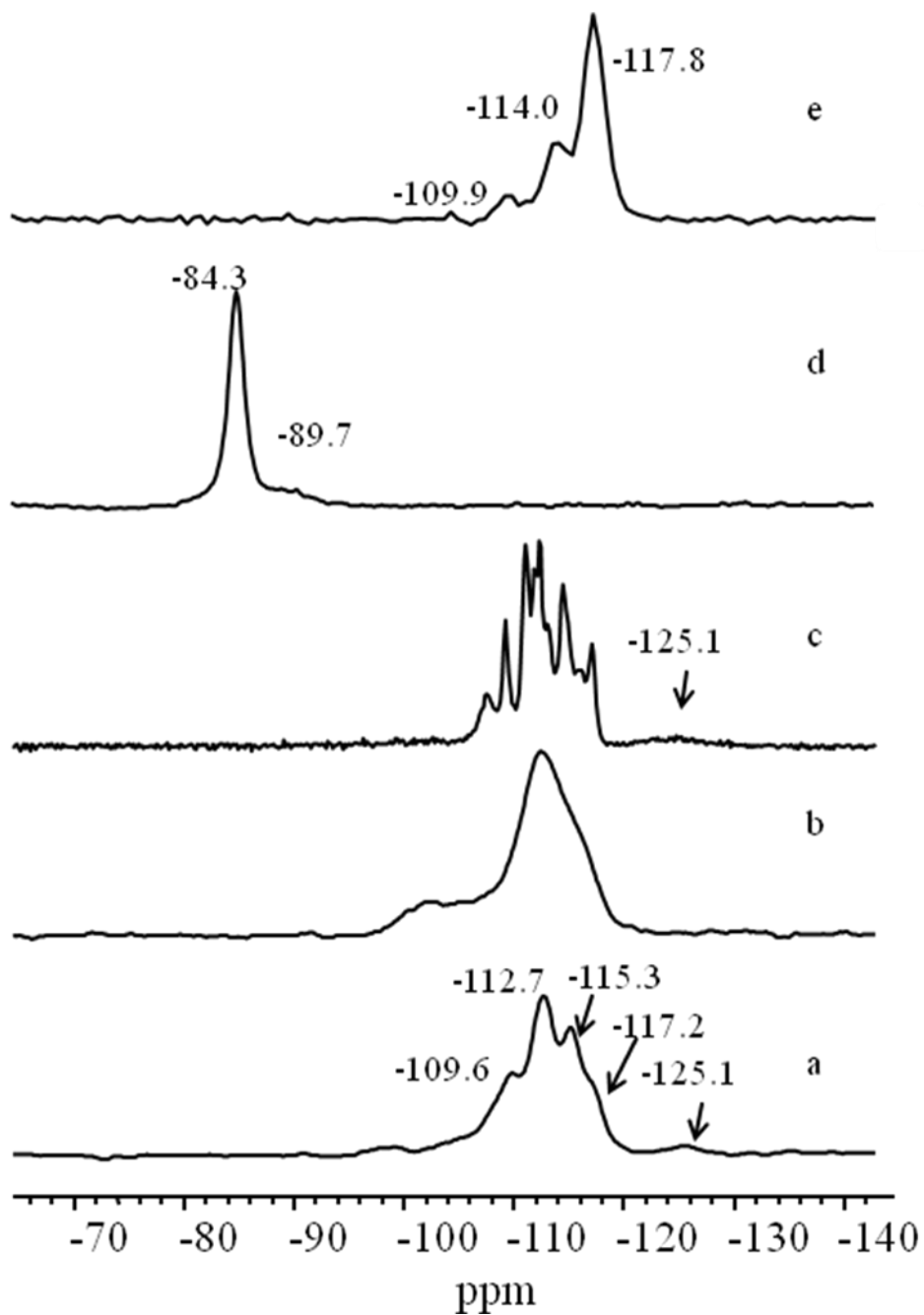


Figure 3.4  $^{29}\text{Si}$  MAS NMR spectra of (a) Silicalite-1 using TPABr and  $\text{NH}_4\text{F}$ , (b) Al-containing ZSM-5 synthesized in NaOH medium, (c) Silicalite-1 synthesized using TEACl and  $\text{NH}_4\text{F}$ , (d) Sodalite, and (e) ZSM-39.

Different types of Ludox containing different amounts of silica were used, and the results of the experiments are shown in Table 3.1 (Samples A2, B1, and B2). Ludox CL-X contains 45% SiO<sub>2</sub>. 5% seeds were added to each of the batches at the beginning of the syntheses. The mole ratios of the starting materials were 1 SiO<sub>2</sub>: 0.6 TPABr: 1.3 PE: 1.6 NH<sub>4</sub>F:  $x$  H<sub>2</sub>O, where  $x = 5.0, 4.1,$  and  $3.3$  when Ludox HS-40, Ludox CL-X, and Ludox TM-50 were used, respectively. No extra water was added to these reactions. From the table, it is apparent that when Ludox TM-50 was used, the reaction time became longer and the yield dropped significantly. This sudden drop in yield was probably due to the lack of water, resulting in the poor dissolution of reactant species in the reaction mixture.

The effect of different TPABr: PE ratios on the formation of MFI were also investigated. In most zeolite syntheses, the organic template is often quite expensive. Thus, it is necessary to use as little template as possible in order to be cost-efficient. The TPABr: PE ratio was 0.42 for most of the reactions in DES medium. The results for experiments involving lowering the TPABr: PE ratios are shown in Table 3.1 (Samples A2, C1-C3). The recovered products were phase-pure siliceous ZSM-5 in all cases. However, when the TPABr: PE ratio decreased, the reaction time became longer, and the reaction yield started to fall. The decrease in yield was probably due to less SDA available in the reaction mixture, resulting in a longer time for the ZSM-5 to form as the TPABr: PE ratio dropped. The case is slightly different in hydrothermal syntheses, where a near 100% yield could be obtained by just using 0.08 TPABr: 1 SiO<sub>2</sub>. This is because in hydrothermal synthesis, the presence of large amount of water facilitates the transport of different particle species. Therefore, high concentration of template is not required in order for zeolite to be formed in a hydrothermal environment.

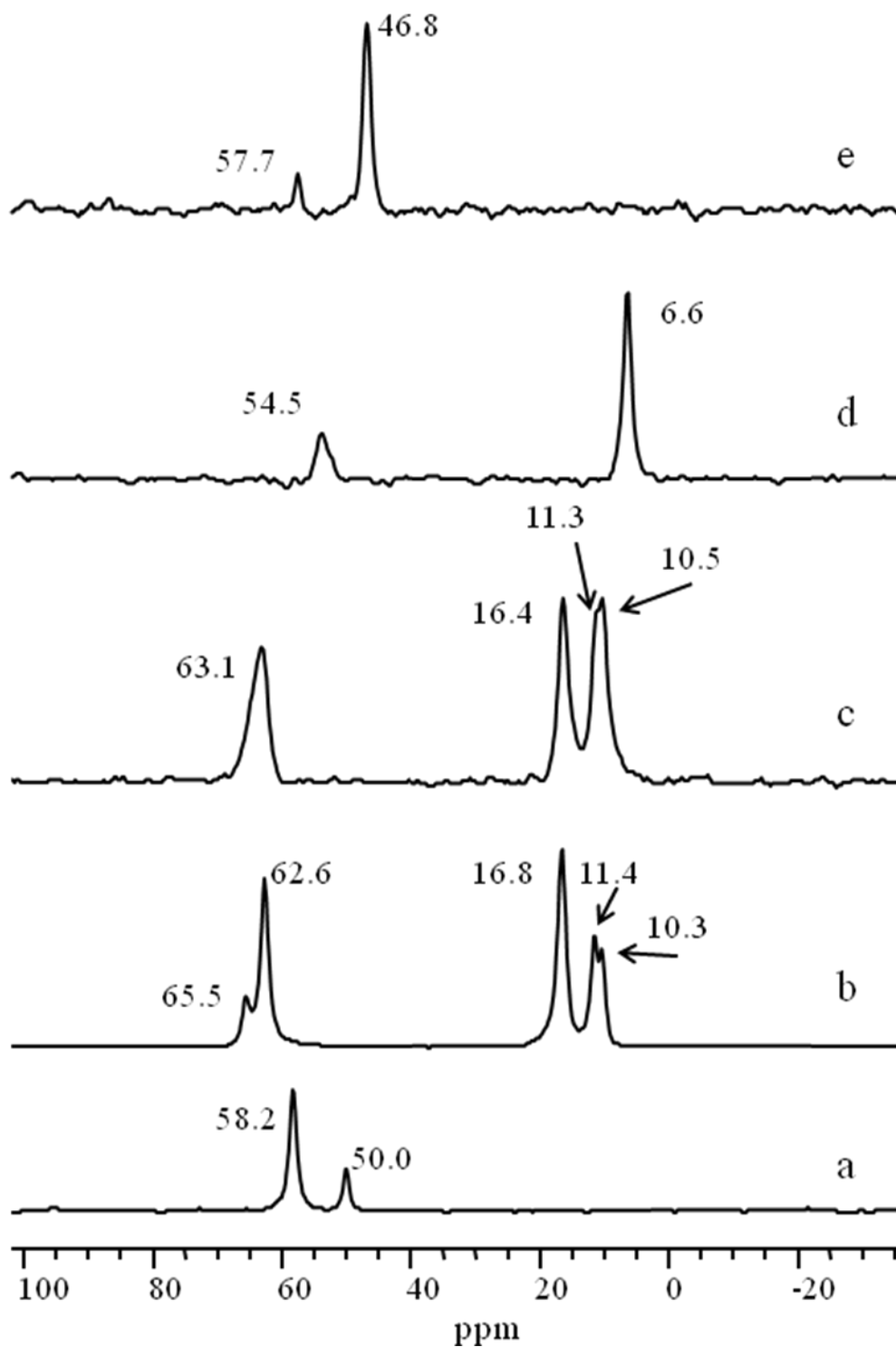


Figure 3.5  $^{13}\text{C}$  CP MAS NMR spectra of (a) pentaerythritol, (b) Silicalite-1 using TPABr and  $\text{NH}_4\text{F}$ , (c) ZSM-5 synthesized in NaOH medium, (d) Silicalite-1 using TEACl and  $\text{NH}_4\text{F}$ , and (e) ZSM-39.



From the  $^{13}\text{C}$  ( $^1\text{H} \rightarrow ^{13}\text{C}$ ) CP MAS spectrum (Figure 3.5a-b), it is clear that only  $\text{TPA}^+$  is present in the as-synthesized ZSM-5 framework. The peaks observed in MFI are due to the presence of tetrapropylammonium bromide. The chemical shifts at 63.3 ppm and 65.5 ppm signals are from the  $\alpha$ -carbons that are directly connected to the nitrogen. There are two signals, because the fluoride is closer to three of the four carbons that are directly connected to the nitrogen of  $\text{TPA}^+$ . The signal at 16.8 ppm comes from the  $\beta$ -carbon. There are two signals for the  $\gamma$ -carbons from the terminal methyl groups, one at 11.4 ppm and the other at 10.3 ppm due to the two types of channels in ZSM-5.<sup>37</sup> The presence of  $\text{TPA}^+$  ion that resides inside the channels of the zeolite was not due to the seeds added at the beginning of the synthesis, because all seeds that were used have been calcined at 350/500 °C, meaning that the organic SDAs have been removed. Furthermore, there is no signal indicating the presence of pentaerythritol inside the MFI framework synthesized under our experimental condition. It was patented that pentaerythritol was used to prepare the zeolite NU-5 (MFI framework).<sup>38</sup> Attempts to reproduce the results from the patent were not successful. The fact that  $\text{TPA}^+$  is the only organic component filling the zeolite channels indicates that the structure-directing ability of  $\text{TPA}^+$  toward the formation of MFI framework is much stronger than that of pentaerythritol.

$^{19}\text{F}$  NMR spectrum (Figure 3.6a) shows one peak at chemical shift of -65.5 ppm of the framework F<sup>-</sup>. The result agrees with previous studies of Silicalite-1 synthesized under hydrothermal conditions. The chemical shift at -65.5 ppm corresponds to F<sup>-</sup> anions that are covalently bonded to the Si atoms. In the case of MFI, the F<sup>-</sup> is jumping between two Si atoms. This is confirmed by the broad feature at 125.1 ppm on the  $^{29}\text{Si}$  MAS spectrum (Figure 3.4a).<sup>39</sup>

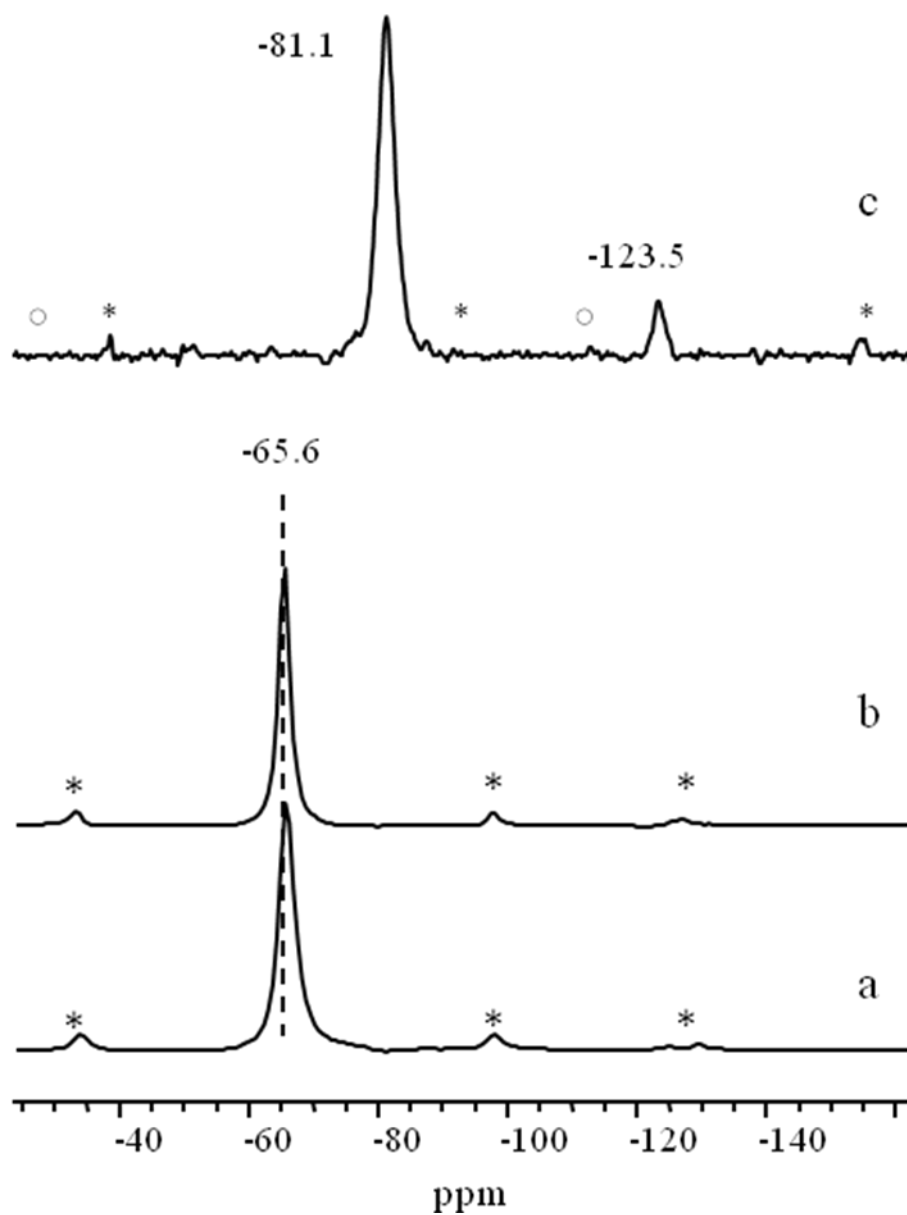


Figure 3.6  $^{19}\text{F}$  MAS NMR spectra of Silicalite-1 synthesized in  $\text{NH}_4\text{F}$  media using (a) TPABr, (b) TEACl as templates, and (c) ZSM-39. Spinning side bands are indicated by “\*”.

### 3.3.1.2 NaOH as the mineralizing agent

To obtain the aluminosilicate form of ZSM-5, syntheses containing different Al sources were performed in the presence of OH<sup>-</sup> ion. The presence of Al in MFI is important in order to obtain the HZSM-5, which is the catalytic form of the zeolite.<sup>1</sup> The initial Si: Al ratios for these samples were 50: 1. The formation of Al-containing ZSM-5 in the presence of NaOH was much slower, probably due to the poor solubility of NaOH in pentaerythritol, as indicated by the longer reaction times and decrease in yields in Table 3.2. The PXRD pattern of an as-synthesized aluminosilicate ZSM-5 in the NaOH medium is shown on Figure 3.2b. The SEM images of these samples show the twinning typical of MFI crystals Figure 3.7. The <sup>29</sup>Si MAS spectrum in Figure 3.4b shows the Q<sup>4</sup> with peaks severely overlapped and some Q<sup>3</sup> due to the presence of defect sites. There are more Q<sup>3</sup> sites in the aluminosilicate MFI than in the siliceous form, because the presence of Al creates more –OH groups in the zeolite structure. Due to the absence of F<sup>-</sup> in the framework, only one signal is observed for the α-carbon atoms that are directly connected to the nitrogen of TPA<sup>+</sup> (Figure 3.5b).<sup>37</sup> The <sup>27</sup>Al MAS spectra for samples prepared using different Al sources are shown in Figure 3.8a-c. The peak at 52.4 ppm represents tetrahedral framework Al, while the resonance at 10.6 ppm represents octahedral Al. EDX data were taken for the samples to determine the Si/Al in the samples. The Si/Al ratios for as-made samples synthesized using Al(O-*i*Pr)<sub>3</sub>, NaAlO<sub>2</sub>, and Al<sub>2</sub>(SO<sub>4</sub>)<sub>3</sub> are 91, 116, and 90. The Si/Al ratios are averages obtained by taking data on different crystals in the sample. We would like to point out that depending on the site the data were taken, the Si/Al can differ significantly. There are two reasons for this. First, the distribution of aluminum is not very uniform. Second, EDX is a surface analysis technique and is only semi-quantitative. For our samples, according to the EDX data, the Si/Al ratios are in the range of 90-115, which is common quite common for the ZSM-5 synthesized hydrothermally.<sup>1</sup>

Table 3.2 ZSM-5 samples synthesized using different Al sources in the presence of NaOH; T = 170 °C. The PXRD patterns of the samples listed in this table are shown in Appendix B.

Sample	Type of Ludox	Al Source	Initial Si:Al	Amount of seeds added (wt % with respect to silica)	TPABr:PE (moles)	H <sub>2</sub> O:SiO <sub>2</sub> (moles)	Reaction time (days)	Yield (%)	Framework Type
D1	HS-40	Al <sub>2</sub> (SO <sub>4</sub> ) <sub>3</sub>	50	5	0.42	5.0:1	28	64	MFI
D2	HS-40	NaAlO <sub>2</sub>	50	5	0.42	5.0:1	28	57	MFI
D3	HS-40	Al(O- <i>i</i> Pr) <sub>3</sub>	50	5	0.42	5.0:1	28	52	MFI

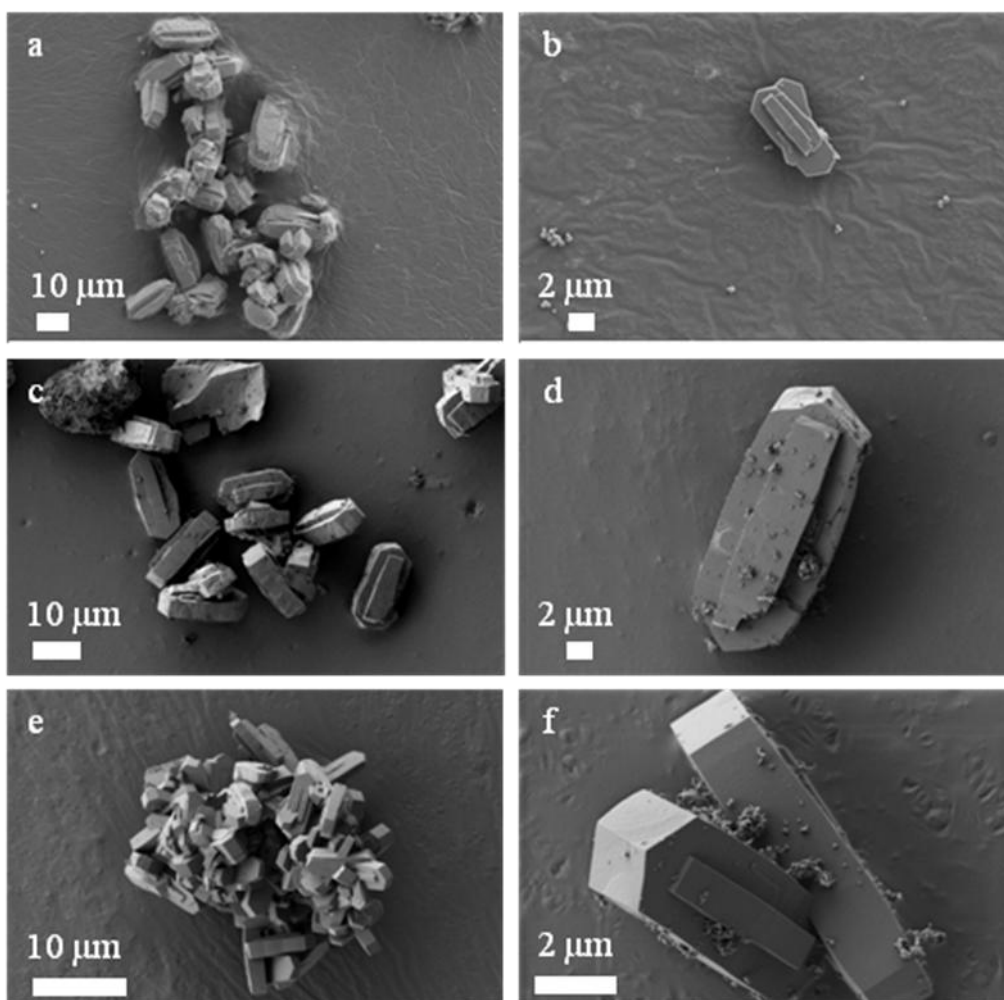


Figure 3.7 SEM images of ZSM-5 samples synthesized using (a-b) Al(O-*i*Pr)<sub>3</sub>, (c-d) NaAlO<sub>2</sub>, and (e-f) Al<sub>2</sub>(SO<sub>4</sub>)<sub>3</sub> as Al sources.

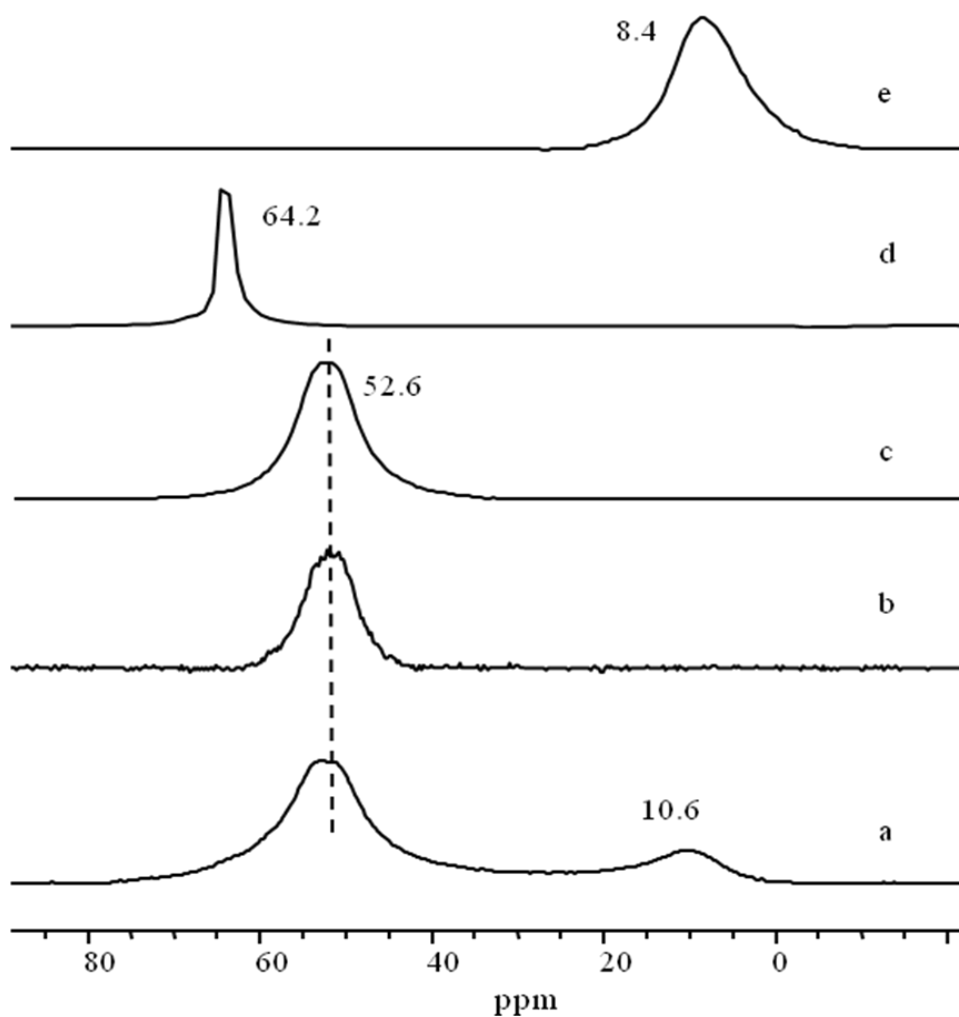


Figure 3.8  $^{27}\text{Al}$  MAS NMR spectra of ZSM-5 (a-c) synthesized in NaOH media using (a)  $\text{Al}(\text{O}-i\text{Pr})_3$ , (b)  $\text{NaAlO}_2$ , (c)  $\text{Al}_2(\text{SO}_4)_3$  as Al sources, (d) sodalite, and (e) ZSM-39.

### 3.3.2 Attempts to synthesize other zeolites using different DES

#### 3.3.2.1 TEACl/pentaerythritol

$\text{TEA}^+$  is known to be a template for MFI.<sup>40</sup> Therefore, not surprisingly, ZSM-5 was produced in a 1: 1 (by weight) TEACl/1, 6-hexanediol mixture in the presence of F<sup>-</sup>. It is worth noting that these reactions were also seeded with calcined ZSM-5 to promote crystallization. The PXRD pattern shows the as-made sample is MFI (Figure 3.2c). The composition of the reaction mixture is given in Table 3.3. The sample where MFI was produced when calcined ZSM-5 was used shows that the crystallization of ZSM-5 is not

promoted by the TPABr in the seed crystals. The SEM images of the sample (Figure 3.9a) show heavily intergrown crystals. However, in this case, the crystals exhibit cubic shape topology with pyramidal at each of the two ends Figure 3.9b. However, it is noted that when TEACl was used instead of TPABr, the reaction time was longer, and the product yield was lower, indicating that the structure-directing effect of TPABr is stronger than that of TEACl. The  $^{13}\text{C}$  CP MAS spectrum indicates that TEACl is present in the as-synthesized zeolite framework (Figure 3.5d). The  $^{29}\text{Si}$  MAS spectrum of an as-synthesized sample contains well-resolved peaks (Figure 3.4d), revealing high crystallinity of the sample. Connectivities between the different T-sites are shown in Figure 3.10a. An expanded version of the  $^{29}\text{Si}$  MAS spectrum is shown in Figure 3.10b, with all the T-sites assigned according to a previous study done by Fyfe *et al.*<sup>41</sup> The  $^{19}\text{F}$  chemical shift is the same as what was observed in the MFI synthesized using TPABr as the template (Figure 3.6b), meaning that the  $\text{F}^-$  is also covalently bonded to the framework silicon atoms. The broad resonance at -125.1 ppm of the  $^{29}\text{Si}$  MAS spectrum indicates that the  $\text{F}^-$  is hopping between the two Si-9 atoms.<sup>41</sup>

Table 3.3 Silicalite-1 sample synthesized using TEACl as the template; T = 170 °C.

Sample	Mole Ratios of Starting Materials						Seeds (5%)	Reaction Time (days)	Yield (%)	Framework Type
	$\text{SiO}_2$	$\text{TEACl}\cdot\text{H}_2\text{O}$	TPABr	PE	$\text{NH}_4\text{F}$	$\text{H}_2\text{O}$ (from starting materials)				
E1	1	0.82	0	1.32	1.62	5.82	Calcined	22	56	MFI

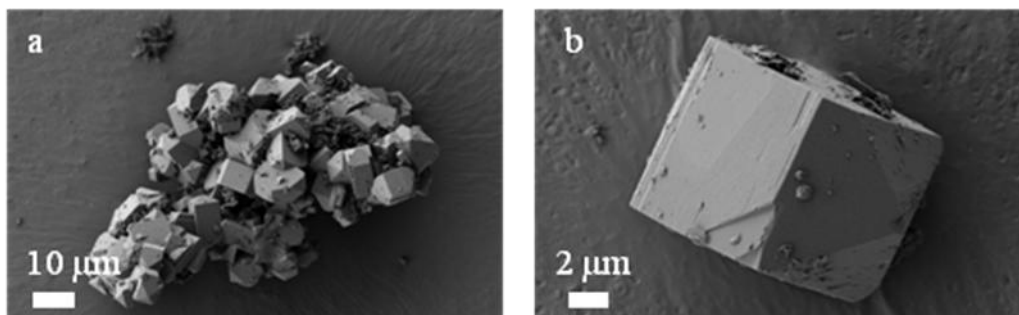


Figure 3.9 SEM images of as-synthesized ZSM-5 using TEACl as the organic SDA.

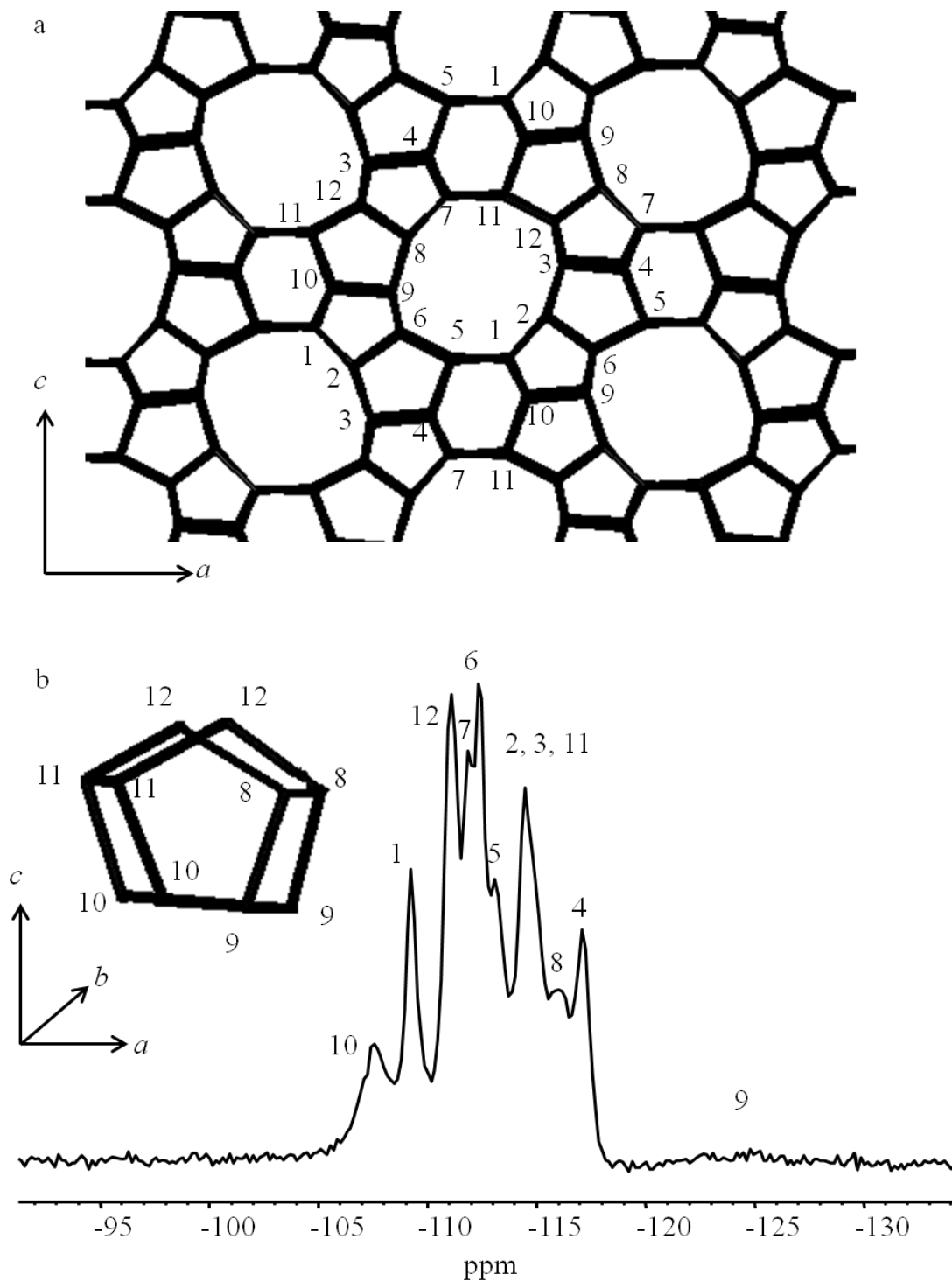


Figure 3.10 (a) Framework of MFI viewed down axis-b; all T-sites are numbered. (b)  $^{29}\text{Si}$  MAS spectrum of as-made MFI using TEACl as the template. The numbers above the peaks correspond to the different T-sites. A small section of the framework showing neighboring Si-9 atoms.

### 3.3.2.2 Sodalite (SOD) and ZSM-39 (MTN)

A DES containing the tetramethylammonium chloride (TMACl) and 1, 6-hexanediol was prepared. The mineralizing agent used in this case was NaOH. Reactions using TMACl/1, 6-hexanediol (m.p. = 39.0-53.1 °C) were conducted at 140 °C. The results of the experiments are summarized in Table 3.4. Sodalite product showing sharp peaks on PXRD was produced (Figure 3.2d), indicating high crystallinity of the sample. SEM images of sodalite shows large aggregations of solid materials consisting of small round balls and cubes (Figure 3.11a-b). TMA<sup>+</sup> is known to occupy the cages in high-silica SOD (Si/Al = 4.7).<sup>42</sup> On the other hand, in our case, no organic species is present inside the channels of the as-made sodalite sample, because no signal was observed during the <sup>13</sup>C NMR experiment. The <sup>27</sup>Al NMR (Figure 3.8d) shows a single peak at 64.2 ppm, corresponding to the tetrahedral Al in the sodalite framework.<sup>43</sup> The <sup>29</sup>Si MAS spectrum (Figure 3.4d) shows a strong peak at -83.4 ppm, corresponding to the Si atoms bonded to four Al atoms via oxygen (Si-4Al).<sup>44</sup> The relatively weak signal at 89.7 ppm is assigned to Si atoms bonded to one Si and three Al atoms via oxygen (Si-3Al).<sup>45</sup> The EDX data of our sodalite sample reveals the Si/Al ratio to be around 1.1. This is different from the case of the high-silica sodalite containing the framework TMA<sup>+</sup> ions. In the case where TMA<sup>+</sup> ions are trapped inside the sodalite cages, there are three different signals on the <sup>29</sup>Si MAS spectrum due to the presence of Si-0Al, Si-1Al, and Si-2Al.<sup>42</sup>

Table 3.4 Mole ratios of SOD and MTN samples synthesized using TMACl as the template; T = 140 °C. M. I. = mineralizing agent

Sample	SiO <sub>2</sub>	NaAlO <sub>2</sub>	TMACl	1, 6-hexanediol	NaOH/NH <sub>4</sub> F	M. I.	H <sub>2</sub> O	Seeds	Time (days)	Yield (%)	Framework
F1	1	0.7	2.1	2.4	NaOH	2.2	5.3	0	18	65	SOD
F2	1	0.7	2.1	2.4	NH <sub>4</sub> F	2.2	5.3	0	18	100	MTN

By changing the mineralizing agent from NaOH to NH<sub>4</sub>F, the product of the reaction became ZSM-39 (MTN). The PXRD pattern is shown in Figure 3.2e. Big crystals in the shape of dodecahedron with dimensions of 100 × 100 μm could be



obtained when the reaction was allowed to proceed for 14 days (Figure 3.11c-d). The  $^{29}\text{Si}$  NMR spectrum of a MTN sample is shown in Figure 3.4e, indicating the presence of three crystallographically distinct sites with ratios of 1: 4: 12.<sup>46</sup> There is only one peak for octahedral Al at 8.4 ppm on the  $^{27}\text{Al}$  MAS spectrum. The lack of signal for tetrahedral Al means that there is no framework Al present (Figure 3.8e). In other words, the ZSM-39 synthesized under such conditions is completely siliceous. The change in the mineralizing agent from  $\text{OH}^-$  to  $\text{F}^-$  caused a change in the framework of the products being formed. The lack of Al in the framework could be due to the formation of  $\text{AlF}_6^{3-}$ .<sup>47</sup> There have been previous studies reporting the synthesis of ZSM-39 in fluoride medium.<sup>48-49</sup> There are two peaks in the  $^{19}\text{F}$  MAS NMR, one at -81.3 ppm and the other is at -123.4 ppm (Figure 3.6c). The -123.4 ppm is assigned to the tetraalkylammonium fluoride species, while the resonance at -81.3 ppm is assigned to the  $\text{F}^-$  anions inside the framework. Unlike the MFI structure, these  $\text{F}^-$  atoms are not covalently bound to the Si atoms.<sup>50</sup> This can also be shown by the lack of a weak but broad signal in the range of -120 to -130 ppm in the  $^{29}\text{Si}$  MAS spectrum. The  $^{13}\text{C}$  CP MAS spectrum (Figure 3.5e) shows signals for two types of organic molecules inside the framework. The signal at 57.7 ppm is due to the tetramethylammonium ( $\text{TMA}^+$ ) ions, while the resonance at 46.8 indicates the presence of trimethylammonium ( $\text{TMAM}^+$ ) species which is the result of the decomposition of  $\text{TMA}^+$ .<sup>51</sup> There are two types of cages in ZSM-39. These organic cations reside in the larger cage which is about 7.5 Å in size.<sup>52</sup> The presence of these  $\text{TMA}^+$  ions inside the zeolite shows that, under our experimental conditions,  $\text{TMA}^+$  has a structure-directing effect toward the formation of MTN type frameworks using  $\text{F}^-$  as the mineralizing agent. Preliminary results for the mechanistic study of the crystallization process of ZSM-39 in  $\text{TMACl}/1$ , 6-hexanediol will be discussed in greater detail in Chapter 5.

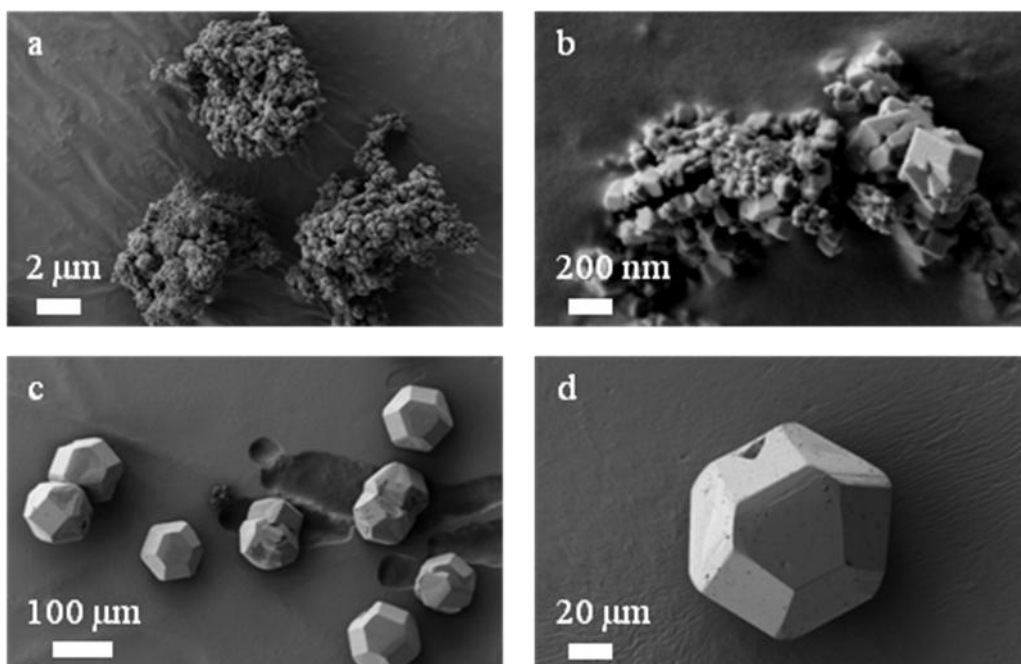


Figure 3.11 SEM images of as-made (a-b) sodalite, and (c-d) ZSM-39.

### 3.4 Conclusions

In conclusion, our experiments present the syntheses of phase-pure high-silica materials in an ionic liquid environment. More specifically, this study shows that the use of a tetraalkylammonium/alcohol DES is not limited for the syntheses of zeolite-like materials. ZSM-5 can be synthesized by using the seeding method in both  $F^-$  and  $OH^-$  media. Furthermore, in the  $OH^-$  medium, Al can be integrated into the MFI framework in the presence of  $OH^-$ . The integration of Al into the zeolite framework allows the formation of aluminosilicate which can then be turned into the catalytically active form. In the case where  $TMA^+$  is the template, SOD and MTN type zeolites can be prepared without seeding in the presence of  $OH^-$  and  $F^-$ , respectively. By using an organic SDA as part of the DES, the reproducibility of the phase purity of the final products is attained. Furthermore, other types of zeolites with different framework topologies can be made by using various organic SDA.

### 3.5 References:

1. Bekkum, H. v.; Jacobs, P. A.; Flanigen, E. M.; Jansen, J. C., *Introduction to Zeolite Science and Practice*. 2001.
2. Dyer, A., *An introduction to zeolite molecular sieves*. J. Wiley & Sons: 1988.
3. Cooper, E. R.; Andrews, C. D.; Wheatley, P. S.; Webb, P. B.; Wormald, P.; Morris, R. E., *Nature* **2004**, *430*, 1012-1016.
4. Cooper, E. R.; Andrews, C. D.; Wheatley, P. S.; Webb, P. B.; Wormald, P.; Morris, R. E., *Stud. Surf. Sci. Catal.* **2005**, *158*, 247-254.
5. Parnham, E. R.; Drylie, E. A.; Wheatley, P. S.; Slawin, A. M. Z.; Morris, R. E., *Angew. Chem. Int. Ed.* **2006**, *45*, 4962-4966.
6. Parnham, E. R.; Morris, R. E., *Chem. Mater.* **2006**, *2006* (18), 4882-4887.
7. Parnham, E. R.; Morris, R. E., *J. Mater. Chem.* **2006**, *16*, 3682-3684.
8. Parnham, E. R.; Wheatley, P. S.; Morris, R. E., *Chem. Commun.* **2006**, 380-382.
9. Xu, Y. P.; Tian, Z. J.; Wang, S. J.; Hu, Y.; Wang, L.; Wang, B. C.; Ma, Y. C.; Hou, L.; Yu, J. Y.; Lin, L. W., *Angew. Chem. Int. Ed.* **2006**, *45*, 3965-3970.
10. Chen, S. M.; Zhang, J.; Bu, X. H., *Inorg. Chem.* **2008**, *47*, 5567-5569.
11. Hogben, T.; Douthwaite, R. E.; Gillie, L. J.; Whitwood, A. C., *Cryst. Eng. Comm.* **2006**, *8*, 866-868.
12. Ji, W. J.; Zhai, Q. G.; Hu, M. C.; Li, S. N.; Jiang, Y. C.; Wang, Y., *Inorg. Chem. Commun.* **2008**, *11*, 1455-1458.
13. Liao, J. H.; Huang, W. C., *Inorg. Chem. Commun.* **2006**, *9*, 1227-1231.
14. Liao, J. H.; Wu, P. C.; Bai, Y. H., *Inorg. Chem. Commun.* **2005**, *8*, 390-392.
15. Liao, J. H.; Wu, P. C.; Huang, W. C., *Cryst. Growth Des.* **2006**, *6*, 1062-1063.
16. Lin, Z. J.; Li, Y.; Slawin, A. M. Z.; Morris, R. E., *Dalton T.* **2008**, 3989-33994.
17. Shi, F. N.; Trindade, T.; Rocha, J.; Paz, F. A. A., *Cryst. Growth. Des.* **2008**, *8*, 3917-3920.
18. Xu, L.; Choi, E. Y.; Kwon, Y. U., *Inorg. Chem.* **2007**, *46*, 10670-10680.
19. Zhang, J.; Chen, S. M.; Bu, X. H., *Angew. Chem. Int. Ed.* **2008**, *47*, 5434-5437.

20. Rogers, R. D.; Seddon, K. R., *Science* **2003**, *302*, 792-793.
21. Luo, H. M.; Baker, G. A.; Dai, S., *J. Phys. Chem. B* **2008**, *112*, 10077-10081.
22. Liu, L.; Li, X. P.; Xu, H.; Li, J. P.; Lin, Z.; Dong, J. X., *Dalton T.* **2009**, (47), 10418-10421.
23. Bibby, D. M.; Baxter, N. I.; Granttaylor, D.; Parker, L. M., *ACS Symp. Ser.* **1989**, *398*, 209-220.
24. Uguina, M. A.; Delucas, A.; Ruiz, F.; Serrano, D. P., *Ind. Eng. Chem. Res.* **1995**, *34* (2), 451-456.
25. Kanno, N.; Miyake, M.; Sato, M., *Zeolites* **1994**, *14* (8), 625-628.
26. Xu, W. Y.; Li, J. Q.; Li, W. Y.; Zhang, H. M.; Liang, B. C., *Zeolites* **1989**, *9* (6), 468-473.
27. Schlenker, J. L.; Dwyer, F. G.; Jenkins, E. E.; Rohrbaugh, W. J.; Kokotailo, G. T.; Meier, W. M., *Nature* **1981**, *294* (5839), 340-342.
28. Shi, Q.; Yu, J. Y.; Liu, L.; Li, J. P.; Dong, J. X., *Shiyou Xuebao, Shiyou Jiagong* **2008**, *24*, 185-187.
29. Xu, H. K., Y.; Liu, L.; Li, J.P.; Wang, J.G.; Dong, J.X., *Acta Petrol. Sin.* **2006**, *22*, 153-155.
30. Brinker, C., *J. Non-Cryst. Solids* **1988**, *100* (1-3), 31-50.
31. Ma, Y. C.; Xu, Y. P.; Wang, S. J.; Wang, B. C.; Tian, Z. J.; Yu, J. Y.; Lin, L. W., *Chem. J. Chinese. U.* **2006**, *27* (4), 739-741.
32. Ma, Y. C.; Wang, S. J.; Song, Y. L.; Xu, Y. P.; Tian, Z. J.; Yu, J. Y.; Lin, L. W., *Chinese. J. Inorg. Chem.* **2010**, *26* (11), 1923-1926.
33. Cai, R.; Liu, Y.; Gu, S.; Yan, Y. S., *J. Am. Chem. Soc.* **2010**, *132* (37), 12776-12777.
34. Wheatley, P. S.; Allan, P. K.; Teat, S. J.; Ashbrook, S. E.; Morris, R. E., *Chem. Sci.* **2010**, *1* (4), 483-487.
35. Ramsharan, S.; Prabir, D., MFI. In *Handbook of Zeolite Science and Technology*, CRC Press: 2003.
36. Chang, C. D.; Bell, A. T., *Catal. Lett.* **1991**, *8*, 305-316.
37. Chézeau, J.-M.; Delmotte, L.; Guth, J.-L.; Soulard, M., *Zeolites* **1989**, *9* (1), 78-80.

38. Whittam, T. V. Zeolites. EP54386A1, 1982.
39. Koller, H.; Wolker, A.; Eckert, H.; Panz, C.; Behrens, P., *Angew. Chem. Int. Ed.* **1997**, *36* (24), 2823-2825.
40. Lok, B. M.; Cannan, T. R.; Messina, C. A., *Zeolites* **1983**, *3* (4), 282-291.
41. Fyfe, C. A.; Brouwer, D. H.; Lewis, A. R.; Chézeau, J.-M., *J. Am. Chem. Soc.* **2001**, *123* (28), 6882-6891.
42. Jarman, R. H., *J. Chem. Soc., Chem. Commun.* **1983**, (9), 512-513.
43. Lambregts, M. J.; Frank, S. M., *J. Am. Ceram. Soc.* **2005**, *88* (8), 2255-2261.
44. Newsam, J. M., *J. Phys. Chem.* **1987**, *91* (5), 1259-1262.
45. Klinowski, J.; Thomas, J. M.; Fyfe, C. A.; Hartman, J. S., *J. Phys. Chem.* **1981**, *85* (18), 2590-2594.
46. Fyfe, C. A.; Gies, H.; Feng, Y., *J. Am. Chem. Soc.* **1989**, *111* (20), 7702-7707.
47. Robson, H.; Lillerud, K. P., *Verified Syntheses of Zeolitic Materials*. 2nd ed.; 2001.
48. Zhao, D. Q.; Qiu, S. L.; Ding, H.; Pang, W. Q., *Chem. J. Chinese. U.* **1992**, *13* (11), 1358-1360.
49. Millar, D. M.; Garces, J. M. In *Synthesis of crystalline porous solids in ammonia*, Materials Research Society: 1999; pp 1535-1542.
50. Zones, S. I.; Darton, R. J.; Morris, R.; Hwang, S. J., *J. Phys. Chem. B* **2005**, *109* (1), 652-661.
51. Dewaele, N.; Gabelica, Z.; Bodart, P.; Nagy, J. B.; Giordano, G.; Derouane, E. G., GEL Composition Versus Organic Directing Agent Effects in the Synthesis of ZSM-39, ZSM-48 and ZSM-50 Zeolites. In *Studies in Surface Science and Catalysis*, Grobet, P. J.; Mortier, W. J.; Vansant, E. F.; Schulz-Ekloff, G., Eds. Elsevier: 1988; Vol. Volume 37, pp 65-73.
52. Gies, H., *Z. Kristallogr.* **1984**, *167* (1-2), 73-82.

## **Chapter 4 : Ionothermal Synthesis of High-Silica Zeolites in Urea/Choline Chloride Deep Eutectic Solvent (DES)**

### 4.1 Introduction

Zeolites, which contains a framework made up of tetrahedral alumina and silica, are extremely important in industries for their roles in catalysis, ion-exchanges processes, and adsorptions processes.<sup>1</sup> Much effort has been put in for the investigations in different synthetic routes in order to discover new types of zeolite or zeolite-like microporous materials. A series of materials, such as the aluminophosphates (AlPO<sub>4</sub>s), metal-organic frameworks (MOFs) and coordination polymers have been made in the past few years using the ionothermal syntheses.<sup>2-18</sup>

An ionothermal synthesis is a reaction in which an ionic liquid (IL) is used. The ILs used in the preparation of zeolite or zeolitic materials need have a melting point below the range of 150-200 °C, the temperature range at which zeolites and zeolitic materials are usually made.<sup>18</sup> 1-ethyl-3-methylimidazolium bromide ([emim]Br) and urea/choline chloride are very common ILs that are used in the synthesis of AlPO<sub>4</sub>. Among these two species, urea/choline chloride is classified as a special class of IL, the deep eutectic solvent (DES). A DES is an IL consisting of two components; the end result is that the melting point of the mixture consisting of the combined species will be lowered. As for the urea/choline chloride mixture, at a 2: 1 ratio, a freezing point of 21 °C can be achieved.<sup>19</sup>

One of the main advantages of using IL in syntheses of zeolite-like materials is that the IL can act as both the solvent and the organic structure-directing agent (SDA). Ideally, this would lower the competition for the SDA between the solvent and the growing framework during crystallization.<sup>18</sup> Indeed, a lot of work has been done on the syntheses of zeolite-like materials in ionic liquids. Nevertheless, the number of reports on the study of high-silica zeolites remains quite limited, mainly due to the poor solubility of silica in the ILs. Furthermore, ionothermal synthetic conditions usually

contain very little amount of water, which plays crucial roles in the dissolution of reactant species and the condensation steps of the framework formation.<sup>20</sup> For the examples of the ionothermal syntheses of zeolites discussed below, water must be added to the initial reaction mixture to ensure the formation of zeolite frameworks.<sup>21-24</sup> An example of a zeolite prepared ionothermally would be sodalite (SOD), which was made in the presence of the [emim]Br IL and hydroxide as the mineralizing agent.<sup>21-22</sup> Later on, it was found that zeolite ZSM-5 (MFI) can be made in 1-butyl-3-methylimidazolium [Bmim] bromide using microwave-heating.<sup>24</sup> Tetrapropylammonium hydroxide (TPAOH), which is an organic SDA for MFI, was added to the reaction mixture to allow for the crystallization of MFI. More recently, siliceous zeolites were made in the [Bmim] bromide/hydroxide IL by adding HF to the starting mixture.<sup>23</sup> Under this reaction condition, phase-pure Silicalite-1 or a mixture of Theta-1 (TON) and MFI could be synthesized.<sup>23</sup> These findings are extremely important for several reasons. First, they set the first examples showing that high-silica zeolites can be produced in an ionothermal environment. Also, the presence of water is essential for the reactions to take place. Finally, an organic SDA needs to be added in order to produce phase-pure materials free of any intergrowths and to reproduce the experimental results.

In the previous chapter, we investigated the synthesis of phase-pure high-silica zeolites in tetraalkylammonium salt/alcohol DES mixture. A disadvantage of this system is the high content of the organic SDA that needs to be added in order to lower the melting point of the DES. Some of the organic SDAs can be expensive and takes long time to synthesized,. However, this problem can be solved by adding a small amount of organic SDA to another DES. The organic SDA in this case must have a strong structure-directing effect, so that only a small amount is needed for the synthesis to occur. Also, the structure-directing abilities of the components of the DES must be minimized so that they cannot compete with the organic SDA to allow the formation different framework types. This chapter will focus on the preparation of high-silica zeolites with different topologies by using different organic SDAs. We will show that ZSM-5, ZSM-11 (MEL), Zeolite Beta (BEA), and ZSM-39 (MTN) can be synthesized in a 2:1 mole ratio of the urea/choline chloride ionic liquid. Among these, the preparation of ZSM-5 and BEA required the presence of 5% calcined seeds, while the other reactions are non-

seeded. All syntheses were performed using fluoride as the mineralizing agent. MFI, MEL, and MTN were prepared using colloidal silica as the silica source, while the silica source for BEA is fumed silica. The organic SDAs used to synthesize MFI, MTN, and BEA are tetrapropylammonium bromide (TPABr), tetramethylammonium chloride (TMACl), and tetraethylammonium hydroxide (TEAOH), respectively. The synthesis of MEL was tried under two different conditions using different organic SDA: *N, N*-dipropylhexamethyleneiminium iodide (DPHMII) and *N, N*-diethyl-3, 5-dimethylpiperidinium iodide (DECDMPI) (Figure 4.1). 5% of calcined siliceous ZSM-11 was added to the initial reaction mixture for the synthesis involving DECDMPI. All as-synthesized materials are phase-pure. Furthermore, it should be noted that under our experimental conditions, no extra water was added to the initial reaction mixture, and that the water content in the reaction comes from the silica and TEAOH, exclusively.

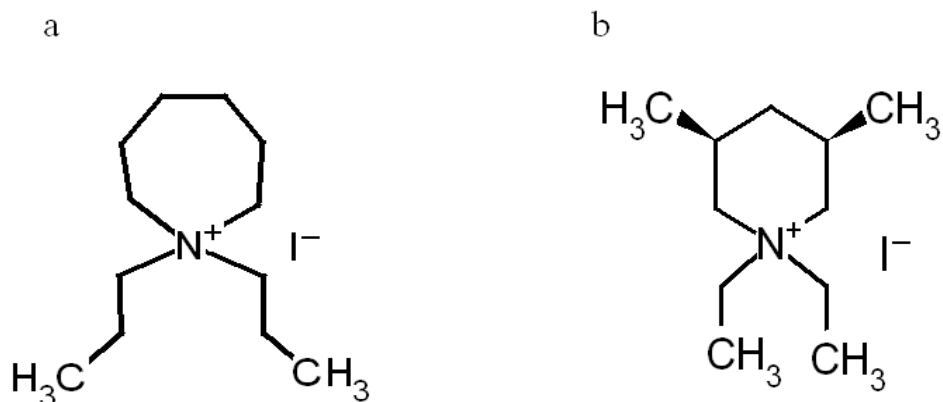


Figure 4.1 organic SDAs used for syntheses of ZSM-11: (a) *N, N*-dipropylhexamethyleneiminium iodide (DPHMII), and (b) *N, N*-diethyl-3,5-dimethylpiperidinium iodide (DECDMPI)

## 4.2 Experimental

### 4.2.1 Syntheses of high-silica zeolites

All reactions were performed in stainless steel autoclaves that are placed in an oven with a temperature of 140 °C unless otherwise stated. The amount of colloidal silica Ludox HS-40 added to each reaction batch was 2.5 g.



### **Urea/Choline Chloride Mixture**

The 2:1 mole ratio of urea/choline chloride mixture is made by mixing urea (99.0-100.5%, Sigma-Aldrich) and choline chloride ( $\geq 98.0\%$ , Sigma-Aldrich). The SEM images were taken using a LEO (ZEISS) 1530 Field Emission Microscope.

### **Synthesis of Siliceous ZSM-5 Zeolites (Silicalite-1)**

The typical procedure is as follows: Ammonium fluoride ( $\geq 98\%$ , Alfa Aesar), tetrapropylammonium bromide (98%, Sigma-Aldrich), and dry calcined ZSM-5 (from hydrothermal synthesis using TPABr) were mixed together with urea and choline chloride quantitatively and ground using a mortar and a pestle. The ground solid mixture was then transferred to a 40 mL Teflon container. To this mixture, a source of colloidal silica, (Ludox HS-40, Sigma-Aldrich) was added. The components were hand-mixed using a spatula until a sticky white paste is formed inside the Teflon cup. The Teflon container was then placed inside a stainless steel autoclave and the reaction mixture would be heated at around  $140\text{ }^{\circ}\text{C}$  for 19-26 days. For every 2.5 g of Ludox HS-40 (colloidal silica that is 40%  $\text{SiO}_2$  and 60%  $\text{H}_2\text{O}$ ), 0.36 g TPABr, 1.9 g urea, 2.2 g choline chloride, 0.62 g  $\text{NH}_4\text{F}$ , and 0.05 g calcined MFI seeds were mixed and ground. Ludox HS-40 was then added to the ground mixture. Each 2.5 g of Ludox HS-40 contains 1.0 g  $\text{SiO}_2$  and 1.5 g  $\text{H}_2\text{O}$ . The typical molar composition of the initial batch is: 1.0  $\text{SiO}_2$ : 1.0  $\text{NH}_4\text{F}$ : 0.08 TPABr: 1.9 urea: 0.95 choline chloride: 5.0  $\text{H}_2\text{O}$ . The final weight of the zeolite produced from was 0.56 g for 2.5 g of Ludox HS-40 in the initial reaction mixture.

### **Synthesis of Zeolite Beta**

In the synthesis of BEA, tetraethylammonium hydroxide (40.0%, Sigma Aldrich) was used as the SDA, and fumed silica (AEROSIL®300, Degussa) was used instead of Ludox HS-40. Seeding was performed by using 0.05 g of dry calcined BEA. The mole ratios of the reaction mixture are 1.0  $\text{SiO}_2$ : 0.5 TEAOH: 1.9 urea: 1.0 choline chloride: 1.0  $\text{NH}_4\text{F}$ : 6.4  $\text{H}_2\text{O}$ . The reaction time ranged from 10-14 days. 1.1 g of zeolite Beta was obtained after the reaction was finished.

### **Synthesis of ZSM-11 (MEL)**

The preparation is similar to those in the synthesis of Silicalite-1. The DPHMII, which was prepared according to Fecant and Bais.<sup>25</sup> The other template, DECDMPI was synthesized according to Nakagawa.<sup>26</sup> The reaction was performed at a temperature of 140 °C; no seeds were added when DPHMII was used. 5% of calcined siliceous ZSM-11 was used in the case of DECDMPI. The mole ratios of the starting materials were 1.0 SiO<sub>2</sub>: 0.08 organic SDA (DPHMII or DECDMPI): 1.9 urea: 1.0 choline chloride: 1.6 NH<sub>4</sub>F: 5.0 H<sub>2</sub>O. Phase-pure MEL was formed after 24 days. 0.8 g and 1.0 g of ZSM-11 were produced when DPHMII and DECDMPI were used as the organic SDA, respectively.

### **Synthesis of ZSM-39 (MTN)**

The preparation is similar to those in the synthesis of Silicalite-1. The SDA used in this case was tetramethylammonium chloride (97%, Sigma-Aldrich). The mole ratios of the starting materials were 1.0 SiO<sub>2</sub>: 1.0 TMACl: 1.9 urea: 1.0 choline chloride: 1.0 NH<sub>4</sub>F: 5.0 H<sub>2</sub>O. The reaction time was 14 days at a temperature of 170 °C. 1.0 g of ZSM-39 was produced when the reaction was completed.

### **Isolation of Product**

The product was obtained by filtration after being three successive washes using deionized water. The filtered solid was washed 5 times with methanol ( $\geq 98\%$ , CALEDON) and 3 times with deionized water again. The product was dried in the oven at 100°C for 24 hours.

#### **4.2.2 Characterization**

The powder X-ray diffractograms of the products were collected on a conventional Rigaku powder diffractometer with Co-K $\alpha$  radiation ( $\lambda = 1.79 \text{ \AA}$ ). The data for the powder X-ray diffraction (PXRD) patterns were collected from 5° to 65° of 2 $\theta$  values.

The solid-state NMR spectra were recorded on an Infinity Plus 400 wide-bore magnet spectrometer. The magic angle of  $54.7^\circ$  was set by the  $^{79}\text{Br}$  signal from KBr.  $^{13}\text{C}$  cross polarization (CP),  $^{29}\text{Si}$ ,  $^{27}\text{Al}$ , and  $^{19}\text{F}$  magic-angle spinning (MAS) NMR spectra were obtained for selected samples. The  $^1\text{H}$ ,  $^{29}\text{Si}$ ,  $^{27}\text{Al}$ ,  $^{19}\text{F}$  and  $^{13}\text{C}$  Larmor frequencies of the spectrometer are 399.5, 79.4, 104.1, 375.9, and 100.5 MHz, respectively.  $^{29}\text{Si}$  one pulse and CP MAS spectra were performed using a 7.5 mm HXY probe. The chemical shifts for the  $^{29}\text{Si}$  spectra were referenced to the standard tetramethylsilane (TMS,  $\delta = 0$  ppm) by using tetrakis(trimethylsilyl)silane (TTMSS) as the secondary standard, which has two peaks, one at -9.8 ppm and the other at -125.2 ppm. The -9.8 ppm signal was used as the reference peak. The spinning rate was 4.0 kHz. The pulse angle was  $30^\circ$  with a pulse delay of 30 s. The  $^{27}\text{Al}$  MAS spectra were collected by using a 5.0 mm HFX probe with a spinning rate of 8 kHz. A pulse angle of  $30^\circ$  with a pulse delay of 1 s was used. The  $^{27}\text{Al}$  NMR chemical shifts were referenced to  $\text{Al}(\text{NO}_3)_3$  (0 ppm) of 1M concentration.  $^{19}\text{F}$  MAS NMR were carried out using the 4.0 mm HXY probe with a pulse angle of  $30^\circ$  and a pulse delay of 10 s. The  $^{19}\text{F}$  shifts were referenced to  $\text{CFCl}_3$ , (0 ppm) by using  $\alpha, \alpha, \alpha$ -trifluorotoluene (-63.7 ppm) as the external reference. The isotropic signals in the  $^{19}\text{F}$  spectra were determined by spinning the sample at two different speeds. Finally, the  $^{13}\text{C}$  CP MAS experiments were performed using the 4.0 mm HXY probe. The Hartmann-Hahn condition was determined on adamantane. The spinning speed for these samples was 10 kHz. The  $^1\text{H}$   $90^\circ$  pulse length was  $4.5 \mu\text{s}$  for the  $^{13}\text{C}$  CP experiments. The contact time was 2 ms, and the pulse delay was 10 s. Adamantane was used as a secondary standard to reference the  $^{13}\text{C}$  chemical shifts to TMS (0 ppm). Adamantane has two  $^{13}\text{C}$  signals at 28.8 and 38.2 ppm. The reference was set by using the signal at 38.2 ppm.

## 4.3 Results and Discussion

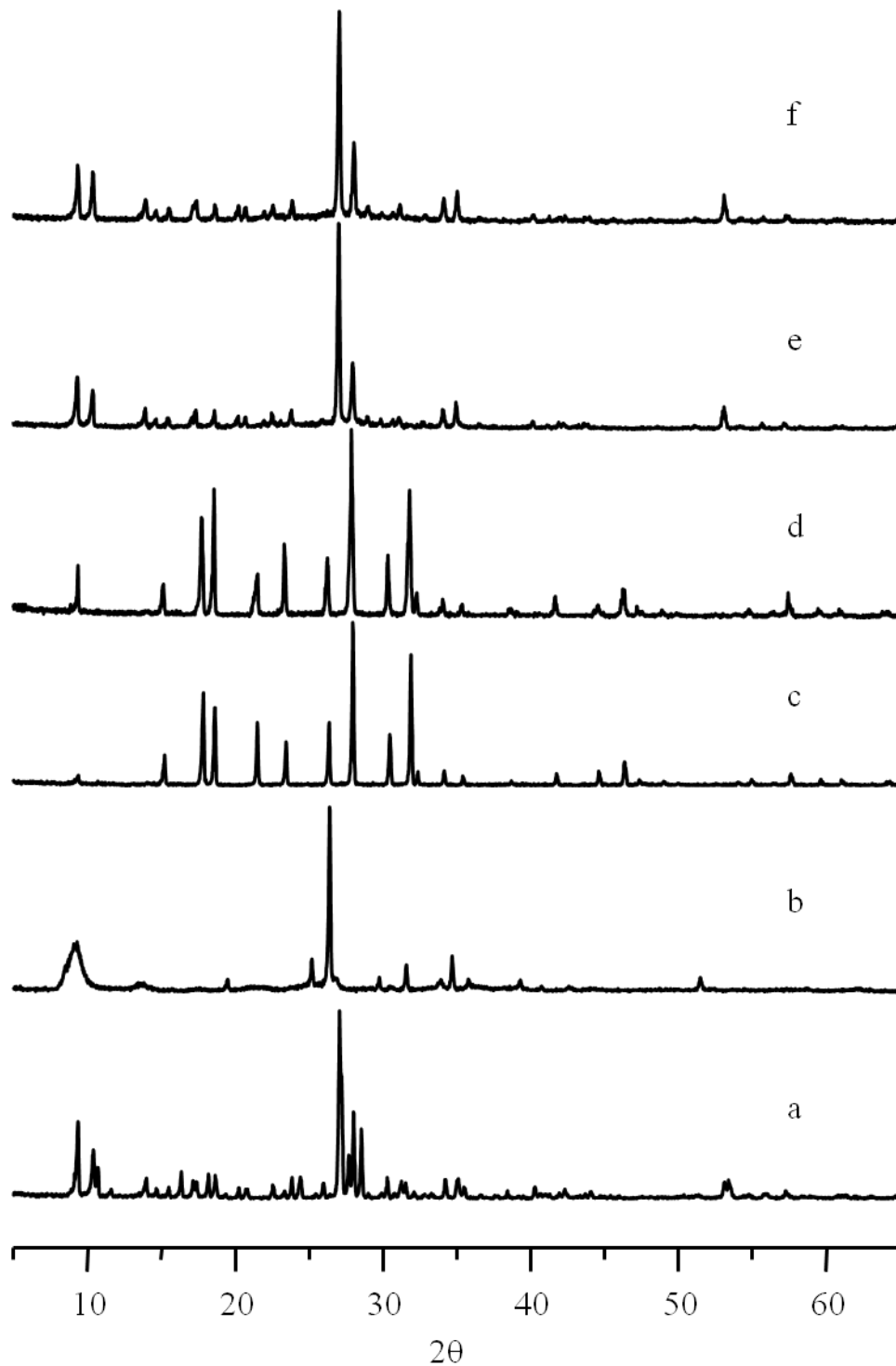


Figure 4.2 PXRD patterns of as-synthesized (A.S.) (a) MFI, (b) BEA, (c) MTN from  $\text{TMA}^+$ , (d) MTN from DPHMII, and (e) MEL from DPHMII, (f) MEL from DECDMPI.

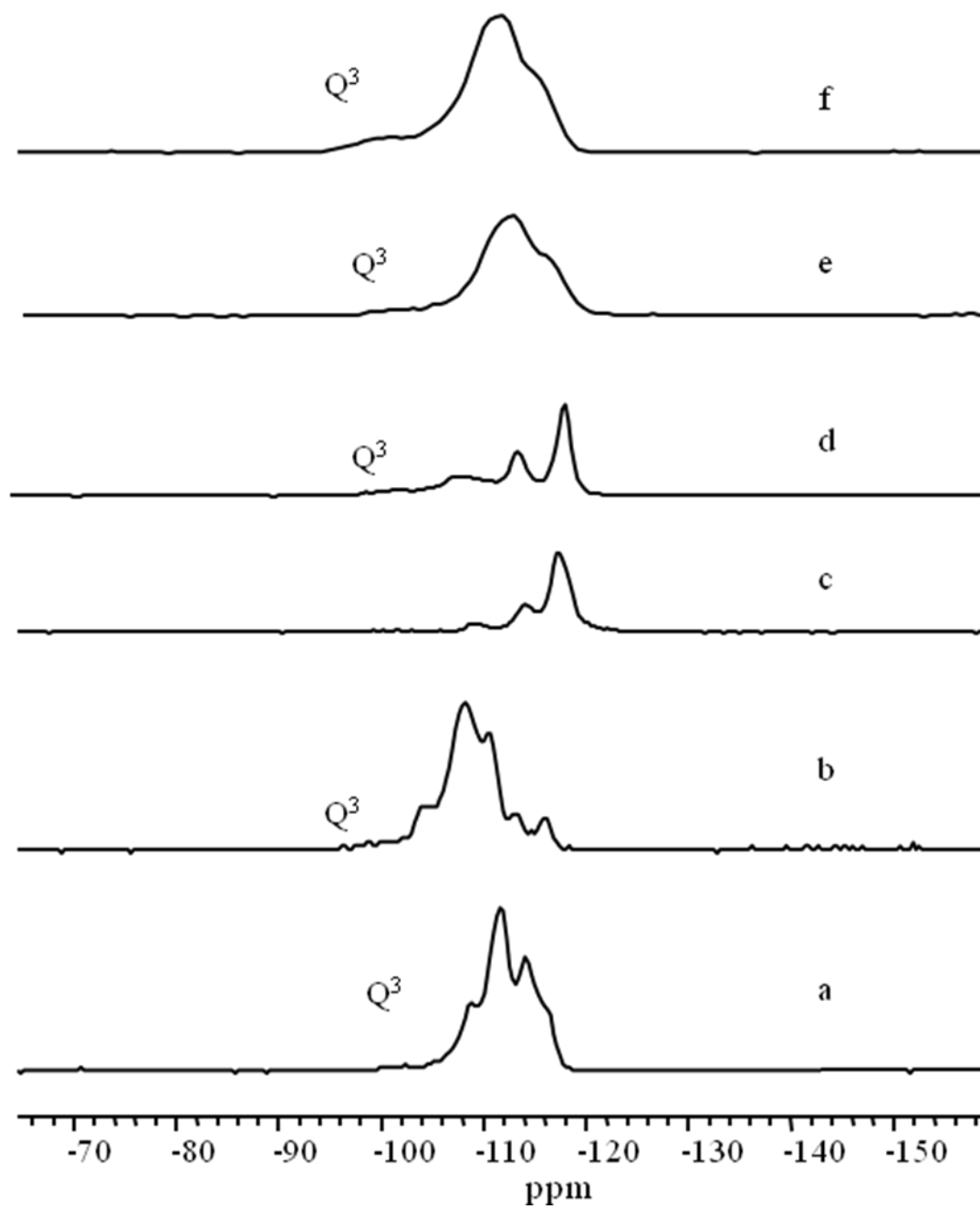


Figure 4.3  $^{29}\text{Si}$  MAS spectra of as-synthesized (a) MFI, (b) BEA, (c) MTN from TMACl, (d) MTN from DPHMII, (e) MEL from DPHMII, and (f) MEL from DECDMPI.

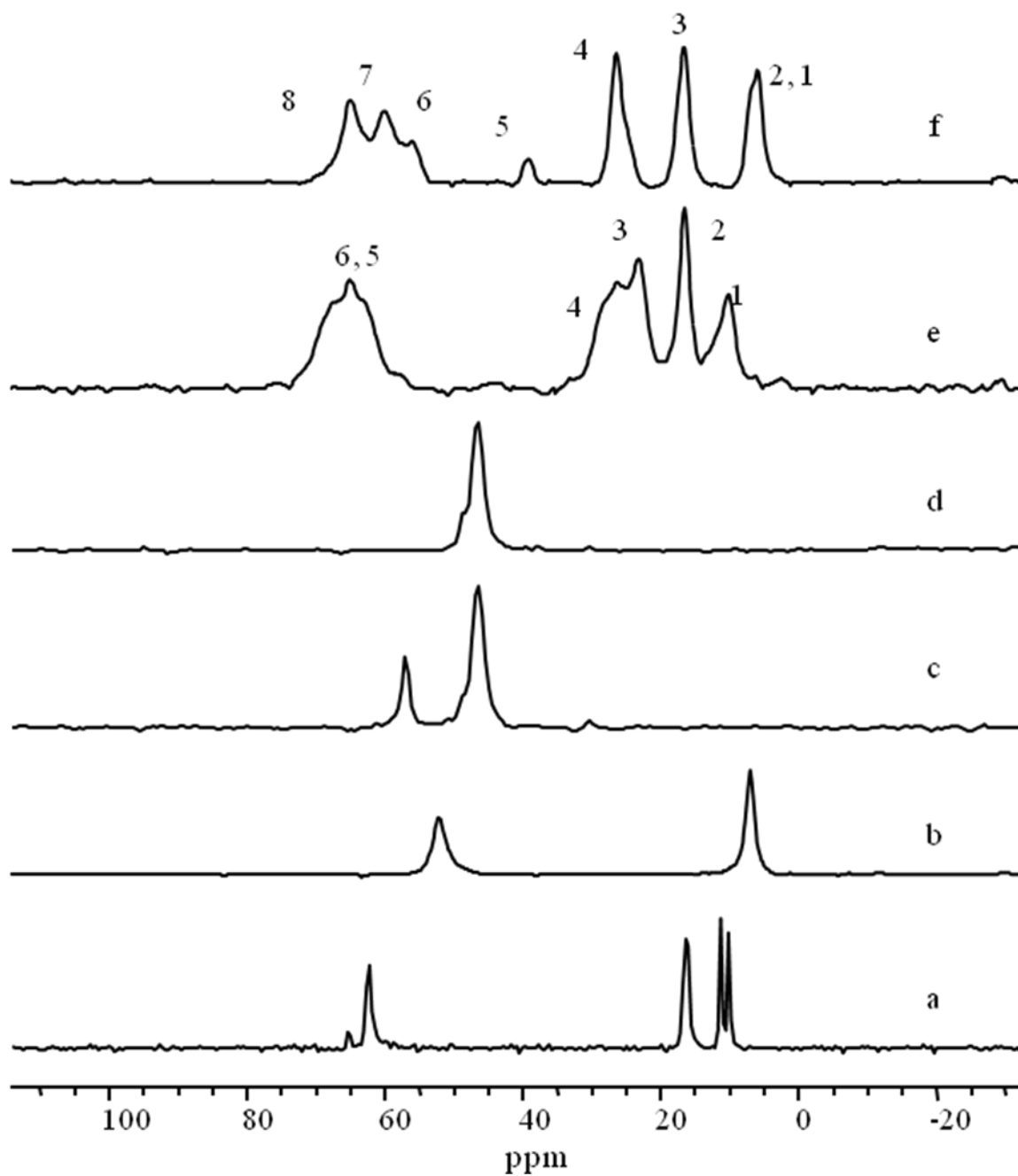


Figure 4.4  $^{13}\text{C}$  CP MAS spectra of as-synthesized (a) MFI, (b) BEA, (c) MTN from TMACl, (d) MTN from DPHMII, (e) MEL prepared using DPHMII as the organic SDA, and (f) MEL prepared using DECDMPI as the organic SDA. The numbers in (e) and (f) are peak assignments corresponding to the different carbon sites on the DPHMII and DECDMPI templates shown in Figure 4.14.

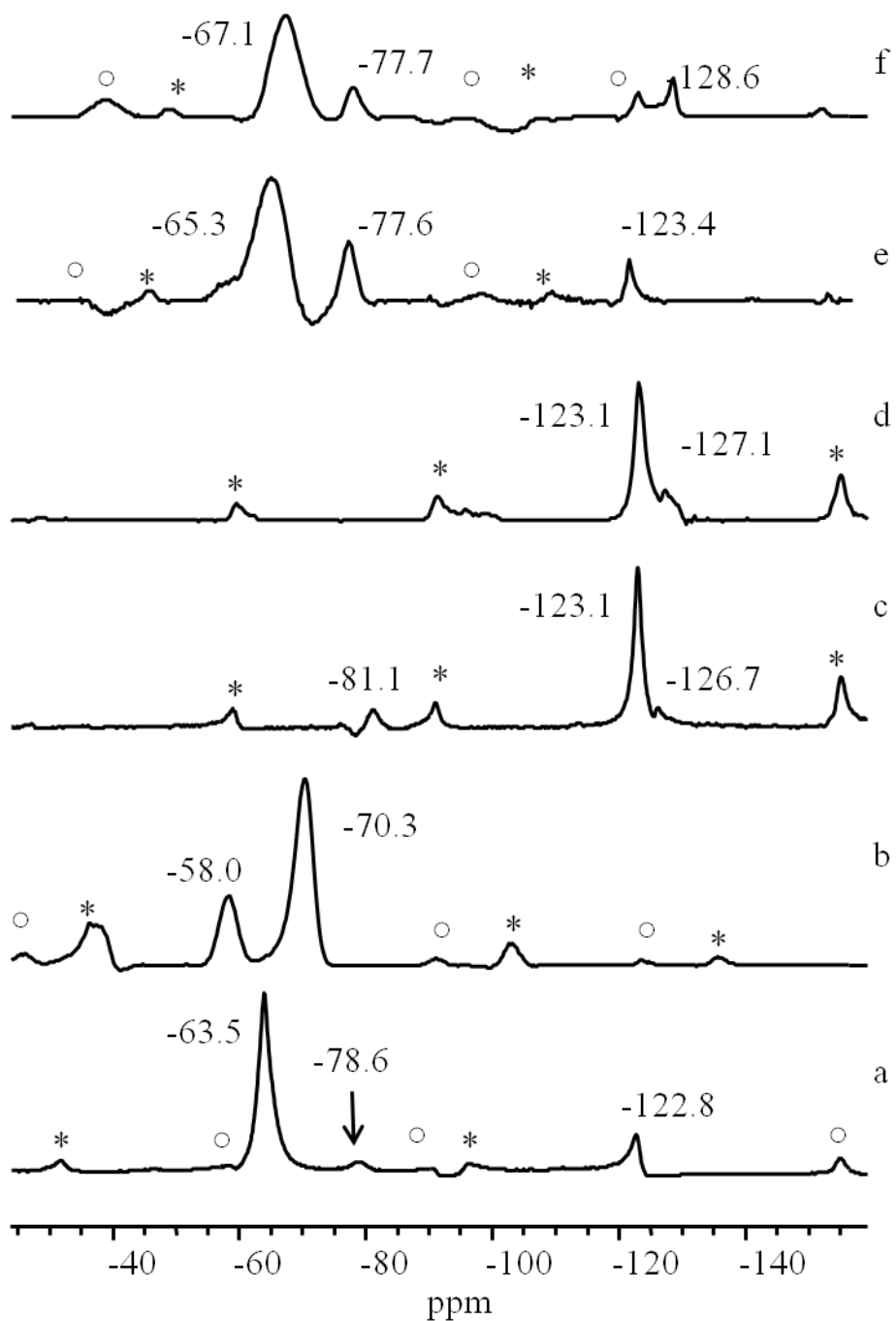


Figure 4.5  $^{19}\text{F}$  MAS spectra of as-synthesized (a) MFI, (b) BEA, (c) MTN from TMACl, (d) MTN from DPHMII, (e) MEL prepared using DPHMII as the organic SDA, and (f) MEL prepared using DECDMPI as the organic SDA. The spinning side bands are indicated by “\*” and “o”.

All zeolites prepared in the urea/choline chloride are siliceous besides Zeolite Beta which has Al in the 5% seeds added to the initial reaction mixture. The calcined BEA seeds contain a Si/Al of greater than 17. For the syntheses of MFI and BEA, 5% calcined seeds were added to the initial reaction mixture to speed up the crystallization process. The use of calcined seeds ensures that, in reactions where seeding was required, the signals in the  $^{13}\text{C}$  MAS spectra given by any organic SDAs occluded in the frameworks of the final products were not due to the organic molecules present in the seeds. In this case, then the tetraalkylammonium ions in the reactions mixtures indeed directed the formation of the final frameworks. No Al sources were added, since in the previous chapter, we found that the addition of Al slows down the reaction of the syntheses of high-silica zeolites. The mineralizing agent used in all four cases was  $\text{F}^-$  which was added to the reaction mixtures in the form of  $\text{NH}_4\text{F}$ .  $\text{F}^-$  ion has been shown to be an effective mineralizing agent that gives siliceous zeolites with fewer defects.<sup>27</sup>

#### 4.3.1 Tetrapropylammonium bromide (TPABr)

Silicalite-1 can be synthesized using 5% of initial seeding. The seeds used were a calcined Silicalite-1 sample, so no Al was present in the reaction and any  $^{13}\text{C}$  signals observed in the  $^{13}\text{C}$  NMR spectra would not be due to the organic SDA present in the seeds. The reaction for the formation of MFI requires the presence of seeds. The presence of seeds in the reaction mixture provided greater surface areas for the solutes to integrate into the solid phase, therefore enhancing the crystallization rate.<sup>28</sup> Figure 4.2a shows the powder X-ray diffraction (PXRD) patterns of the as-synthesized sample. The synthesis of Silicalite-1 was made using  $\text{TPA}^+$  as the organic SDA; the sample is phase-pure with strong reflections. The as-made TPA-MFI is orthorhombic and has 12 crystallographically distinct tetrahedral (T) sites. However, the  $^{29}\text{Si}$  MAS spectrum (Figure 4.3a) shows broad  $\text{Q}^4$  (Si atoms bonded to four other Si atoms through oxygen) peaks. Due to this severe overlap, the peaks for the individual T-sites cannot be distinguished. The  $^{29}\text{Si}$  MAS spectrum also shows a small broad peak for  $\text{Q}^3$  (Si sites containing one SiOH group) Si sites, meaning that the framework is imperfect.

It is clear that the organic SDA is present inside the MFI framework from the  $^{13}\text{C}$  CP MAS spectrum (Figure 4.4a), where the methyl groups give two different signals at



10.2 and 11.2 ppm, because two of the four propyl chains are in the straight channels while the other two are in the sinusoidal channels.<sup>29</sup> The  $^{13}\text{C}$  MAS spectrum also indicates the presence of fluoride in the zeolite framework due to the presence of two signals (65.3 and 65.5 ppm) in the lower field. This is because in the as-synthesized silicalite-1, the fluoride is much closer to three of the  $\alpha$ -carbon atoms (carbon directly bonded to nitrogen atom of  $\text{TPA}^+$ ) than the other.<sup>29</sup>

Unlike the hydrothermally as-synthesized F-MFI (fluoride MFI), there are two signals in the  $^{19}\text{F}$  MAS spectrum aside from the -122.8 ppm (Figure 4.5a). This band usually indicates the presence of  $\text{SiF}_6^{2-}$ , which is an impurity that is often present in the final product of the zeolite synthesis. The chemical shift for  $\text{SiF}_6^{2-}$  has been reported in several studies and usually falls in the range of -120 to -130 ppm.<sup>30-32</sup> The resonance at -68.5 ppm corresponds to the fluoride that is covalently bonded to Si-9 of the ZSM-5 framework, which has been shown in Figure 3.10 from the previous chapter.<sup>33</sup> There is also a weak signal at -78.6 ppm which is not usually seen in the high-temperature hydrothermally synthesized F-MFI. Similar situation has been reported in the dense-gel synthesis of F-MFI and F-MEL (fluoride MEL).<sup>34-35</sup> The presence of this second site is probably due to another fluoride species or fluoride that is covalently bonded to another Si atom in the framework. However, the identity of the species has not been determined yet.

The SEM images show that the crystals aggregate together to form a large cluster (Figure 4.6a). At a higher magnification, we can see that the crystal is heavily intergrown. The surface of the crystal is quite rough, containing defects and is also adhered by small particles, which may be amorphous (Figure 4.6b).

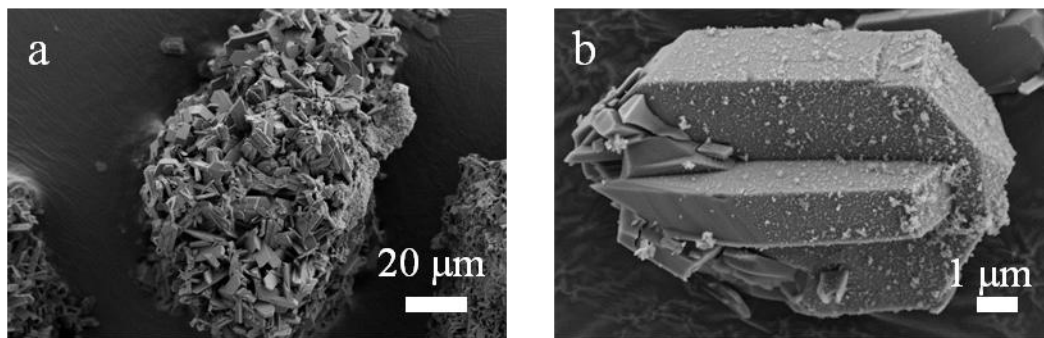


Figure 4.6 SEM images showing (a) an overview and (b) a single crystal of the as-made Silicalite-1.

#### 4.3.2 Tetraethylammonium hydroxide (TEAOH)

The synthesis of zeolite Beta, which is a high-silica zeolite having 12-membered ringed channels and consisted of the intergrowths of two or more polymorphs, also requires the addition of seeds in the initial reaction batch for the product to be formed.<sup>36</sup> Without seeding, MFI becomes the competing phase in the reaction. This is not surprising since  $\text{TEA}^+$  can also be a organic SDA for MFI in hydrothermal synthesis.<sup>37</sup> The BEA seeds used for the reactions were calcined at 350/500 °C, so any signals observed in the  $^{13}\text{C}$  MAS spectrum of the final product are not due to the SDA molecules present in the seeds. The PXRD pattern of the as-synthesized sample is shown in Figure 4.2b; the resulting product of the reaction is consisted of a mixture of the different polymorphs. The  $^{29}\text{Si}$  MAS spectrum of the as-synthesized sample (Figure 4.3b) shows five signals which are due to the  $\text{Q}^4$  Si atoms and  $\text{Q}^3$  Si atoms that are bonded to one Al through oxygen are in the range of -108.3 — -116ppm, while the  $\text{Q}^3$  SiOH sites are represented by the broad peak at -104.0 ppm.<sup>38-39</sup> The Al present in the seeds ( $\text{Si}/\text{Al} > 17$ ) is the sole source of Al for the reaction. However, the exact percentage of Al in the as-made sample was not detectable by x-ray fluorescence (XRF).  $^{27}\text{Al}$  MAS spectrum of the as-made final product shows two resonances (Figure 4.7a). The signal at 55.1 ppm represents tetrahedral Al in the BEA framework, while the signal close to 0 ppm represents extraframework Al atoms, which are octahedrally coordinated. The  $^{13}\text{C}$  NMR (Figure Figure 4.4b) shows the presence of  $\text{TEA}^+$  ions inside the channels of BEA. The chemical shift at 6.7 ppm corresponds to the terminal methyl carbons, while the one at 52.3 ppm correspond to the methylene carbons that are directly bonded to the nitrogen.

$^{19}\text{F}$  MAS spectrum of the as-synthesized sample contains two signals at -58.0 and -70.3 ppm (Figure 4.5b). The results agree with the hydrothermally as-made TEA-BEA.<sup>32</sup> The presence of these two signals means that there are two different  $\text{F}^-$  sites at which the fluoride atoms that are covalently bonded to Si atoms inside the framework.<sup>32</sup> It has been proposed that the fluoride anions are located inside the  $[4^35^4]$  cage of the framework (Figure 4.8).<sup>32</sup> The zeolite BEA synthesized under our condition has relatively small crystal sizes as shown in the SEM images (Figure 4.9a and b). Under higher magnification, we can see that the F-BEA made under our condition shows the truncated squared pyramidal shape of the highly faulted BEA structure.

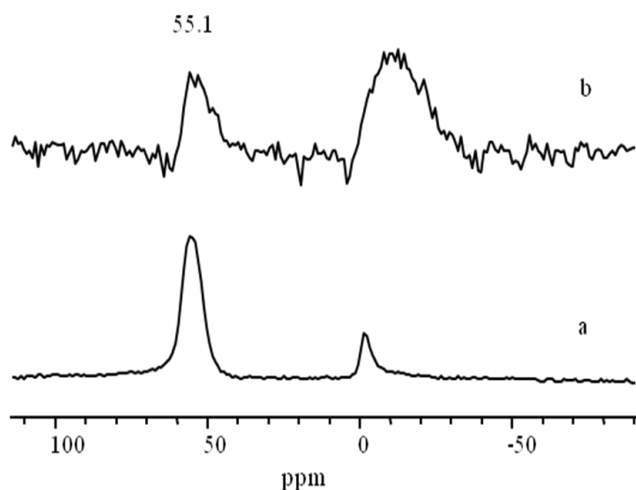


Figure 4.7  $^{27}\text{Al}$  MAS spectra of as-made BEA (a) and calcined BEA (b).

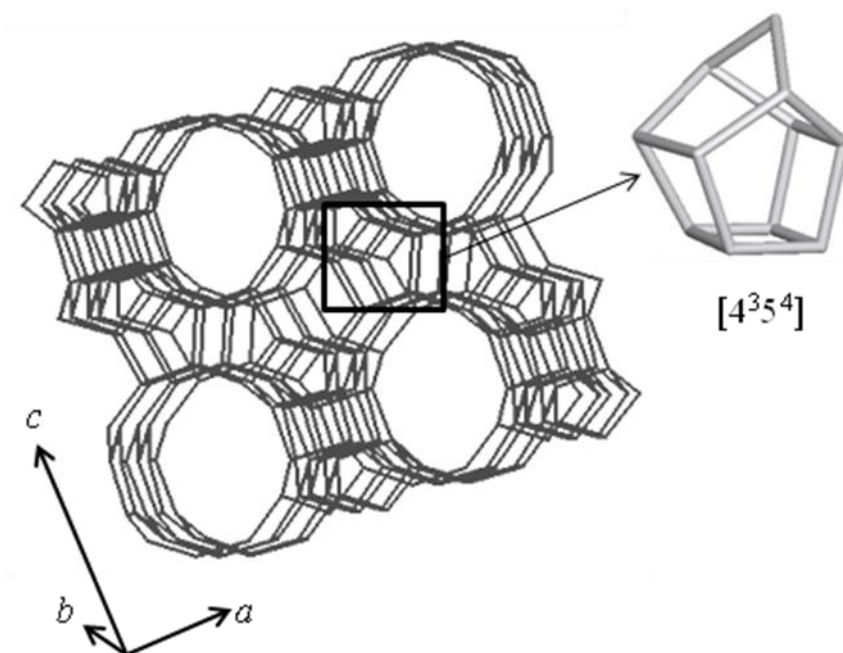


Figure 4.8  $[4^3 5^4]$  cage in BEA.

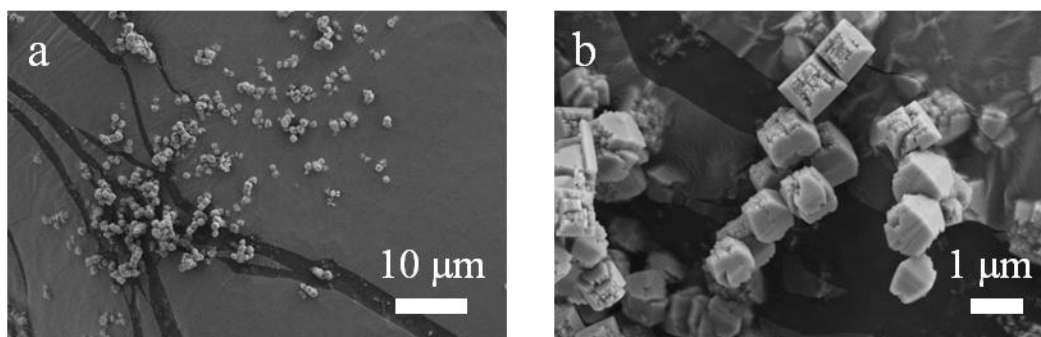


Figure 4.9 SEM images showing (a) an overview and (b) expanded view of as-synthesized BEA.

After the sample is being calcined at 350/500 °C, the  $^{29}\text{Si}$  MAS spectrum shows well resolved peaks instead of the broad overlap of signals we see in the as-synthesized material. PXRD pattern was obtained for the calcined sample as well to show that the BEA has not been broken down into amorphous material after the calcination treatment (Figure 4.10). Calcination is known to remove the defects within the zeolite frameworks.<sup>40</sup> The  $^{29}\text{Si}$  MAS shows nine crystallographically inequivalent T-sites within the framework of BEA similar to the highly siliceous dealuminated BEA prepared in hydrothermal conditions (Figure 4.11).<sup>38</sup> The  $^{29}\text{Si}$  MAS spectrum of the calcined sample

does not show a signal at -104.0 ppm, which was assigned to the -SiOH groups present in the as-synthesized materials. By calcining the sample, these defects are “healed.” There is a small and weak signal at -108.2 ppm, which can be due to the Q<sup>3</sup> Si sites containing Si atoms connected to one Al and three other Si atoms via oxygen. Compared with the as-synthesized BEA, the calcined sample contains less framework-Al. The peak responsible for the octahedral Al site (~ -11 ppm) in the <sup>27</sup>Al MAS spectrum has a higher intensity than the one for the tetrahedral Al (55.1 ppm) (Figure 4.7b). Upon calcination, some of the tetrahedrally coordinated Al (framework Al) were converted into octahedral Al (extraframework Al).<sup>40</sup>

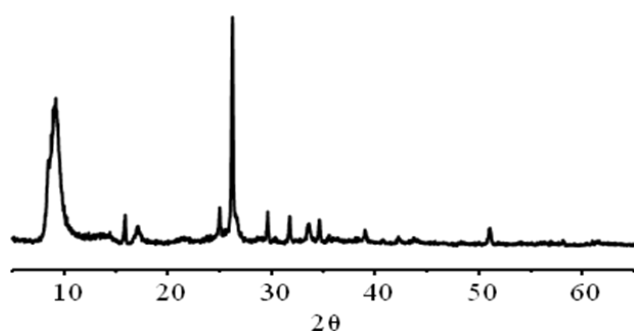


Figure 4.10 PXRD pattern of calcined BEA.

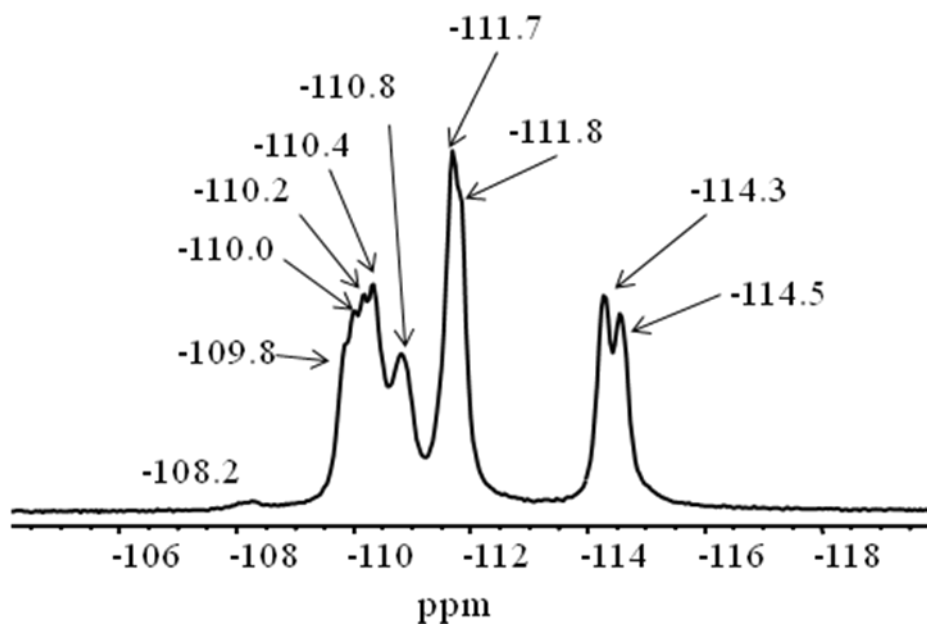


Figure 4.11 <sup>29</sup>Si MAS spectrum of calcined BEA.

### 4.3.3 Tetramethylammonium chloride (TMACl)

When the organic SDA was changed to TMACl, ZSM-39 was produced after 2 weeks of reaction at 170 °C. The PXRD (Figure 4.2c) of this product with cubic framework shows peaks with sharp reflections. From the  $^{29}\text{Si}$  MAS spectrum, the signals at -109.2, -114.1, and -117.3 ppm (1: 4: 12) correspond to the three different tetrahedral sites (T-sites) in the cubic framework (Figure 4.3c).<sup>41-43</sup> Although  $\text{TMA}^+$  is known to be one of the organic SDA for MTN type zeolites, the  $^{13}\text{C}$  CP MAS NMR (Figure 4.4c) spectrum reveals that during the course of the reaction, some of the  $\text{TMA}^+$  molecules have decomposed into trimethylammonium ions (46.4 ppm), the result of which is in agreement with previous studies.<sup>44</sup> Only a small signal for  $\text{TMA}^+$  is shown at 57.1 ppm. According to other studies, the trimethylammonium ions are in equilibrium with trimethylamine, which gives a signal at 51.3 ppm. However, based on the  $^{13}\text{C}$  MAS spectrum, trimethylamine is not adsorbed on the crystal surface nor occluded in the pores of the ZSM-39 we synthesized. It is possible that the trimethylamine was washed away along with the urea and choline chloride during the clean-up process of the sample. Based on previous works, organic species are resided in the larger of the two types of cages in MTN (7.5 Å).<sup>45</sup> The  $^{19}\text{F}$  NMR shows a major signal at -123 ppm, which is assigned to fluoride that acts as the counterion for the organic SDA (Figure 4.5c). There is a weak signal at -126.7 ppm which is due to the  $\text{SiF}_6^{2-}$  impurity.<sup>30-32</sup> The signal at -81.1 ppm is assigned to  $\text{F}^-$  inside the framework. This signal is much weaker than that observed in the MTN made from TMACl/1, 6-hexanediol, meaning that there is less  $\text{F}^-$  being trapped inside the smaller cages of the framework. SEM images shows the samples crystals often aggregate together (Figure 4.12a). Furthermore, although they exhibit the dodecahedral morphology, the surfaces of the crystals are not very smooth and are sometimes covered by debris (Figure 4.12b).

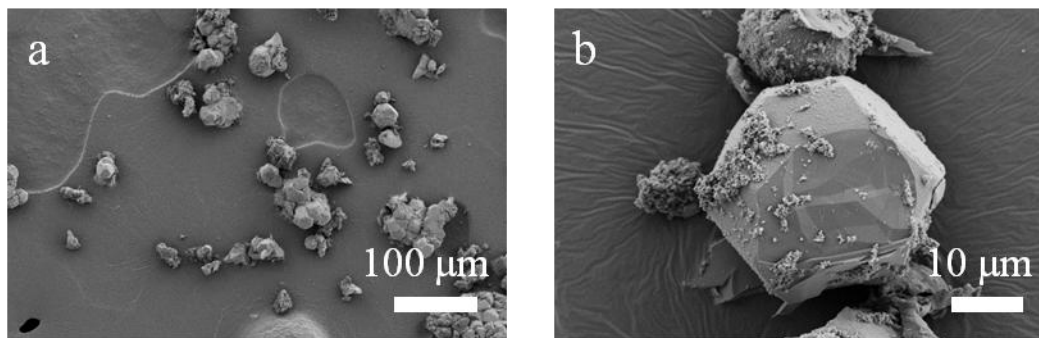


Figure 4.12 SEM images showing (a) an overview and (b) expanded view of as-synthesized TMA-MTN.

#### 4.3.4 *N, N*-dipropylhexamethylene imminium iodide (DPHMII) and *N, N*-diethyl-3, 5-dimethylpiperidinium iodide (DECDMPI)

A zeolite closely related to the MFI structure is the ZSM-11, which is tetragonal and has two intersecting channels consisted of 10-membered ring openings. However, unlike the case in ZSM-5, in the MEL framework, the pentasil chains are connected to each other by a reflection instead of by an inversion centre.<sup>46</sup> The organic SDA used in our experiment is DPHMII. Based on the results, the effect of temperature on MEL synthesis is apparent. Instead of producing MEL, the reaction mixture gave MTN at 170 °C after 3 weeks as shown by the PXRD pattern in Figure 4.2d. The <sup>29</sup>Si MAS spectrum (Figure 4.3d) shows the three crystallographically distinct T-sites in the structure framework. There may be two reasons accounted for the production of MTN. First, dense frameworks are preferred at higher temperatures. Furthermore, the reaction time for these reactions in ionic liquids tends to be longer than what is observed in hydrothermal synthesis due to the lack of water for the solubility and transportation of species in the mixture. Therefore, the DPHMII could be decomposed at 170 °C over the course of the reaction. The <sup>13</sup>C CP MAS (Figure 4.4d) shows that the organic species occluded inside the pores of the final product is the trimethylammonium ion, which is what was observed in the MTN synthesized using TMACl.<sup>44</sup> The <sup>19</sup>F MAS spectrum of this sample does not contain any resonances in the -80 ppm region (Figure 4.5d). Only the strong peak at -123.1 ppm is shown, meaning that F<sup>-</sup> is acting as the counterion for the organic SDA. There is also a small amount of SiF<sub>6</sub><sup>2-</sup> as indicated by the weak signal at -127.1 ppm.<sup>30-32</sup> The lack of F<sup>-</sup> peak at around -80 ppm suggests that the formation of

MTN under this condition is largely due to the high reaction temperature but not the structure-directing effect of the F<sup>-</sup>. The sample contains both single and intergrown crystals (Figure 4.13a). Unlike the TMA-MTN (discussed in previous section) which shows a dodecahedral morphology, these MTN crystals obtained from the urea/choline chloride mixture containing DPHMII in the starting material are perfect octahedral (Figure 4.13b). Such morphology has been reported in the non-aqueous synthesis of ZSM-39 in the presence of propylamine and NaOH.<sup>47</sup> This octahedral morphology is also very common for solids in the cubic crystal system.<sup>48</sup> The crystals in this case have much smoother surfaces than the TMA-MTN mentioned in the previous section. This can be attributed to the longer reaction time, which heals the crystal defects.<sup>49</sup>

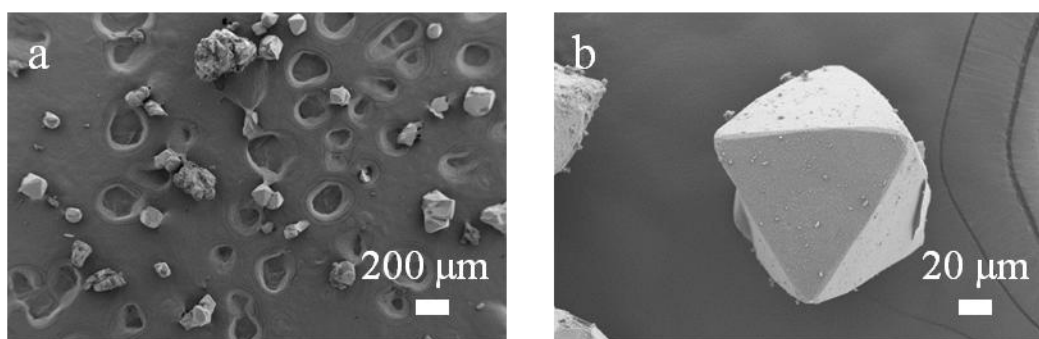


Figure 4.13 SEM images showing (a) an overview and (b) expanded view of as-synthesized MTN from a reaction mixture containing DPHMII at 170 °C.

To avoid the formation of dense frameworks, a lower temperature must be used for the preparation of MEL. Indeed, when the temperature was lowered to 140 °C, phase-pure MEL free of any MFI intergrowths was produced as indicated by the weak reflection at  $2\theta = 21.8^\circ$  and a strong single peak reflection at  $2\theta = 53.1^\circ$  on the PXRD pattern (Figure 4.2e).<sup>50</sup> The <sup>29</sup>Si MAS spectrum in Figure 4.3e shows the sample contains some Q<sup>3</sup> Si atoms, indicating the presence of defects in the final product. The broad peak for Q<sup>4</sup> Si atoms is the result of the overlap of the seven crystallographically non-equivalent Si in the crystal lattice.<sup>51</sup> Despite the presence of defects, the Q<sup>4</sup> signal is much larger than the Q<sup>3</sup>. The <sup>13</sup>C CP MAS spectrum (Figure 4.4e) reveals the presence of DPHMII inside the as-synthesized framework structure. There are six different carbon environments in total, where the signals for the two methylene carbons (one from the propyl chain and the other from the hexamethyleneiminium ring) closest to the nitrogen



overlap, giving a broad peak. The assignments are shown in Figure 4.14a. The ionothermal preparation of MEL in the absence of seeding using DPHMII is highly reproducible, which suggests the strong structure-directing ability of this organic SDA. The  $^{19}\text{F}$  MAS spectrum (Figure 4.5e) contains two major peaks at -65.3 and -77.6 ppm similar to the case observed in MFI in Section 4.3.1. However, in this case, the signal at -77.6 ppm is stronger in intensity. The overall results agree with the findings in the dense gel synthesis of ZSM-11.<sup>35</sup> The signal at -65.3 ppm is assigned to  $\text{F}^-$  atoms that are covalently bonded to one of the Si sites.<sup>30</sup> However, given the current data, the exact location of the  $\text{F}^-$  and the identity of the  $\text{F}^-$  species which gives the -77.6 ppm signal cannot be identified. There is a small amount of  $\text{SiF}_6^{2-}$  as indicated by the shift at -123.4 ppm.<sup>30-32</sup> The sample contains long needles clumped together shown by the SEM (Figure 4.15a). At higher magnification (Figure 4.15b), each end of the needle contains a pyramid. Furthermore, the needles are covered by some small particles, which can be amorphous.

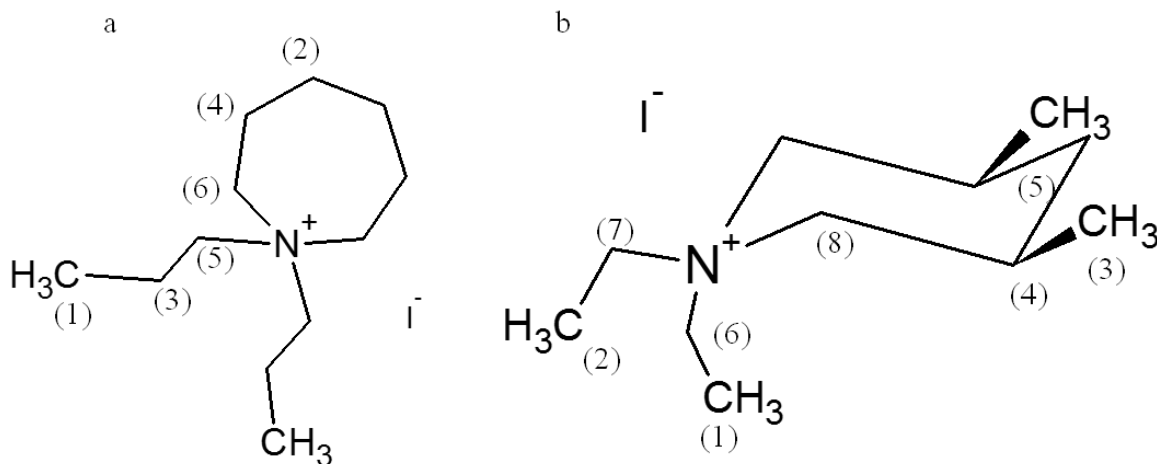


Figure 4.14 DPHMII (a) and DECDMPI (b). The carbon atoms are labeled to represent the peak assignments for  $^{13}\text{C}$  MAS spectra in Figure 4.4 (e) and (f).

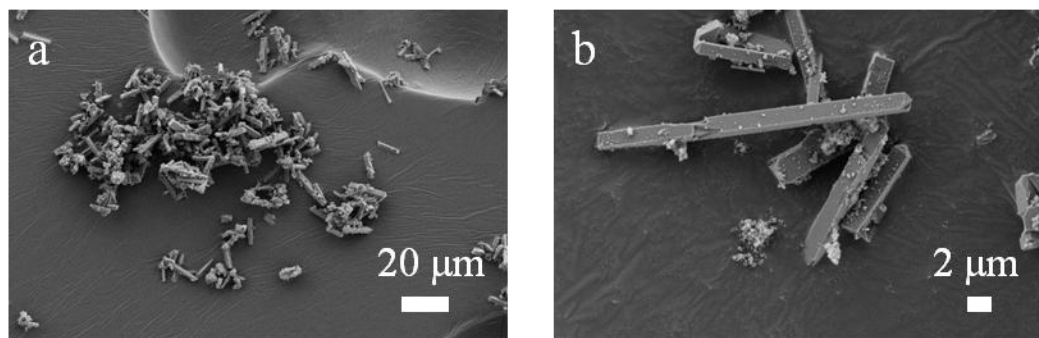


Figure 4.15 SEM images showing (a) an overview and (b) expanded view of as-synthesized DPHMI-MEL.

The other organic SDA, DECDMPI has been known to give phase-pure MEL in hydrothermal and dense gel conditions.<sup>26,35</sup> For our experiments, to investigate the effect of SDA on the reaction, DPHMII was replaced with DECDMPI. The organic SDA: SiO<sub>2</sub> ratio remained at 0.08: 1, and the temperature of the reaction was also 140 °C. Figure 4.2f shows the PXRD of the as-made MEL where 5% of calcined MEL seeds were added to the initial mixture. The ZSM-11 product obtained after 24 days of reaction was phase-pure and free of any MFI intergrowths as indicated by the weak reflection at  $2\theta = 21.8^\circ$  and a strong single peak reflection at  $2\theta = 53.1^\circ$ .<sup>50</sup> The <sup>29</sup>Si MAS spectrum shows a Q<sup>4</sup> region with severe overlap of the seven T-sites (Figure 4.3f).<sup>51</sup> Like the DPHMII-MEL, there is also a small amount of Q<sup>3</sup> Si atoms, meaning that the framework contains defects. The <sup>13</sup>C CP MAS (Figure 4.4f) shows that DECDMP<sup>+</sup> is present inside the framework. The peak assignments are labeled in Figure 4.14b. There are two signals for the –CH<sub>2</sub>CH<sub>3</sub> groups hanging off from the nitrogen of the piperidinium ring, since one ethyl group is at the equatorial position while the other is at the axial position. The chemical shift for the equatorial groups are in the lower field, because they are more deshielded than the ethyl groups in the axial position. The <sup>19</sup>F MAS spectrum (Figure 4.5f) for the as-made DECDMP-MEL is similar to what has been observed in the DPHMI-MEL case, where there are two major peaks. The signal corresponding to the fluoride that forms a covalent bond with Si is at -67.7 ppm, this can be a result of the change in the organic SDA. The weak resonance at -128.6 ppm represents the SiF<sub>6</sub><sup>2-</sup> impurity.<sup>30-32</sup> The SEM pictures (Figure 4.16a and b) of the as-synthesized sample also shows the long needles like we see in the DPHMII-MEL. The needles are often clumped together. Furthermore,

there is a greater size distribution in this case: Some crystals are larger than the others (Figure 4.16a). This is probably due to the use of seeds. During crystallization, crystal growth can occur on the surfaces of the seeds. Some of the seeds might have been dissolved into smaller pieces, which can also provide sites for the amorphous silica to adhere.

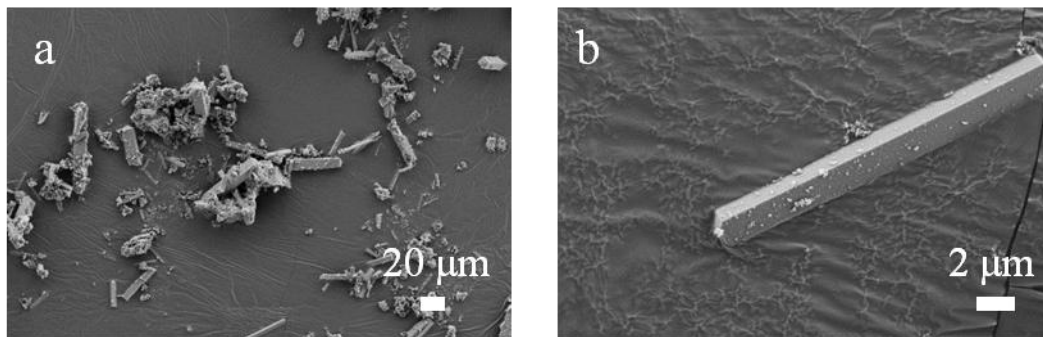


Figure 4.16 SEM images showing (a) an overview and (b) expanded view of as-synthesized DECDMP-MEL.

The crystallization process involving DECDMPI as the organic SDA was much slower when no seeds were present at the initial stage (Figure 4.17). Crystallization only started at around 24 day, while the reaction was finished in the seeded case. The addition of seeds speeds up the reaction by providing a greater surface area for the solutes to integrate into the solid phase.<sup>28</sup> The choice of the MEL organic SDA has been shown to be important in both hydrothermal and low temperature dense gel syntheses.<sup>35</sup> This requirement for the presence of seeds for MEL preparation in urea/choline chloride mixture is similar to that in the dense gel condition, in which the fluoride synthesis of ZSM-11 using DECDMPI as the organic SDA must be initiated by seeding.<sup>35</sup> Comparing this result with what we had for the DPHMII discussed in the previous paragraph, we can conclude that the DECDMPI's structure-directing ability toward the MEL type framework is much weaker than that of DPHMII.

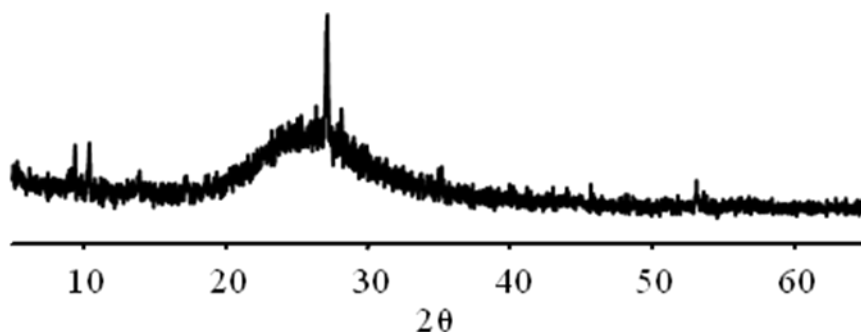


Figure 4.17 PXRD pattern of the solid obtained after 24 days of reaction using DECDMPI as the organic SDA.

#### 4.4 Conclusions

In summary, our results present the first example of high-silica and siliceous zeolite synthesis in the ionic liquid urea/choline chloride mixture using  $F^-$  as the mineralizing agent. The water content in all of our reactions came from the chemical reagents exclusively. Furthermore, we have shown that by using different organic SDA, several types of framework structures can be achieved. The disadvantage of this system is the long reaction times compared to those in the hydrothermal conditions. Also, some framework structures require the addition of seeds to the initiation of the reaction or the shortening of the crystallization time. Nevertheless, the zeolites obtained in our conditions are all phase-pure (with the exception of zeolite beta where a mixture of polymorphs were obtained), and the results exhibit high reproducibility. Upon calcination, zeolite Beta synthesized in urea/choline chloride exhibits high crystallinity. With our results of ZSM-11 preparation, both DPHMII and DECDMPI generate phase-pure MEL free of any MFI intergrowths. However, the choice of organic SDA is critical to our reaction conditions as it is in the hydrothermal and dense gel syntheses. The DPHMII molecule has a much stronger structure-directing power toward the MEL framework in the urea/choline chloride mixture, allowing the reaction to proceed without the addition of calcined seeds.

## 4.5 References:

1. Bekkum, H. v.; Jacobs, P. A.; Flanigen, E. M.; Jansen, J. C., *Introduction to Zeolite Science and Practice*. 2001.
2. Cooper, E. R.; Andrews, C. D.; Wheatley, P. S.; Webb, P. B.; Wormald, P.; Morris, R. E., *Stud. Surf. Sci. Catal.* **2005**, *158*, 247-254.
3. Parnham, E. R.; Drylie, E. A.; Wheatley, P. S.; Slawin, A. M. Z.; Morris, R. E., *Angew. Chem. Int. Ed.* **2006**, *45*, 4962-4966.
4. Parnham, E. R.; Morris, R. E., *Chem. Mater.* **2006**, *2006* (18), 4882-4887.
5. Parnham, E. R.; Morris, R. E., *J. Mater. Chem.* **2006**, *16*, 3682-3684.
6. Parnham, E. R.; Wheatley, P. S.; Morris, R. E., *Chem. Commun.* **2006**, 380-382.
7. Xu, Y. P.; Tian, Z. J.; Wang, S. J.; Hu, Y.; Wang, L.; Wang, B. C.; Ma, Y. C.; Hou, L.; Yu, J. Y.; Lin, L. W., *Angew. Chem. Int. Ed.* **2006**, *45*, 3965-3970.
8. Chen, S. M.; Zhang, J.; Bu, X. H., *Inorg. Chem.* **2008**, *47*, 5567-5569.
9. Hogben, T.; Douthwaite, R. E.; Gillie, L. J.; Whitwood, A. C., *Cryst. Eng. Comm.* **2006**, *8*, 866-868.
10. Ji, W. J.; Zhai, Q. G.; Hu, M. C.; Li, S. N.; Jiang, Y. C.; Wang, Y., *Inorg. Chem. Commun.* **2008**, *11*, 1455-1458.
11. Liao, J. H.; Huang, W. C., *Inorg. Chem. Commun.* **2006**, *9*, 1227-1231.
12. Liao, J. H.; Wu, P. C.; Bai, Y. H., *Inorg. Chem. Commun.* **2005**, *8*, 390-392.
13. Liao, J. H.; Wu, P. C.; Huang, W. C., *Cryst. Growth Des.* **2006**, *6*, 1062-1063.
14. Lin, Z. J.; Li, Y.; Slawin, A. M. Z.; Morris, R. E., *Dalton T.* **2008**, 3989-33994.
15. Shi, F. N.; Trindade, T.; Rocha, J.; Paz, F. A. A., *Cryst. Growth. Des.* **2008**, *8*, 3917-3920.
16. Xu, L.; Choi, E. Y.; Kwon, Y. U., *Inorg. Chem.* **2007**, *46*, 10670-10680.
17. Zhang, J.; Chen, S. M.; Bu, X. H., *Angew. Chem. Int. Ed.* **2008**, *47*, 5434-5437.
18. Cooper, E. R.; Andrews, C. D.; Wheatley, P. S.; Webb, P. B.; Wormald, P.; Morris, R. E., *Nature* **2004**, *430* (7003), 1012-1016.
19. Abbott, A. P.; Capper, G.; Davies, D. L.; Rasheed, R. K.; Tambyrajah, V., *Chem. Commun.* **2003**, (1), 70-71.

20. de Moor, P. P. E. A.; Beelen, T. P. M.; Komanschek, B. U.; Beck, L. W.; Wagner, P.; Davis, M. E.; van Santen, R. A., *Chem. Eur. J.* **1999**, *5* (7), 2083-2088.
21. Ma, Y. C.; Wang, S. J.; Song, Y. L.; Xu, Y. P.; Tian, Z. J.; Yu, J. Y.; Lin, L. W., *Chinese. J. Inorg. Chem.* **2010**, *26* (11), 1923-1926.
22. Ma, Y. C.; Xu, Y. P.; Wang, S. J.; Wang, B. C.; Tian, Z. J.; Yu, J. Y.; Lin, L. W., *Chem. J. Chinese. U.* **2006**, *27* (4), 739-741.
23. Wheatley, P. S.; Allan, P. K.; Teat, S. J.; Ashbrook, S. E.; Morris, R. E., *Chem. Sci.* **2010**, *1* (4), 483-487.
24. Cai, R.; Liu, Y.; Gu, S.; Yan, Y. S., *J. Am. Chem. Soc.* **2010**, *132* (37), 12776-12777.
25. Fecant, A.; Bats, N. Preparation of MEL-type zeolites and their use. FR2914635A1, 2008.
26. Nakagawa, Y. Preparation of zeolite ZSM-11 using a 3,5-dimethylpiperidinium templating agent. US5645812A, 1997.
27. Cambor, M. A.; Villaescusa, L. A.; Diaz-Cabanas, M. J., *Top. Catal.* **1999**, *9* (1-2), 59-76.
28. Gonthier, S.; Thompson, R. W., Effects of Seeding on Zeolite Crystallisation, and the Growth Behavior of Seeds. In *Studies in Surface Science and Catalysis*, J.C. Jansen, M. S. H. G. K.; Weitkamp, J., Eds. Elsevier: 1994; Vol. Volume 85, pp 43-73.
29. Chézeau, J.-M.; Delmotte, L.; Guth, J.-L.; Soulard, M., *Zeolites* **1989**, *9* (1), 78-80.
30. Zones, S. I.; Darton, R. J.; Morris, R.; Hwang, S. J., *J. Phys. Chem. B* **2005**, *109* (1), 652-661.
31. Villaescusa, L. A.; Bull, I.; Wheatley, P. S.; Lightfoot, P.; Morris, R. E., *J. Mater. Chem.* **2003**, *13* (8), 1978-1982.
32. Cambor, M. A.; Barrett, P. A.; Díaz-Cabañas, M.-J.; Villaescusa, L. A.; Puche, M.; Boix, T.; Pérez, E.; Koller, H., *Microporous Mesoporous Mater.* **2001**, *48* (1-3), 11-22.
33. Fyfe, C. A.; Brouwer, D. H.; Lewis, A. R.; Chézeau, J.-M., *J. Am. Chem. Soc.* **2001**, *123* (28), 6882-6891.
34. Fyfe, C. A.; Darton, R. J.; Mowatt, H.; Lin, Z. S., *Microporous Mesoporous Mater.* **2011**, *144* (1-3), 57-66.

35. Fyfe, C. A.; Lin, Z. S.; Tong, C.; Darton, R. J., *Microporous Mesoporous Mater.* **2012**, *150* (0), 7-13.
36. Newsam, J. M.; Treacy, M. M. J.; Koetsier, W. T.; Gruyter, C. B. D., *Proceedings of the Royal Society of London. Series A, Mathematical and Physical Sciences* **1988**, *420* (1859), 375-405.
37. Lok, B. M.; Cannan, T. R.; Messina, C. A., *Zeolites* **1983**, *3* (4), 282-291.
38. Fyfe, C. A.; Strobl, H.; Kokotailo, G. T.; Pasztor, C. T.; Barlow, G. E.; Bradley, S., *Zeolites* **1988**, *8* (2), 132-136.
39. Lemos de Macedo, J.; Ferreira Ghesti, G.; Alves Dias, J.; Claudia Loureiro Dias, S., *PCCP* **2008**, *10* (11), 1584-1592.
40. Hunger, M., Catalytically Active Sites: Generation and Characterization. In *Zeolites and Catalysis*, Wiley-VCH Verlag GmbH & Co. KGaA: 2010; pp 493-546.
41. Schlenker, J. L.; Dwyer, F. G.; Jenkins, E. E.; Rohrbaugh, W. J.; Kokotailo, G. T.; Meier, W. M., *Nature* **1981**, *294* (5839), 340-342.
42. Higgins, J. B.; Woessner, D. E.; Trewella, J. C.; Schlenker, J. L., *Zeolites* **1984**, *4* (2), 112-113.
43. Fyfe, C. A.; Gies, H.; Feng, Y.; Kokotailo, G. T., *Nature* **1989**, *341* (6239), 223-225.
44. Dewaele, N.; Gabelica, Z.; Bodart, P.; Nagy, J. B.; Giordano, G.; Derouane, E. G., GEL Composition Versus Organic Directing Agent Effects in the Synthesis of ZSM-39, ZSM-48 and ZSM-50 Zeolites. In *Studies in Surface Science and Catalysis*, P.J. Grobet, W. J. M. E. F. V.; Schulz-Ekloff, G., Eds. Elsevier: 1988; Vol. Volume 37, pp 65-73.
45. Gies, H., *Z. Kristallogr.* **1984**, *167* (1-2), 73-82.
46. Kokotailo, G. T.; Chu, P.; Lawton, S. L.; Meier, W. M., *Nature* **1978**, *275* (5676), 119-120.
47. Qisheng, H.; Shouhua, F.; Ruren, X., Syntheses of Pentasil Silica-Zeolites From Nonaqueous Systems. In *Studies in Surface Science and Catalysis*, Jacobs, P. A.; Santen, R. A. v., Eds. Elsevier: 1989; Vol. 9, pp 291-298.
48. Anderson, M. W.; Agger, J. R.; Thornton, J. T.; Forsyth, N., *Angew. Chem. Int. Ed. Engl.* **1996**, *35* (11), 1210-1213.
49. Kim, I. J.; Zhao, W.; Fan, X.; Chang, J. H.; Gauckler, L. J., *J. Ceram. Process Res.* **2010**, *11* (2), 158-163.

50. Millward, G. R.; Ramdas, S.; Thomas, J. M.; Barlow, M. T., *J. Chem. Soc., Faraday Trans. 2* **1983**, 79 (7), 1075-1082.
51. Fyfe, C. A.; Gies, H.; Kokotailo, G. T.; Pasztor, C.; Strobl, H.; Cox, D. E., *J. Am. Chem. Soc.* **1989**, 111 (7), 2470-2474.



## **Chapter 5 : Preliminary Studies on the Formation of ZSM-39 (MTN) Zeolite in Tetramethylammonium Chloride (TMACl)/1, 6-Hexandiol Deep Eutectic Mixture**

### **5.1 Introduction**

Zeolites are crystalline microporous silicate or aluminosilicate structures with that are important in various industrial processes.<sup>1</sup> The formation of zeolites often requires the presence of an organic structure-directing agent (SDA), which tend to be occluded in the pores of the final product.<sup>2</sup> Studying the location of these SDAs in the framework allow us to have a better understanding of the crystallization process of these microporous materials.

Zeolite ZSM-39 is a clathrate and the silicate analogue of the 17Å cubic gas hydrate.<sup>3</sup> ZSM-39 has been made in hydrothermal and non-aqueous conditions.<sup>4-8</sup> One of the most commonly seen SDA in the synthesis of ZSM-39 is the tetramethylammonium ion (TMA<sup>+</sup>). The building units of the MTN framework consist of [5<sup>12</sup>] and [5<sup>12</sup>6<sup>4</sup>] tetrahedral silica (Figure 5.1).<sup>3, 5, 9</sup> Due to its small diameter of the [5<sup>12</sup>6<sup>4</sup>] cages (6.2-7.5 Å), ZSM-39 has very limited sorption ability.<sup>6, 9</sup> From previous studies, it is well known that structure-directing agent (SDA) molecules are often occluded into the zeolite frameworks when the reactions are finished.<sup>10</sup> Due to the small cages present in ZSM-39's clathrate type structure, any molecules that have entered the system cannot escape. Therefore, despite of its limited sorption abilities, ZSM-39 is an excellent candidate for studying guest-host interactions under different conditions. For instance, any changes occur to the structure will be dependent on the type of guest molecules being incorporated into the framework. Studying these interactions and monitoring the changes in the chemical environment during the reaction will give us insights on the mechanism of the framework formation. A previous study has been performed on the formation mechanism of ZSM-39 using tetramethylethylenediamine (TMEDA) as the organic

SDA under hydrothermal conditions.<sup>11</sup> The study found that the silica species in the gel first aggregate around the TMEDA. Then, condensation of silica occurs to form the zeolite framework. The TMEDA is now incorporated into the ZSM-39 structure.<sup>11</sup>

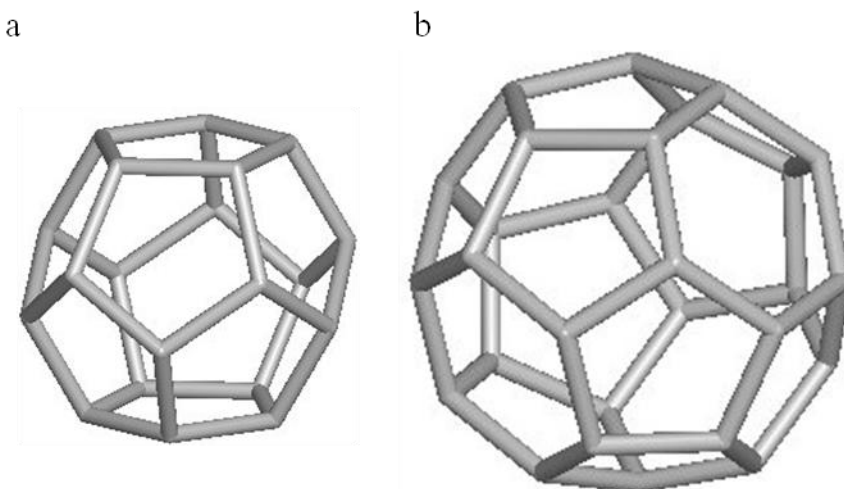


Figure 5.1 Two types of cages that build up ZSM-39: (a)  $[5^{12}]$  and (b)  $[5^{12}6^4]$

Typically speaking, zeolites are synthesized hydrothermally at temperatures of 150-200 °C by mixing silica, water, base, and the SDA. Over the past few decades, there have been attempts to synthesize zeolites in non-aqueous systems containing organic solvents or mixed solvents.<sup>12-19</sup> More recently, a new synthetic strategy using ionic liquid (IL) to prepare framework structures has been developed. To be considered as an IL for the synthesis of microporous materials, the salt needs to have a melting point below 150-200 °C. Using IL as the major component of the reaction mixture would therefore yield a lower vapour pressure in the system. Furthermore, in the synthesis of microporous framework materials, the interactions between the growing solid, SDA, and solvents are crucial to the formation of the final product. It is believed that the use of ILs will lower the competitions existing between the solvent and SDA for the growing solid.<sup>20</sup> Previous studies have shown ILs are successful in generating framework structures such as aluminophosphates ( $\text{AlPO}_4\text{s}$ ), metal oxide clusters, and metal-organic frameworks (MOFs).<sup>21</sup> One of the classes of ILs is the deep eutectic solvents (DES). A DES is a mixture containing two

compounds that has the lowest melting point. Dong's group first demonstrated that  $\text{AlPO}_4$ 's can be prepared in a DES containing an organic salt SDA and pentaerythritol.<sup>22</sup>

Whether in the presence of ILs involving the imidazolium ion or a DES containing the tetraalkylammonium SDA, the examples of silicate or aluminosilicate species are very limited.<sup>23-26</sup> The reason for this is due to the low solubility of silica in ILs. However, as shown in the previous chapters, the crystallization of different types of high-silica zeolites can be achieved by changing the SDA and the solvent. Although there have been reports on the crystallization of zeolites in hydrothermal conditions, no mechanistic studies have been performed on the formation of zeolites in the ionothermal reaction environment. Such investigations are necessary for understanding the high-silica zeolite production in ionic liquids, the preparation of other framework types, and the development of new structures under such conditions. As mentioned in the previous two chapters, zeolites with different framework topologies have been successfully produced under different conditions. For the purpose of this chapter, the reactions were performed in a deep eutectic solvent (DES) system composed of TMACl and 1, 6-hexanediol at a 1: 1 mole ratio and fluoride as the mineralizing agent. In this chapter, we present the findings in the preliminary investigations on the crystallization process of ZSM-39 in this medium by powder X-ray diffraction (PXRD),  $^{29}\text{Si}$  CP and MAS NMR,  $^{13}\text{C}$  CP MAS NMR,  $^{19}\text{F}$  MAS NMR, and scanning electron microscopy (SEM). The water content in the reaction mixtures comes from the chemical reagents exclusively, and no extra water was added.

## 5.2 Experimental Section

### 5.2.1 Sample preparation

Ammonium fluoride ( $\geq 98\%$ , Alfa Aesar), 1, 6-hexanediol (97%, Sigma-Aldrich), tetramethylammonium chloride (TMACl, 97%, Sigma-Aldrich) were mixed quantitatively and ground using a mortar and pestle. The ground solid mixture was then transferred to a 40 mL Teflon container. To this mixture, a source of colloidal silica

(Ludox HS-40, Sigma-Aldrich) was added. Ludox HS-40 contains 40% SiO<sub>2</sub> and 60% water. The components were hand-mixed using a spatula until a sticky white paste is formed inside the Teflon cup. The Teflon container was then placed inside a stainless steel autoclave and the reaction mixtures were heated at 140 °C. To obtain the intermediates for this reaction, autoclaves were taken out from the oven at different time periods and immediately quenched in cold water to prevent the reaction from happening further. The cooled down sample was then washed in an excess of solvent mixture containing 1: 1 volume ratio of water/ethanol. The solid component was obtained by vacuum filtration and then dried in an oven at 100 °C for 24 hours. The mole ratios of the reagents are as follows: 1.0 SiO<sub>2</sub>: 0.9 TMACl: 0.9 1, 6-hexanediol: 1.0 NH<sub>4</sub>F: 5.0 H<sub>2</sub>O.

### 5.2.2 Sample characterization

Powder X-ray diffraction patterns were collected for the white powders obtained on a conventional Rigaku powder diffractometer with Co-K $\alpha$  radiation ( $\lambda = 1.79 \text{ \AA}$ ) for  $2\theta$  values in the range of 5° – 65°. The SEM images were taken using a LEO (ZEISS) 1530 Field Emission Microscope.

Solid-state magic-angle spinning (SSMAS) NMR technique was used to characterize the chemical environments in the samples. The measurements were done on an Infinity Plus 400 spectrometer with a wide-bore magnet operating at a field strength of 9.4 T. The magic angle of 54.7° was set from the <sup>79</sup>Br signal from KBr. The <sup>1</sup>H channel has a frequency of 399.5 MHz. The frequencies for <sup>29</sup>Si, <sup>13</sup>C and <sup>19</sup>F are 79.4, 100.5, and 375.9 MHz, respectively. The cross polarization (CP) experiments were set up according to the Hartmann Hahn conditions on TTMSS and adamantane for <sup>1</sup>H  $\rightarrow$  <sup>29</sup>Si CP and <sup>1</sup>H  $\rightarrow$  <sup>13</sup>C CP, respectively. The <sup>29</sup>Si CP and MAS NMR spectra were collected using a 9.5 mm HXY probe at a spinning rate of 3.5 kHz. The <sup>29</sup>Si chemical shifts were referenced to the standard sample which is tetramethylsilane (TMS,  $\delta = 0$  ppm) using tetrakis(trimethylsilyl)-silane (TTMSS) as the secondary standard (-9.8 ppm was used as the reference peak. The other signal was at -125.2 ppm). For the MAS experiments, a 30° pulse with a pulse delay of 30 s was used. For the <sup>29</sup>Si CP experiments, a <sup>1</sup>H 90° pulse length of 9.5  $\mu$ s and a contact time of 0.5 and 5.0 ms were used depending on the

experimental conditions of the sample. The pulse delay in this case was 10 s. The  $^{13}\text{C}$  CP MAS spectra of the samples were collected using a 4.0 mm MAS HXY probe; the spinning rate was 10.0 kHz.  $^{13}\text{C}$  chemical shifts were referenced to the zero standard TMS ( $\delta = 0$  ppm) by using adamantane as the external standard, which has signals at 28.8 and 38.2 ppm. The resonance at 38.2 ppm was used as the reference peak. The  $^1\text{H}$   $90^\circ$  pulse length was  $4.5 \mu\text{s}$ . The contact time used was 3.0 ms, and the pulse delay was 10.0 s.  $\alpha, \alpha, \alpha$ -trifluorotoluene was used as an external standard (-63.7 ppm) to reference the  $^{19}\text{F}$  chemical shifts to  $\text{CFCl}_3$  ( $\delta = 0$  ppm). For the  $^{19}\text{F}$  MAS experiments, a  $30^\circ$  pulse with a pulse delay of 10 s was used. The  $^{19}\text{F}$  MAS spectra shown were collected by spinning the samples at 12 kHz. The spinning side bands of these  $^{19}\text{F}$  spectra were determined by using a different spinning rate at 10 kHz.

Scanning electron microscope (SEM) images of the samples were collected on a LEO (Zeiss) 1530 Field Emission SEM. A 3 nm conductive layer of amorphous osmium was coated onto the samples using an Osmium Plasma Coater.

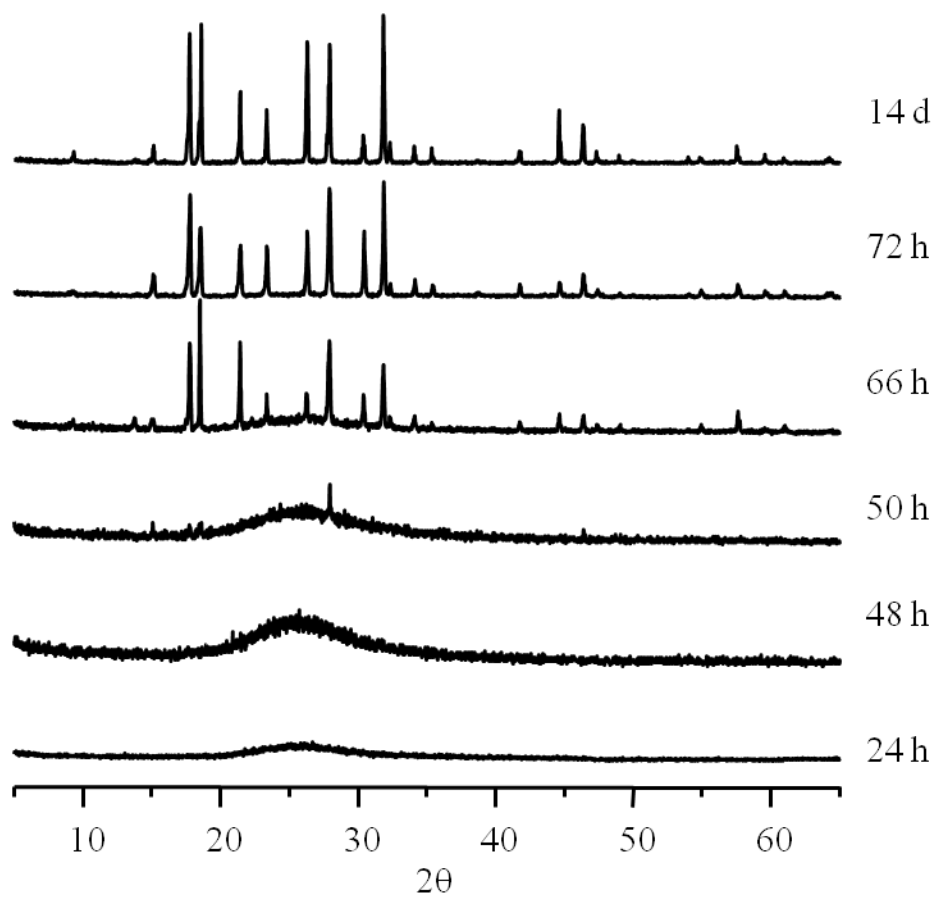


Figure 5.2 PXRD patterns of samples obtained from reactions stopped at different time intervals.

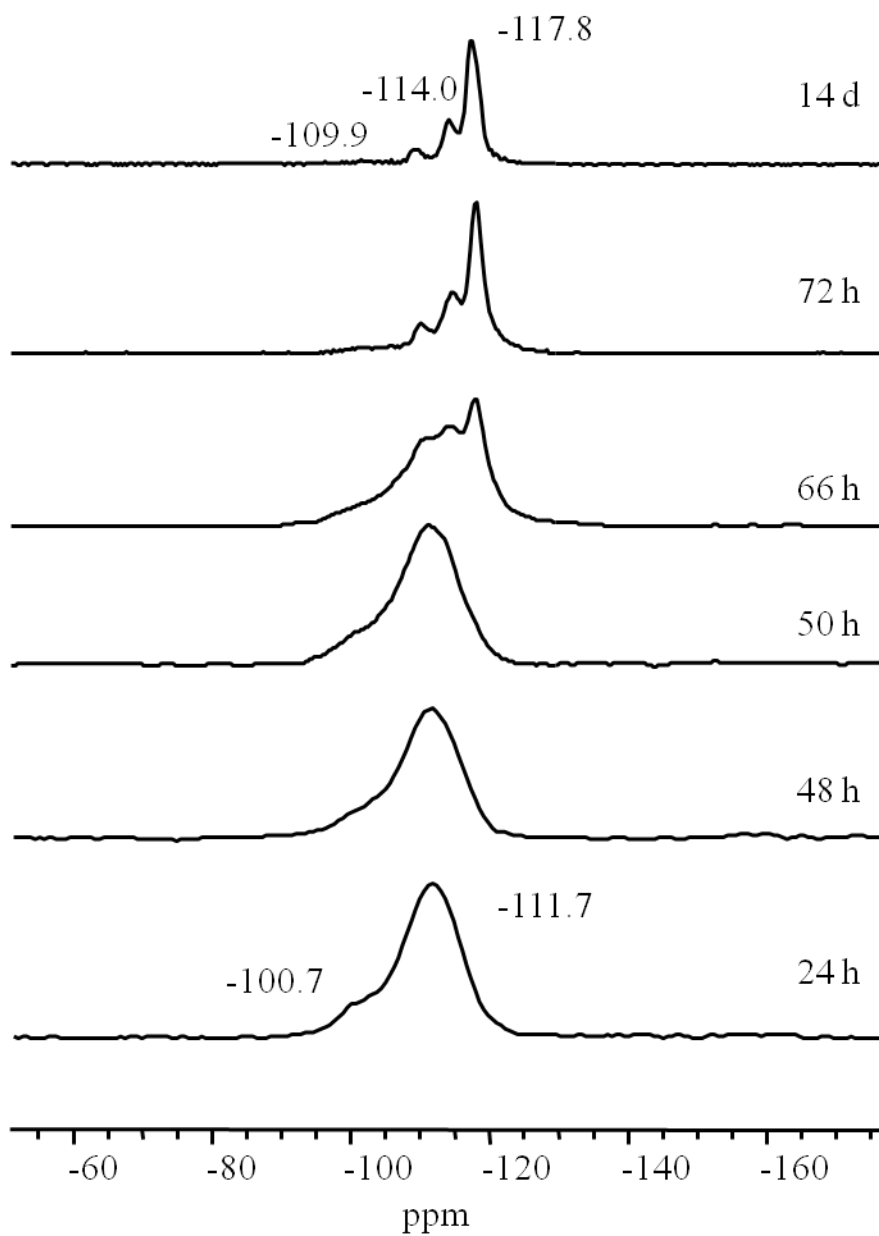


Figure 5.3  $^{29}\text{Si}$  MAS NMR spectra of samples obtained from reactions stopped at different time intervals.

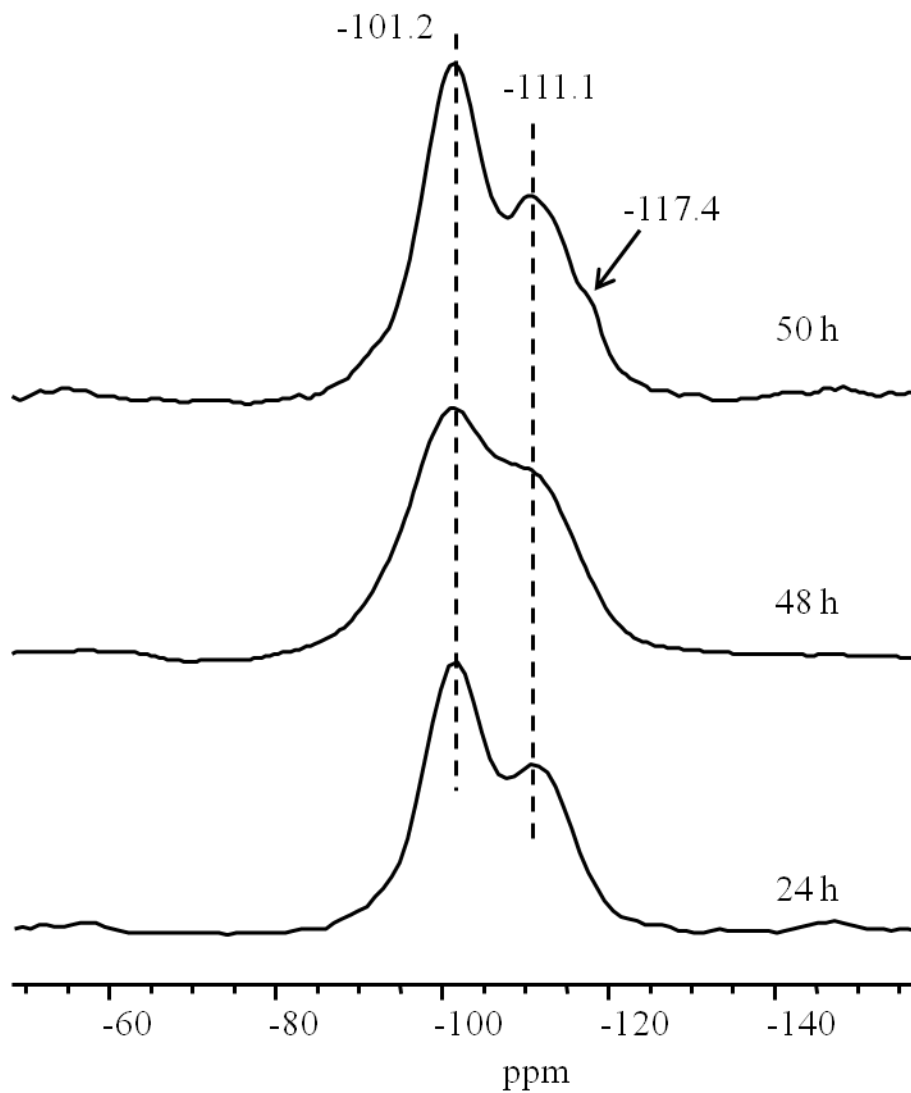


Figure 5.4  ${}^1\text{H} \rightarrow {}^{29}\text{Si}$  CP MAS NMR spectra of samples obtained from reactions stopped at early stages of crystallization (24-50 hr). Contact time = 0.5 ms.



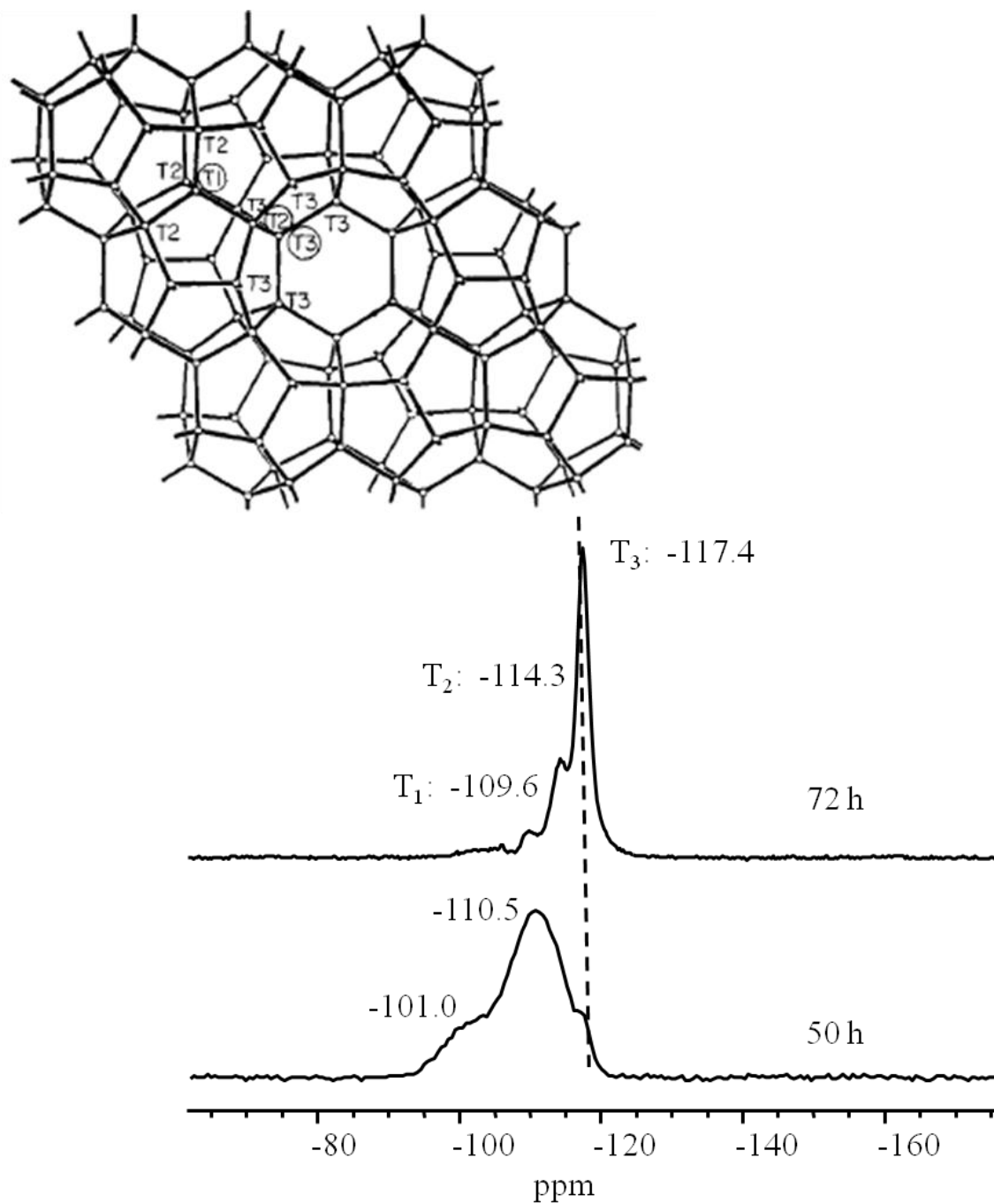


Figure 5.5  $^1\text{H} \rightarrow ^{29}\text{Si}$  CP MAS NMR spectra of a 50 hr sample (ct = 10 ms) and a 72 hr sample (for comparison). The framework structure of ZSM-39 with T-sites assigned are shown.<sup>27</sup>

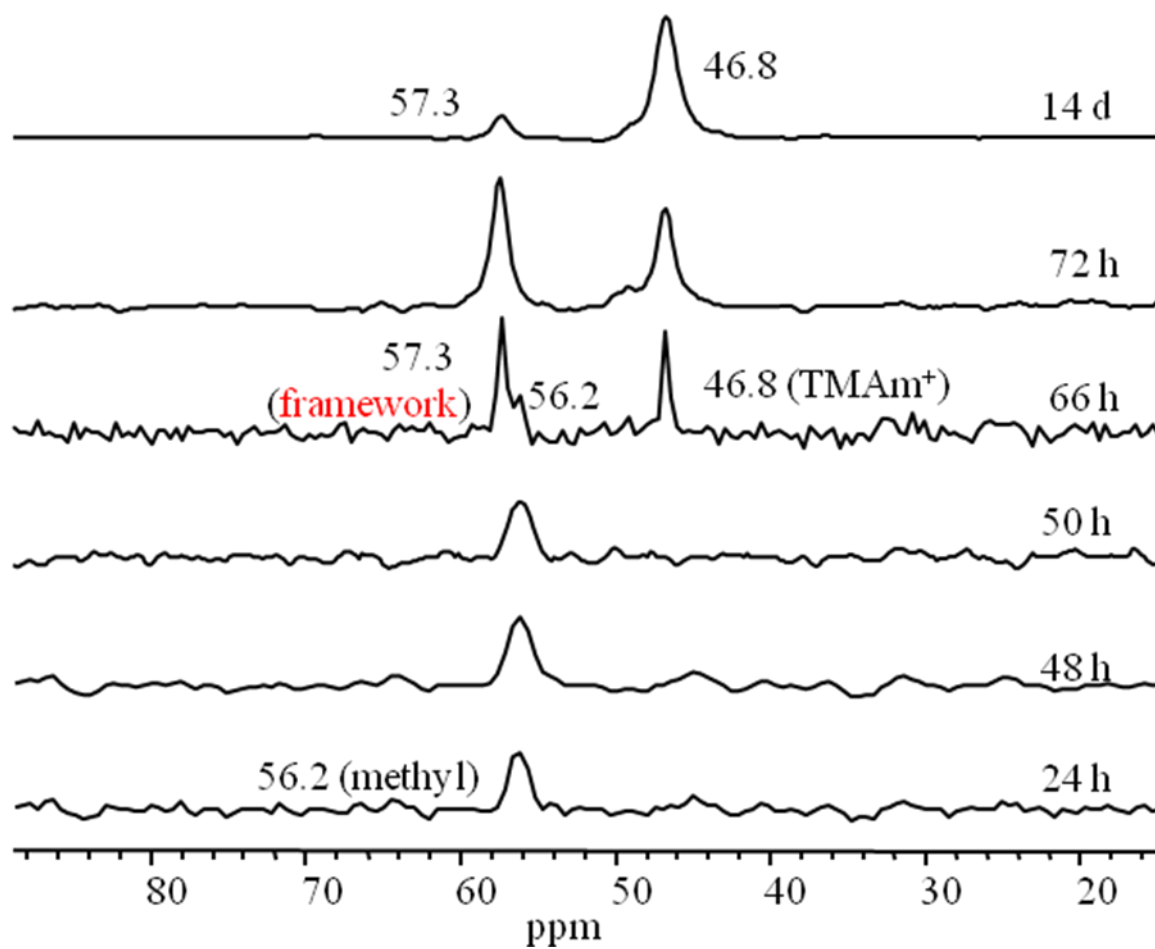


Figure 5.6 :  $^{13}\text{C}$  CP MAS NMR spectra of samples obtained from reactions stopped at different time intervals. TMAm<sup>+</sup>: trimethylammonium ion

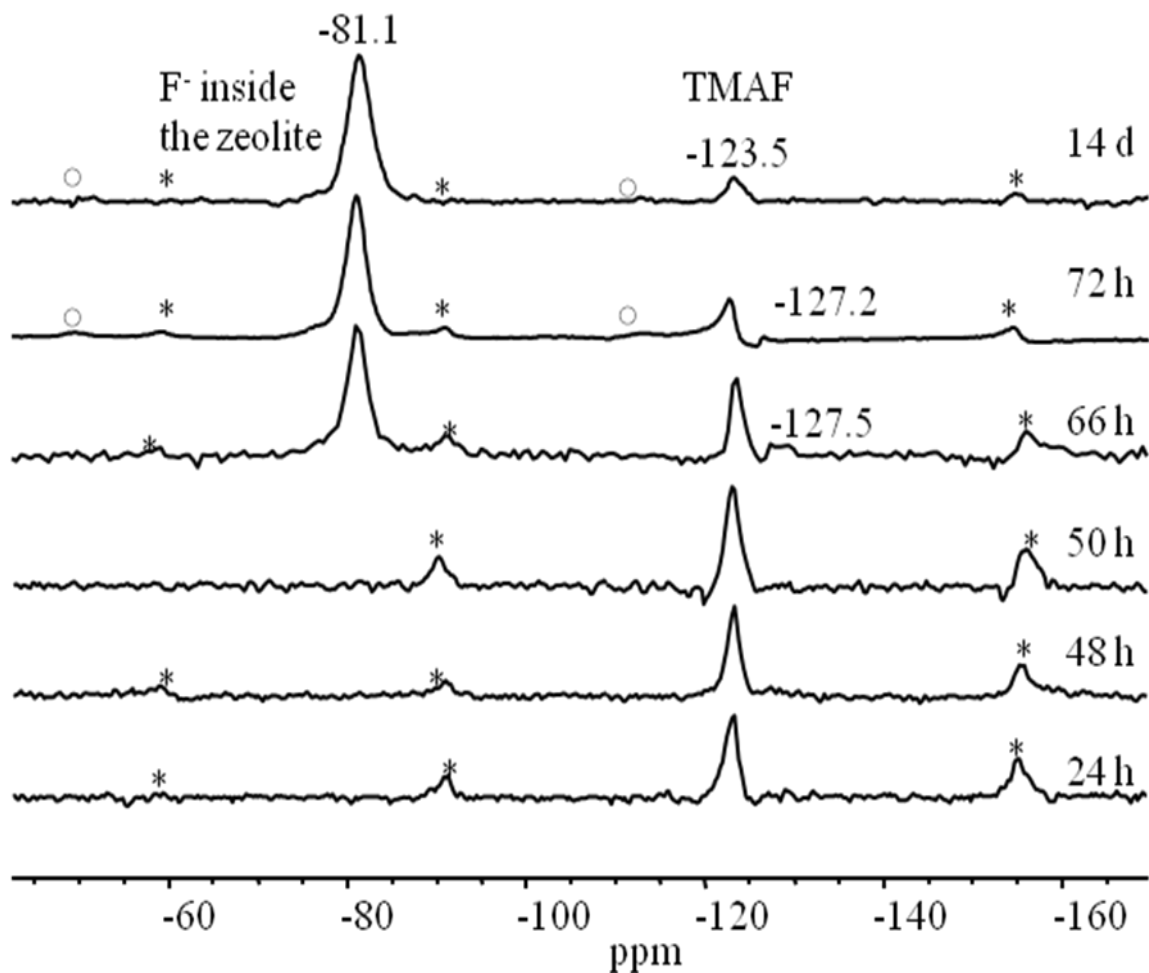


Figure 5.7  $^{19}\text{F}$  MAS NMR spectra of samples obtained from reactions stopped at different time intervals. Spinning speed = 12 kHz. The spinning side bands are shown by "\*" and "o". TMAF = tetramethylammonium fluoride

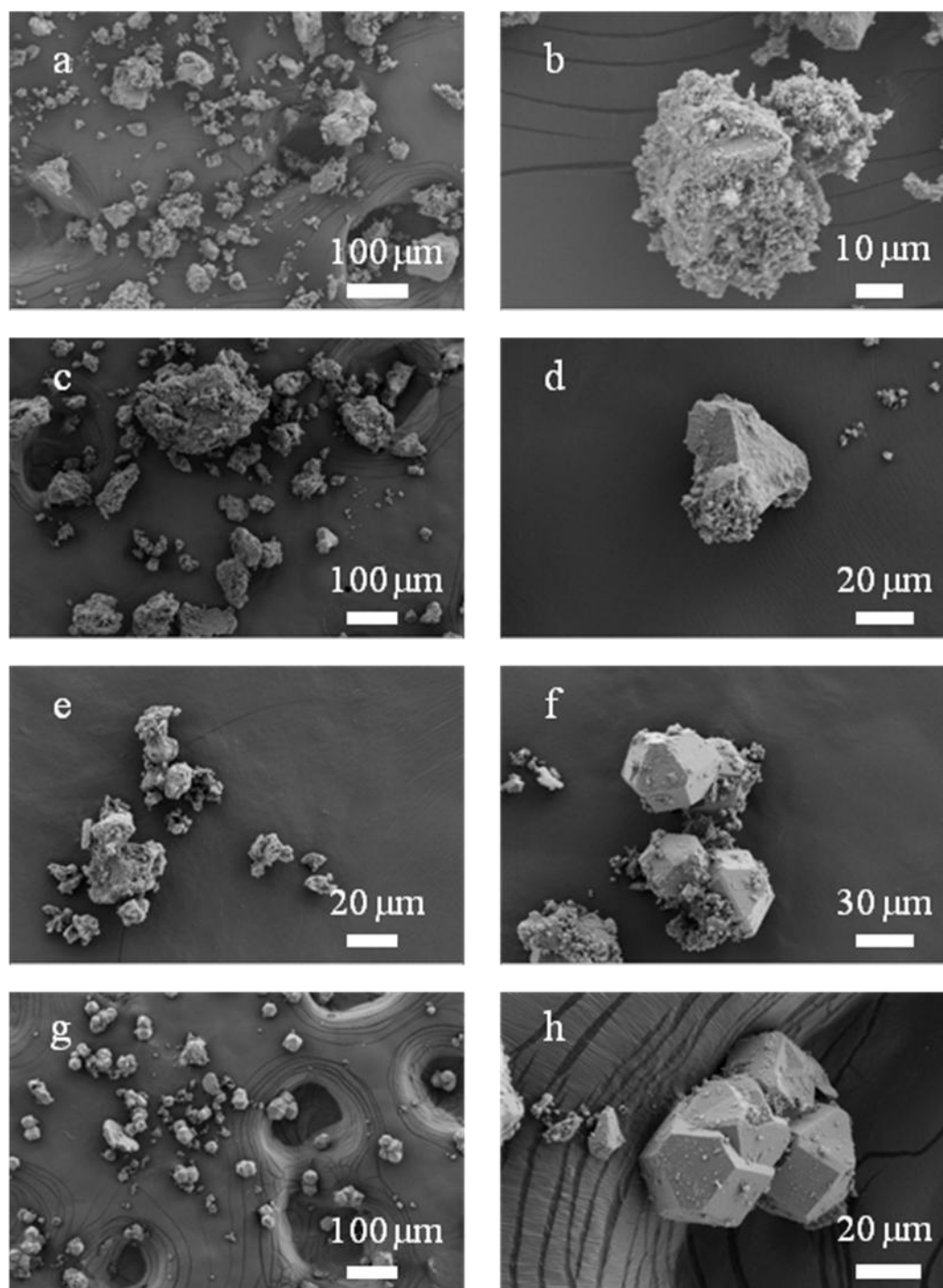


Figure 5.8 SEM images of samples obtained from reactions stopped at 48 hr (a-b), 50 hr (c-d), 66 hr (e-f), and 72 hr (g-h).

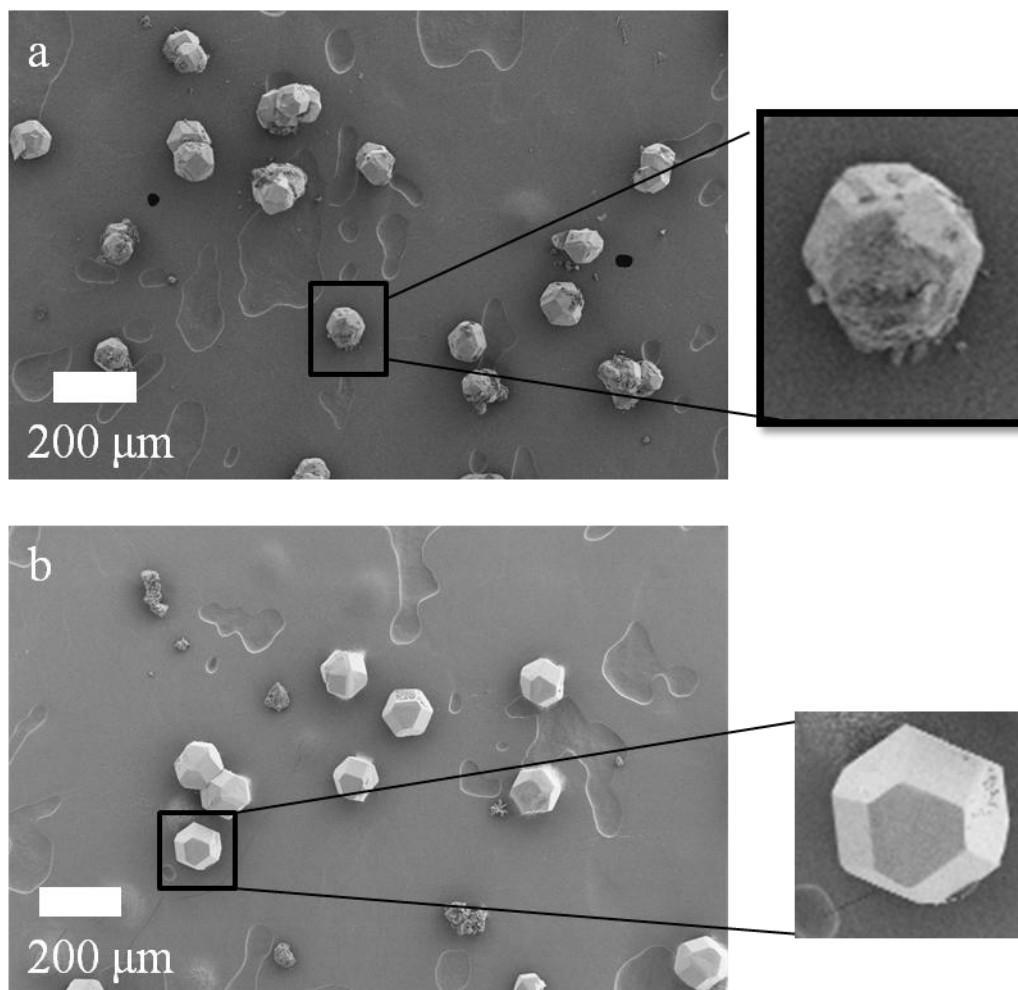


Figure 5.9 SEM images of samples obtained from reactions stopped at (a) 4, and (b) 14 days.

### 5.3 Results and Discussion

The crystallization process of siliceous ZSM-39 at 140 °C without seeding was studied by taking intermediates at different reaction time intervals from 24 hours to 14 days throughout the course of the reaction. The autoclaves were quenched into cold water once they were taken out from the oven. PXRD patterns,  $^{29}\text{Si}$  MAS,  $^{13}\text{C}$  CP MAS, and  $^{19}\text{F}$  MAS NMR spectra were collected for samples stopped at the following time intervals: 24 h, 48 h, 50 h, 66 h, 72 h, and 14 days.  $^{29}\text{Si}$  CP MAS and SEM images were obtained for selected samples.

At the beginning of the reaction at 24 h, the PXRD pattern indicates the sample is completely amorphous at this stage (Figure 5.2). On the  $^{29}\text{Si}$  MAS NMR spectrum, the solid component of the reaction mixture contains of  $\text{Q}^4$  silicon atoms (Si bounded to four other neighboring Si atoms via oxygen) and  $\text{Q}^3$  silicon (silicon atoms bounded to three other neighboring Si atoms via oxygen and one neighboring -OH) (Figure 5.3). The chemical shift for  $\text{Q}^3$  silicon atoms is at around -100.7 ppm, while the  $\text{Q}^4$  Si sites has a chemical shift of around -111.7 ppm.<sup>28</sup> The  $^1\text{H} \rightarrow ^{29}\text{Si}$  CP MAS spectrum at 24 hr of reactions shows the enhancement of the  $\text{Q}^3$  peak (Figure 5.4). The  $\text{Q}^3$  signal is more intense than the  $\text{Q}^4$  signal in the CP MAS spectrum, because CP relies on the proximity between the atoms in the framework. At the early stages of the reaction, there are unreacted amorphous silica with silanol groups being on the surfaces. Due to the close proximity between the Si to the hydrogen of the -OH group, the  $\text{Q}^3$  signal is enhanced by CP. The peak at 56.2 ppm on the  $^{13}\text{C}$  CP MAS spectrum is assigned to the - $\text{CH}_3$  carbon on the  $\text{TMA}^+$  (Figure 5.6). This  $^{13}\text{C}$  signal indicates the presence of  $\text{TMA}^+$  ions inside the gel even before crystallization has started. The nature of the  $\text{TMA}^+$  species is likely to be TMAF, since a signal at -123.5 ppm is shown on the  $^{19}\text{F}$  NMR (Figure 5.7).<sup>29</sup>

From the PXRD patterns, the reaction mixture remains amorphous at 48 hours. There is not much change observed on the  $^{29}\text{Si}$  MAS and  $^{13}\text{C}$  CP MAS spectra (Figure 5.3 and Figure 5.6). The  $^1\text{H} \rightarrow ^{29}\text{Si}$  CP MAS spectrum shows enhancement of  $\text{Q}^3$  sites. However, there is a signal enhancement for the  $\text{Q}^4$  peak compared to the 24 hr sample. Between 24 to 48 hours of reaction, the silica starting material that was previously

dissolved is now re-condensed to form the precursor for MTN. The SEM image (Figure 5.8a) shows that the majority of the sample is composed of amorphous material. However, at a higher magnification (Figure 5.8b), the amorphous particles wrap around a chunk of solid, which can be the precursors for the crystallization. After 50 hours of reaction, the emergence of several sharp peaks belonging to ZSM-39 on the PXRD pattern marks the onset of crystallization (Figure 5.2). However, no change in chemical shifts can be observed on both  $^{29}\text{Si}$  MAS and  $^{13}\text{C}$  CP MAS NMR spectra at this point. The  $^{29}\text{Si}$  MAS spectrum consists of a rather featureless  $\text{Q}^4$  peak having a chemical shift of -111.7 ppm and a broad  $\text{Q}^3$  peak (Figure 5.3). Nevertheless, on the  $^1\text{H} \rightarrow ^{29}\text{Si}$  CP spectrum (Figure 5.4) using a 0.5 ms contact time, there is a shoulder at -117.4 ppm. The intensity of this peak is enhanced by using a longer contact time (10 ms), and the chemical shift coincides with the T3 (the third tetrahedral site) Si chemical shift (Figure 5.5).<sup>27</sup> The longer contact time discriminates against the gel phase due to the fact that the proton spin-lattice relaxation time in the gel phase is usually shorter than that in the crystalline zeolites. Therefore, the  $^{29}\text{Si}$  signals from the more crystalline material can be enhanced. Furthermore, it is very interesting that the  $\text{Q}^4$  peaks are further enhanced as the reaction proceeds. This means that there are more  $\text{Si}(\text{OSi})_4$  being organized to form MTN. The  $^{13}\text{C}$  spectrum (Figure 5.6) shows only one signal for the  $-\text{CH}_3$  carbon at 56.2 ppm. The lack of change in chemical shifts on the  $^{13}\text{C}$  spectrum indicates that the  $\text{TMA}^+$  ions are still mostly occluded inside the amorphous silica gel. As shown by SEM, the majority of the sample is still quite amorphous; however, the solid particles now seem to have more defined faces, which take the shape of a triangle (Figure 5.8c-d). However, at this stage, we are unable to tell which face of the crystal they belong to. If we look at the structure of the MTN framework (Figure 5.5), we will notice that the T3 silicon atoms form the six-membered ring window of the  $[5^{12}6^4]$  cage, in which the organic SDA resides.<sup>30</sup> The enhancement of the -117.4 ppm  $^{29}\text{Si}$  signal indicates that the T3 sites are being formed first. The explanation behind can be that there is an aggregation of silica species around the  $\text{TMA}^+$ . However, we do not observe any changes in the chemical shifts in the  $^{13}\text{C}$  MAS spectrum yet. This is probably due to the fact that the crystalline framework has not been fully formed. Furthermore, there is no change in the  $^{19}\text{F}$  MAS

spectrum at this point (Figure 5.7), meaning that the  $F^-$  anions have not been occluded into the zeolite framework yet.

The ZSM-39 forms very quickly after the onset of crystallization. At 66 hours of reaction, we can see that the reaction mixtures now contains mainly crystallized product and a small amount of amorphous materials as marked by the broad bump at around  $20-30^\circ$  of  $2\theta$  on the PXRD pattern (Figure 5.2). New peaks belonging to the  $Q^4$  region appear on the  $^{29}\text{Si}$  MAS spectrum at -109.9, -114.0, and -117.8 ppm (Figure 5.3). These peaks correspond to the three different types of Si environments in the MTN framework.<sup>27, 31-33</sup> The peaks are not very well separated yet, and there are still some  $Q^3$  silicon sites as indicated by the broad band next to the T-site with chemical shift of -109.9 ppm. However, it is clear that the MTN structure forms very quickly after the formation of the  $[5^{12}6^4]$  cages in the framework. SEM images reveal the presence of both amorphous species and intergrown crystals of ZSM-39 (Figure 5.8e-f). The peaks at 57.2 and 56.2 ppm in the  $^{13}\text{C}$  CP MAS spectrum (Figure 5.6) are both due to the carbon from  $-\text{CH}_3$  on  $\text{TMA}^+$ . The split of the  $-\text{CH}_3$  carbon signal is due to the presence of both crystalline and amorphous materials at this period of the reaction process. In the  $^{13}\text{C}$  CP MAS spectrum for the 66 hr sample (Figure 5.6), the 57.2 ppm is assigned to the  $-\text{CH}_3$  carbon atoms on the  $\text{TMA}^+$  ions which are resided in the crystalline ZSM-39, since this peak can be seen in the final product of the synthesis as well. The 56.2 ppm signal is due to the resonance of  $-\text{CH}_3$  of  $\text{TMA}^+$  ions that are still surrounded by the amorphous gel present in the reaction mixture, because the reaction is not at completion. Formation of the 3D structure traps the  $\text{TMA}^+$  inside the cages of ZSM-39. As the distance between the  $-\text{CH}_3$  carbon atoms and the oxygen atoms of MTN becomes closer, some of the electron densities from the methyl groups are drawn toward the oxygen atom, causing a downfield shift of the carbon signal from the  $\text{TMA}^+$ . This indicates that the proximity of the methyl group to the oxygen atom is closer in the 3D structure than in the amorphous gel. Furthermore, the occlusion of the  $\text{TMA}^+$  into the final product's framework shows that the  $\text{TMA}^+$  ions direct the formation of ZSM-39. Finally, the chemical shift at 46.8 ppm is due to the trimethylammonium ( $\text{TMAm}^+$ ) species formed from the decomposition of  $\text{TMA}^+$  ions during the process of crystallization.<sup>34</sup> There are two types of cages present in ZSM-39. The smaller cavity is around  $5.7 \text{ \AA}$ , while the larger cage is around



7.5 Å. Since the diameters of TMA<sup>+</sup> and TMAm<sup>+</sup> are around 6.9 and 6.6 Å respectively, these two species can only reside inside the larger of the two cavities in MTN.<sup>30</sup> Unlike the 50 hr sample, the 66 hr sample shows the incorporation of fluoride into the framework. A new signal at -81.1 ppm in the <sup>19</sup>F MAS spectrum appears (Figure 5.7). Fluoride is known to be covalently bonded to Si atoms in some of the zeolite frameworks, forming the pentacoordinated silicon species.<sup>35</sup> However, in our case, the chemical shift for the fluoride anion in this case does not correspond to the fluoride that forms a covalent bond with Si atoms. Since the organic SDA species are occupying the [5<sup>12</sup>6<sup>4</sup>] cages, the fluoride anions are more likely to be in the form of fluoride anions resided inside or in between the smaller of the two cages of MTN. There is a small signal at around -127 ppm in the 66 hr and the 72 hr samples, which can be due to the presence of the impurity species, SiF<sub>6</sub><sup>2-</sup>.<sup>36</sup>

From 55 hr to 66 hr, what used to be aggregates around the organic SDA molecules have transformed into crystalline materials. The [5<sup>12</sup>6<sup>4</sup>] cages are linked together through the [5<sup>12</sup>] cages. This is also indicated by the <sup>29</sup>Si MAS spectra that the signals for T1 and T2 Si sites appear later than the T3. The shift to lower field of the TMA<sup>+</sup> peak on the <sup>13</sup>C MAS spectrum signals the formation of the [5<sup>12</sup>6<sup>4</sup>] cages. The occlusion of the fluoride into the framework does not happen at early stages of the synthesis but rather during the formation of crystalline ZSM-39. This in a way explains the downfield shift we see on the <sup>13</sup>C MAS spectrum. As the [5<sup>12</sup>6<sup>4</sup>] cages are being formed, there must be an anion present in order to obtain an overall neutral framework. Thus, anions must be then incorporated into the structure.

The reaction is near completion as it proceeds from 66 hours to 72 hours. At 72 hours, the PXRD pattern shows sharp peaks with strong reflections that are indicative of crystalline ZSM-39 (Figure 5.2). On the <sup>13</sup>C MAS spectrum, the signal at 56.2 ppm now disappears. Only signals at 57.2 and 46.8 ppm can be seen (Figure 5.3). The diminishment of the 56.2 ppm peak on the <sup>13</sup>C MAS spectrum supports what we see on the PXRD pattern: The sample is now highly crystalline, and any signals we see on the <sup>13</sup>C MAS spectrum must be due to the organic species resided inside the framework. The peaks corresponding to the three T (tetrahedral)-sites on the <sup>29</sup>Si MAS spectrum are much

better resolved compared to those observed at 66 hours of reaction. However, there is still a small amount of  $Q^3$  silicon atoms present ( $\sim -106$  ppm), indicating the imperfection of the product's framework at this stage (Figure 5.5). The  $-123.5$  ppm signal on the  $^{19}\text{F}$  MAS spectrum has decreased as a result of the formation of more crystalline materials (Figure 5.7). The SEM images of the 72-hour-sample are shown in Figure 5.8g-h. At higher magnification, it can be seen that the product crystals are often intergrown together. Furthermore, the rough surfaces of the crystals contain defects such as the edges and kinks. Some of the surfaces are also covered by some unreacted amorphous materials.

The 4 day sample is very similar to the 72 hr sample and still consists of intergrown crystals (Figure 5.9a). After 14 days of reaction, the sample obtained is highly crystalline. The  $^{29}\text{Si}$  MAS spectrum shows well separated peaks for the three different T-sites of the Si atoms. The broad peak of the  $Q^3$  Si sites is disappeared, meaning that the MTN framework formed at this point is close to perfection. Although there are still intergrown crystals in the final product, there are also many single crystals exhibiting the dodecahedral morphology (Figure 5.9b).<sup>3</sup> Also, the surface of the crystals obtained after 14 days of reaction are much smoother compared to those after 4 days of reaction and are mostly free from the covering of unreacted amorphous silica. These results indicate that treating the reaction mixture for a longer time helps to heal the defects in the framework and allows the production of high quality crystals.<sup>37</sup> The peak due to the  $\text{TMAm}^+$  at  $46.8$  ppm on the  $^{13}\text{C}$  MAS spectrum is now much stronger than the signal for  $\text{TMA}^+$  at  $57.2$  ppm. This shows that more  $\text{TMA}^+$  ions have decomposed when the reaction was reacted for a longer time. The  $^{19}\text{F}$  MAS spectrum of the 14-day-sample contains two peaks, the stronger one at  $-81.1$  ppm, which corresponds to the  $\text{F}^-$  inside the smaller cages of MTN, and a weak signal at  $-123.5$  ppm. This means that there is still a small amount of TMAF species present.<sup>35</sup>

We would like to point out that throughout the course of the reaction, the other species present in the reaction mixture, 1, 6-hexanediol, is not found in the solid we obtained by vacuum filtration, because only the peaks due to  $\text{TMA}^+$  and  $\text{TMAm}^+$  were observed on the  $^{13}\text{C}$  NMR spectra. The 1, 6-hexanediol must have been dissolved and

washed away by the 1: 1 water/ethanol mixture during the cleansing process. This finding shows that 1, 6-hexanediol is not occluded in ZSM-39 at any point of the crystallization process, indicating that the  $\text{TMA}^+$  species is indeed the sole structure-directing component for MTN formation.

## 5.4 Conclusions

From the above results on the formation of ZSM-39 in  $\text{TMACl}/1$ , 6-hexanediol, the crystallization probably starts with amorphous  $-\text{Si-O-Si}-$  units arranged around the  $\text{TMA}^+$  ions, gradually forming the  $[5^{12}6^4]$  cavity of the MTN structure. As the 3D framework of ZSM-39 is being established, the  $\text{TMA}^+$  became trapped inside the cavities of the zeolite. Connectivity within the MTN framework is then achieved by the formation of the  $[5^{12}]$  cages, in which the  $\text{F}^-$  anions reside. The crystallization of the 3D structure can be seen by the appearance of the three  $\text{Q}^4$  peaks corresponding to the three crystallographically distinct Si sites on the  $^{29}\text{Si}$  MAS spectrum and the downfield shift of the signal due to the  $-\text{CH}_3$  group from  $\text{TMA}^+$  on the  $^{13}\text{C}$  MAS spectrum. The crystallization process is also accompanied by the decomposition of  $\text{TMA}^+$  into  $\text{TMAm}^+$  species. More  $\text{TMAm}^+$  species are formed as the reaction mixture is allowed to react for longer times. Allowing the mixture to react for a longer time at high temperature yields single crystals with low defects.

Our preliminary investigation provides the first example of the study on completely siliceous zeolite formation in DES. The combination of PXRD, NMR and SEM is effective and sensitive to the changes in the chemical environment in the crystallization process. Such methods can be employed for the mechanistic studies of the formation of other zeolite frameworks in ionic liquids.

## 5.5 References

1. Camblor, M. A.; Bong Hong, S., Synthetic Silicate Zeolites: Diverse Materials Accessible through Geoinspiration. In *Porous Materials*, John Wiley & Sons, Ltd: 2010; pp 265-325.
2. Bekkum, H. v.; Jacobs, P. A.; Flanigen, E. M.; Jansen, J. C., *Introduction to Zeolite Science and Practice*. 2001.
3. Schlenker, J. L.; Dwyer, F. G.; Jenkins, E. E.; Rohrbaugh, W. J.; Kokotailo, G. T.; Meier, W. M., *Nature* **1981**, 294 (5839), 340-342.
4. Bibby, D. M.; Parker, L. M., *Zeolites* **1983**, 3 (1), 11-12.
5. Long, Y.; He, H.; Zheng, P.; Wu, G.; Wang, B., *J. Inclusion Phenom. Macrocyclic Chem.* **1987**, 5 (3), 355-362.
6. Marler, B.; Dehnbostel, N.; Eulert, H. H.; Gies, H.; Liebau, F., *J. Inclusion Phenom. Macrocyclic Chem.* **1986**, 4 (4), 339-349.
7. Long, Y., *Chem. J. Chinese Univ.* **1987**, 8, 492.
8. Ripmeester, J. A.; Desando, M. A.; Handa, Y. P.; Tse, J. S., *J. Chem. Soc., Chem. Comm.* **1988**, 608.
9. Zheng, P.; Wang, B.; Wu, G., *Chem. J. Chinese Univ.* **1988**, 9, 1.
10. Anthony, J. L.; Davis, M. E., Assembly of Zeolites and Crystalline Molecular Sieves Self-Organized Nanoscale Materials. Adachi, M.; Lockwood, D. J., Eds. Springer New York: 2006; pp 159-185.
11. Tang, X.; Sun, Y.; Wu, T.; Wang, L.; Fei, L.; Long, Y., *J. Chem. Soc., Faraday Trans.* **1993**, 89 (11), 1839-1841.
12. Bibby, D. M.; Baxter, N. I.; Granttaylor, D.; Parker, L. M., *ACS Symp. Ser.* **1989**, 398, 209-220.
13. Uguina, M. A.; Delucas, A.; Ruiz, F.; Serrano, D. P., *Ind. Eng. Chem. Res.* **1995**, 34 (2), 451-456.
14. Kanno, N.; Miyake, M.; Sato, M., *Zeolites* **1994**, 14 (8), 625-628.
15. Xu, W. Y.; Li, J. Q.; Li, W. Y.; Zhang, H. M.; Liang, B. C., *Zeolites* **1989**, 9 (6), 468-473.
16. Wenyang, X.; Jianquan, L.; Guanghuan, L., *Zeolites* **1990**, 10 (8), 753-759.

17. Caullet, P.; Hazm, J.; Guth, J. L.; Joly, J. F.; Lynch, J.; Raatz, F., *Zeolites* **1992**, *12* (3), 240-250.
18. Xu, H. K., Y.; Liu, L.; Li, J.P.; Wang, J.G.; Dong, J.X., *Acta Petrol. Sin.* **2006**, *22*, 153-155.
19. Shi, Q.; Yu, J. Y.; Liu, L.; Li, J. P.; Dong, J. X., *Shiyou Xuebao, Shiyou Jiagong* **2008**, *24*, 185-187.
20. Cooper, E. R.; Andrews, C. D.; Wheatley, P. S.; Webb, P. B.; Wormald, P.; Morris, R. E., *Stud. Surf. Sci. Catal.* **2005**, *158*, 247-254.
21. Morris, R. E., Ionothermal Synthesis of Zeolites and Other Porous Materials. In *Zeolites and Catalysis*, Wiley-VCH Verlag GmbH & Co. KGaA: 2010; pp 87-105.
22. Liu, L.; Li, X. P.; Xu, H.; Li, J. P.; Lin, Z.; Dong, J. X., *Dalton T.* **2009**, (47), 10418-10421.
23. Ma, Y. C.; Wang, S. J.; Song, Y. L.; Xu, Y. P.; Tian, Z. J.; Yu, J. Y.; Lin, L. W., *Chinese J. Inorg. Chem.* **2010**, *26* (11), 1923-1926.
24. Ma, Y. C.; Xu, Y. P.; Wang, S. J.; Wang, B. C.; Tian, Z. J.; Yu, J. Y.; Lin, L. W., *Chem. J. Chinese U.* **2006**, *27* (4), 739-741.
25. Cai, R.; Liu, Y.; Gu, S.; Yan, Y. S., *J. Am. Chem. Soc.* **2010**, *132* (37), 12776-12777.
26. Wheatley, P. S.; Allan, P. K.; Teat, S. J.; Ashbrook, S. E.; Morris, R. E., *Chem. Sci.* **2010**, *1* (4), 483-487.
27. Fyfe, C. A.; Gies, H.; Feng, Y., *J. Am. Chem. Soc.* **1989**, *111* (20), 7702-7707.
28. J, B. N.; Derouane, E. G., NMR Spectroscopy and Zeolite Chemistry. In *Perspectives in Molecular Sieve Science*, American Chemical Society: 1988; Vol. 368, pp 2-32.
29. Christe, K. O.; Wilson, W. W., *J. Fluorine Chem.* **1990**, *46* (2), 339-342.
30. Gies, H., *Z. Kristallogr.* **1984**, *167* (1-2), 73-82.
31. Higgins, J. B.; Woessner, D. E.; Trewella, J. C.; Schlenker, J. L., *Zeolites* **1984**, *4* (2), 112-113.
32. Fyfe, C. A.; Gies, H.; Feng, Y.; Kokotailo, G. T., *Nature* **1989**, *341* (6239), 223-225.
33. Fyfe, C. A.; Gies, H.; Feng, Y., *J. Chem. Soc., Chem. Commun.* **1989**, (17), 1240-1242.

34. Dewaele, N.; Gabelica, Z.; Bodart, P.; Nagy, J. B.; Giordano, G.; Derouane, E. G., GEL Composition Versus Organic Directing Agent Effects in the Synthesis of ZSM-39, ZSM-48 and ZSM-50 Zeolites. In *Studies in Surface Science and Catalysis*, Grobet, P. J.; Mortier, W. J.; Vansant, E. F.; Schulz-Ekloff, G., Eds. Elsevier: 1988; Vol. Volume 37, pp 65-73.
35. Zones, S. I.; Darton, R. J.; Morris, R.; Hwang, S. J., *J. Phys. Chem. B* **2005**, *109* (1), 652-661.
36. Cambor, M. A.; Barrett, P. A.; Díaz-Cabañas, M.-J.; Villaescusa, L. A.; Puche, M.; Boix, T.; Pérez, E.; Koller, H., *Microporous Mesoporous Mater.* **2001**, *48* (1-3), 11-22.
37. Boris, S.; Josip, B., Theoretical and Practical Aspects of Zeolite Crystal Growth. In *Handbook of Zeolite Science and Technology*, CRC Press: 2003.

## Chapter 6 : Conclusions and Future Works

### 6.1 Conclusions

The studies in this thesis are mainly focusing on the preparation of high-silica zeolites in the presence of ionic liquids (ILs). While there is an increasing interest in the investigations for discoveries of new types of microporous materials, studies in the synthetic strategies for high-silica or siliceous zeolites remain important due to the high chemical, thermal and hydrothermal stabilities of the high-silica zeolites. Our studies have shown that phase-pure high-silica zeolites can be made by adding organic SDAs to the DES.

In Chapter 3, the organic SDA is part of the DES component. Studies were focused on the types of zeolites produced and different factors which can affect the reactions in a tetraalkylammonium/alcohol DES mixture. We found that both siliceous and high-silica zeolites can be prepared under such conditions. By varying the organic SDA and also the mineralizing agent, we were able to synthesize phase-pure ZSM-5, sodalite, and ZSM-39. For MFI, the reaction rate is decreased when the amount of seeds, water, and organic SDA are lowered. Aluminosilicate MFI with Si/Al ratio of around 100 can be prepared by employing NaOH as the mineralizing agent. In the case where TMACl was the organic SDA (no seeds were added), by changing the mineralizing agent from fluoride to hydroxide, ZSM-39 was produced instead of sodalite. This shows that in an ionothermal environment, the formation of a particular zeolite framework can be affected by the choice of mineralizing agent present.

Chapter 4 explores the preparation of different types of zeolite frameworks in urea/choline chloride mixture. By using different organic SDAs, ZSM-5, zeolite Beta, ZSM-39, and ZSM-11 can be made. Under these reaction conditions and the presence of fluoride as the mineralizing agent, the zeolite Beta produced is extremely high in quality, especially after calcination. The studies also show the importance of reaction temperature on the type of zeolites being produced. High reaction temperature can cause the formation of denser frameworks despite the strong structure-directing ability of the

SDA. When there are different choices of SDAs available for the generation of the same framework, the reaction can proceed in the absence of seeds if the SDA with stronger structure-directing ability is used.

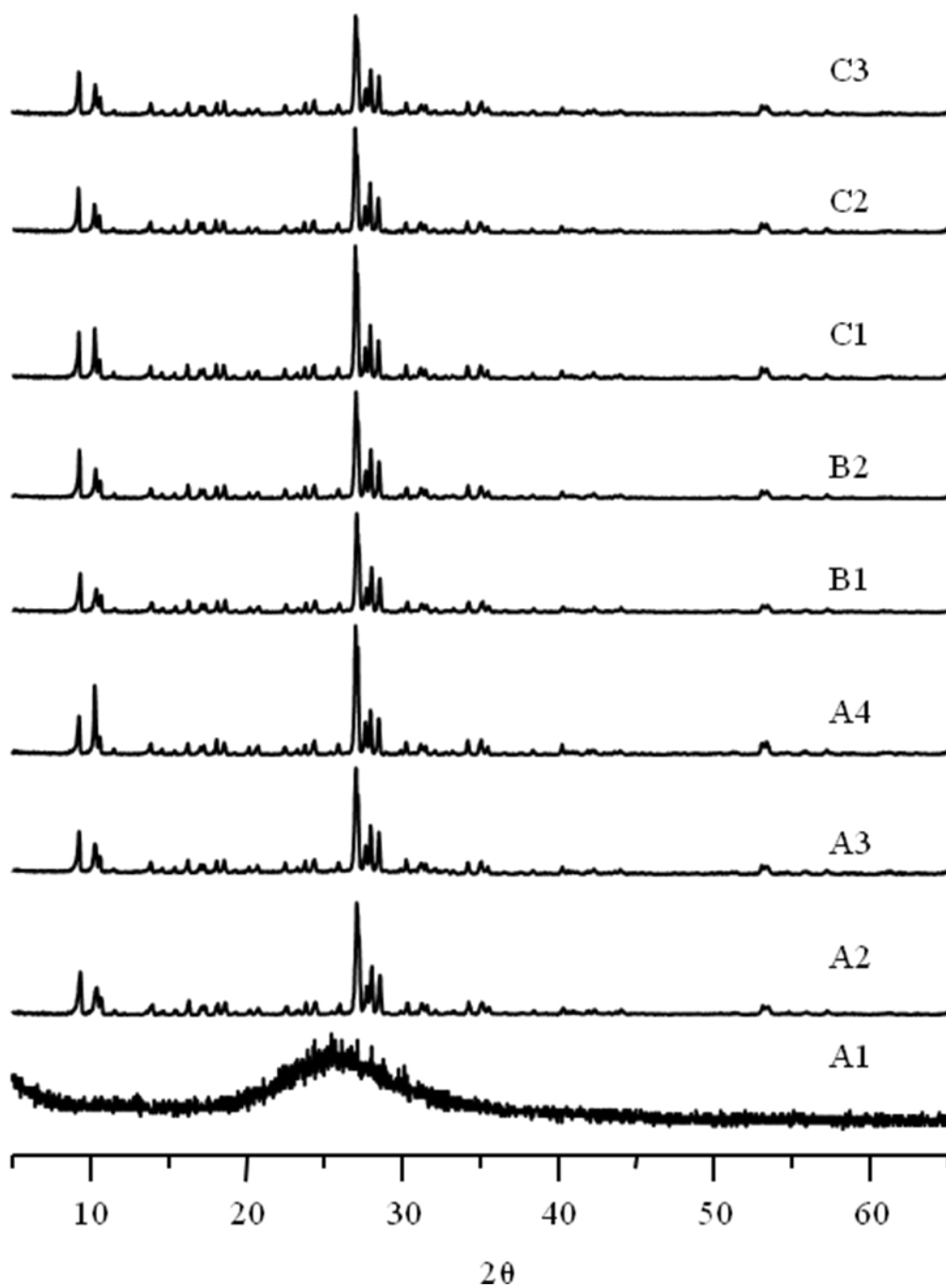
The crystallization process of ZSM-39, a cubic hydrate containing two types of cages, in TMACl/1, 6-hexanediol DES was explored in Chapter 5. Based on NMR, PXRD, and SEM results, the crystallization starts with Si species dissolved from silica forming an aggregate around the  $\text{TMA}^+$ . As the reaction proceeds, the aggregates rearrange themselves to form the larger cage ( $[5^{12}6^4]$ ) of the framework. To achieve the 3D framework, the larger cages are then joined together by the smaller cages ( $[5^{12}]$ ). During this period, the fluoride anions also became trapped inside the zeolite framework. However, the exact location of the  $\text{F}^-$  cannot be determined given the data available at this point.

## 6.2 Future Works

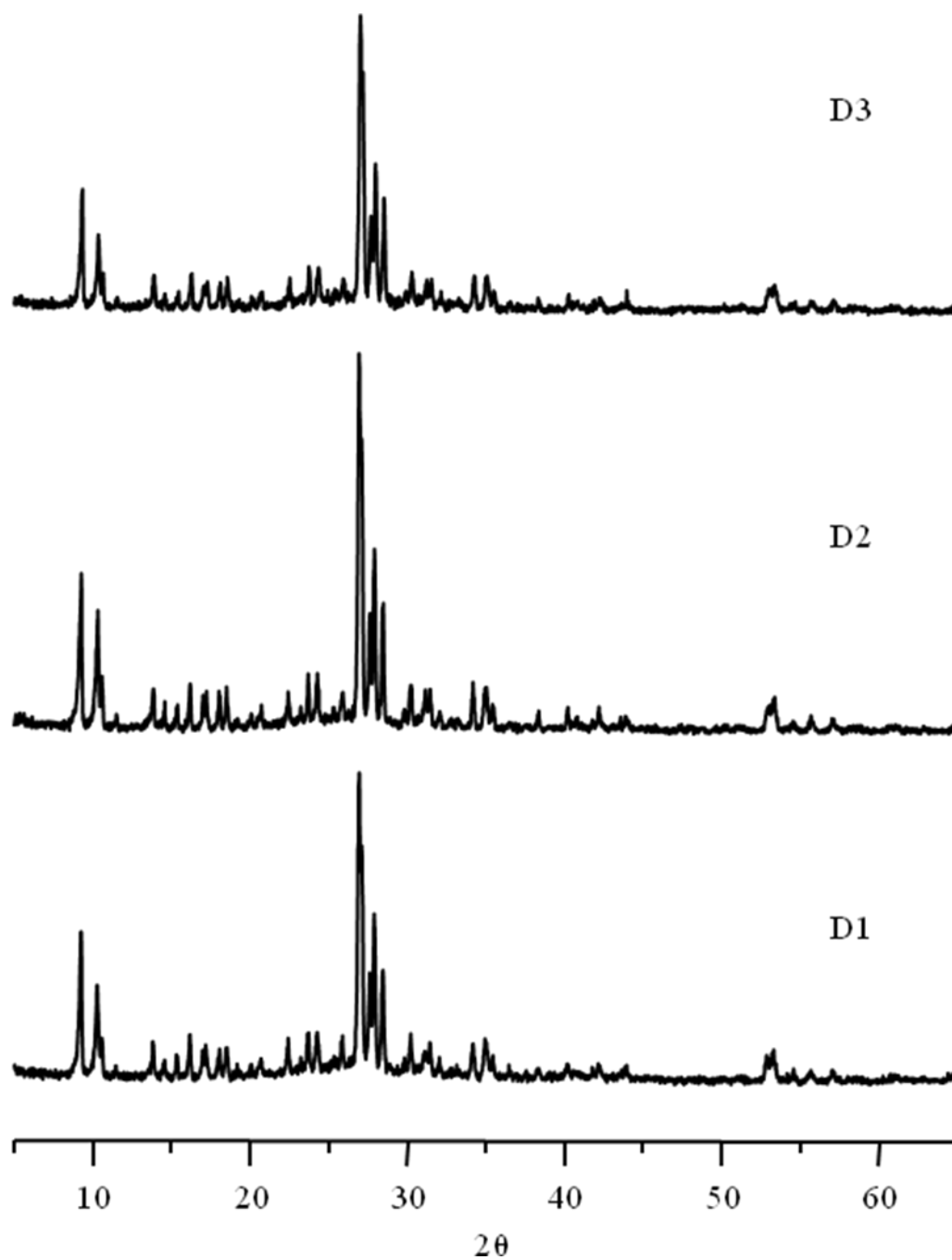
For the studies performed on the crystallization process of ZSM-39 in TMACl/1, 6-hexanediol,  $^{19}\text{F} \rightarrow ^{29}\text{Si}$  CP NMR needs to be done in order to acquire more information regarding the location of the  $\text{F}^-$  atoms in the framework. However, the choice of DES used may have an effect on the crystallization of the same type of zeolite. Nevertheless, the details of the process can be obtained by using the combination of NMR, PXRD, and SEM techniques. Therefore, this characterization method can be applied to other zeolites made in a different DES mixture. Finally, we have shown that different zeolites can be made in an ionothermal environment. By optimizing the reaction conditions, other types of frameworks can be made. Among these, it is very likely that the other members of the pentasil family can be prepared by choosing an SDA that is specific to the production of the desired framework. For instance, the preparation of ZSM-12 using N, N-dimethylhexamethyleneiminium iodide in ILs can be examined.



## Appendices



Appendix A: PXRD patterns of Silicalite-1 samples listed in Table 3.1.



Appendix B: PXRD patterns of aluminosilicate ZSM-5 samples prepared using different sources of aluminum. These are the PXRD patterns for the samples listed in Table 3.2.

## Curriculum Vitae

**Name:** Zheng Sonia Lin

**Post-secondary Education and Degrees:** The University of British Columbia  
Vancouver, British Columbia, Canada  
2004-2009 B.Sc.

The University of Western Ontario  
London, Ontario, Canada  
2010-2012 M.Sc.

**Honours and Awards:** Western Graduate Research Scholarship  
Fall 2011, Winter 2012

**Related Work Experience** Work Study Student  
UBC Mass Spectrometry/Microanalysis  
2007-2009

Research Assistant  
The University of British Columbia (Dr. Fyfe's Group)  
2009-2010

Research Assistant (Dr. Huang's Group)  
The University of Western Ontario  
2010-2012

Teaching Assistant (C2213a and C2223b)  
The University of Western Ontario  
2010-2012

### Publications:

1. Fyfe, C.A., Lin, Z.S., Tong, C., Darton, R.J. (2012) Simple, efficient synthesis of zeolite ZSM-11 (MEL) at temperatures below 100 °C using very dense gels, *Microporous and Mesoporous Materials*. 150, 7-13
2. Fyfe, C.A., Darton, R.J., Mowatt, H., Lin, Z.S. (2011) Efficient, low-cost, minimal reagent syntheses of high silica zeolites using extremely dense gels below 100 °C, *Microporous and Mesoporous Materials*. 144, 57-66

### Presentations:

1. 43<sup>rd</sup> Inorganic Discussion Weekend (IDW). Niagara Falls, Ontario, Canada (2011). Zheng Sonia Lin and Yining Huang. Presentation: Synthesis of ZSM-5 zeolite Using deep eutectic solvents (DES)

2. Centre for Advanced Materials and Biomaterials Research (CAMBR) Distinguished Lecturer and Research Day. London, Ontario, Canada (2011). Zheng Sonia Lin and Yining Huang. Poster: Ionothermal Synthesis of ZSM-5 Zeolite Using Deep Eutectic Solvents (DES)